

Graduate School of
Systemic Neurosciences

LMU Munich

Transcriptional specification and dendritic growth patterns of motion-sensing neurons in *Drosophila* during development

Nikolai Li-Heng HÖRMANN

supervised by
Prof. Dr. Alexander Borst

Dissertation at the

Graduate School for Systemic Neurosciences
Ludwig-Maximilians-Universität München

9th of January 2023

Supervisor

Prof. Dr. Alexander Borst

Max Planck Institute for Biological Intelligence, Martinsried, Germany

First reviewer

Prof. Dr. Alexander Borst

Second reviewer

Prof. Dr. Magdalena Götz

External third reviewer

Filipe Pinto Teixeira, PhD

Date of submission

9th of January 2023

Date of defense

2nd of May 2023

Abstract

The development of functional circuits in the brain requires neuronal morphogenesis combined with specificity in synapse formation. Diverse morphologies of neurons are generated by the precise interactions between transcription factors in gene regulatory networks. These networks specify the development of neurons, creating elaborate branching patterns of dendrites and axons. During this growth process, synaptic partners are located in close proximity to each other within the neuropil for synapse formation. The *Drosophila* motion vision circuit is well understood in the adult animal regarding morphology and function. Therefore, this system provides the necessary background to study the development of motion selective neurons. In combination with the genetic accessibility of *Drosophila* neurons and recent advances in transcriptomic profiling approaches, it is the ideal model system for the study the development of neuronal circuits.

In my PhD, I focused on primary visual motion-sensing neurons in *Drosophila*. These neurons, T₄ and T₅, exist in four subtypes (*a*, *b*, *c*, *d*), each responding preferentially to visual motion in one of the four cardinal directions. Their dendrites are oriented according to their functional response and innervate the same neuropil layer, in the medulla or lobula for T₄ and T₅, respectively. Their axon terminals are located in one of the four layers of the lobula plate separated by their functional identity. These two morphological characteristics, the dendrite orientation and the layer of axonal arborisation, are the only difference between T₄ and T₅ subtypes. Therefore, it is possible to investigate how genes specify neuronal morphologies through transcriptomic profiling by studying the growth patterns of T₄ and T₅ dendrites.

For the first manuscript of my PhD, I performed single-cell RNA sequencing of T₄ and T₅ neurons at different stages of dendritic development. I found multiple transcriptional differences between subtypes. In particular, I discovered that the transcription factor *grain* separates *a/d* from *b/c* subtypes. *grain* is additionally required to specify the morphological characteristics of *b/c* subtypes, while suppressing *a/d* morphologies. Through overexpression experiments *a/d* subtypes could be transformed to *b/c* and *b/c* could be transformed to *a/d* subtypes using RNA interference experiments, morphologically. Furthermore, overexpression experiments combined with recordings of neuronal activity, mainly showed preferred direction responses of *b/c* subtypes. It is, thus, a necessary component of the gene regulatory network to specify T₄ and T₅ subtype morphologies. Additionally, I identified many differentially expressed cell surface proteins that potentially play a role in guiding the growth of T₄ and T₅ dendrites.

In the second manuscript of this thesis, I used an *ex vivo* brain preparation to image single T4 dendrites during their growth phase. I could distinguish horizontal, *a/b*, and vertical, *c/d*, subtypes of T4 neurons only by their dendritic growth pattern. Furthermore, horizontal subtypes could be split into *a* and *b* subtypes based on their direction of growth. Their growth pattern shows a sequential order growing from their proximal to their distal compartment.

In conclusion, this work discovered the specification of T4 and T5 neurons through transcription factors, which, combined with their dendritic growth pattern, can help us understand how gene expression determines morphologies necessary to form neuronal circuits.

CONTENTS

1 INTRODUCTION	1
1.1 Brain development	2
1.1.1 Neuronal lineages and specification	2
1.1.2 Extrinsic cues guiding neuronal development	4
1.2 Neuronal development	5
1.2.1 Axon growth and guidance	7
1.2.2 Dendritic growth rules	7
1.3 Neuronal cell types	8
1.3.1 Combinatorial transcription factor codes	9
1.3.2 Protein expression	10
1.3.3 Morphology	10
1.3.4 Function	11
1.3.5 Classifying neurons	11
1.4 Advancements in the field of <i>Drosophila</i> neuroscience and development	11
1.5 <i>Drosophila</i> vision as a model system for neurodevelopment	13
1.5.1 <i>Drosophila</i> visual system	13
1.5.2 Computation of motion	16
1.5.3 Motion vision circuit	16
1.5.4 Local motion detectors in <i>Drosophila</i>	17
1.5.5 T4/T5 development	19
1.6 Motivation for the choice of model system	19
2 MANUSCRIPTS	21
2.1 Manuscript 1	21
2.2 Manuscript 2	51

3 DISCUSSION	77
3.1 Transcriptional regulation in T4 and T5 neurons	78
3.1.1 Expression patterns of transcription factors in T4 and T5 neurons	78
3.1.2 Temporal expression profiles	79
3.1.3 Differentially expressed genes between T4 and T5 subtypes	80
3.2 Variability of gene expression in T4 and T5 neurons	81
3.2.1 Technical variability in scRNA-seq experiments	81
3.2.2 Biological variability in gene expression	82
3.3 Morphological analysis of T4 dendrites during development	82
3.3.1 Dendritic morphometrics	83
3.3.2 Morphological identification of T4 subtypes during development	85
3.3.3 T4 morphologies during development	86
3.4 Dendritic growth strategies	87
3.4.1 Dendritic growth patterns of T4 neurons	87
3.4.2 Medulla topology	88
3.4.3 Synaptotrophic hypothesis	89
3.4.4 Developmental comparison between T4 and T5 neurons	89
3.5 Conclusions and outlook	90
LIST OF FIGURES	93
LIST OF ABBREVIATIONS	95
REFERENCES	97
DECLARATION OF AUTHORSHIP	117

1

INTRODUCTION

During morphogenesis, genes are translated to proteins, through an intermediate step of RNA, giving rise to an entire, functioning organism from a single cell. While almost every cell contains the same genome, their morphologies and functions diverge immensely. To generate the diversity, cells interpret the genetic code [1] differentially to produce organs and structures constituting the adult animal. Large numbers of different proteins, nucleic acids, and other organic molecules are required to interact in the process of development, impeding our understanding of the molecular mechanism underlying morphogenesis. Therefore, developmental biology studies how the genetic code is implemented at different stages of development to coordinate DNA, RNA and proteins and build a functional, multicellular organism [2].

The brain is, arguably, the most complex structure organisms built during morphogenesis. The two major challenges for brain development are, first, diverse neuronal morphologies [3] that must be formed to bring synaptic partners into close proximity for synapse formation [4]; and second, neurons need to be connected to their specific pre- and postsynaptic partners for the formation of neuronal circuits [5]. The translation of the genetic code used in each individual neuron is determined through epigenetic and transcriptional regulation. Developing complex morphologies in neurons requires intracellular interactions between proteins, e.g., intrinsic signaling pathways [6], and extracellular interactions of proteins with the surrounding matrix, e.g., sensing concentration gradients [7].

These molecular mechanisms relevant for development have been studied for long, especially in *Drosophila*, and have led to fundamental discoveries, such as the genetic control of segment generation in the *Drosophila* embryo [8, 9]. However, the translation of the genetic code to specific neuronal morphologies has not been fully understood

so far. The motion vision circuit of *Drosophila* offers a morphologically well-described model in the adult for the investigation of molecular mechanisms during development. Additionally, thanks to recent technological advances in microscopy [10], image analysis [11] and molecular biology [12], neuronal development can be studied in far more detail nowadays than in the past [13]. Applying these novel methods to the *Drosophila* visual system can facilitate the investigation of how genes control the diversity of neurons [14] [15] and the molecular mechanism underlying neuronal morphogenesis [16] [17].

In the following, I provide the relevant background to understand neuronal morphogenesis with a focus on the visual system of *Drosophila*. First, I introduce the developmental mechanisms generating diverse neuronal morphologies and topographic maps in the process of brain development. Subsequently, I describe how neurons are classified into cell types for consistent identification. Then, I will introduce the *Drosophila* visual system and a selection of novel tools with a high potential of leading to fundamental discoveries in the field of developmental neuroscience. Lastly, I elaborate on my motivation of studying this system in the context of neuronal specification and morphogenesis.

1.1 Brain development

During embryogenesis, three cell layers are generated in a process called 'gastrulation': the endoderm, the mesoderm, and the ectoderm. Brain development starts with the specification of neuronal progenitor cells that originate from the ectoderm and are arranged in the antero-posterior, rostral-caudal, and the dorso-ventral axis [21-23]. Progenitors in the embryo assume cell fates dependent on their spatial position, a process called patterning. The molecular mechanism underlying 'patterning' can range from mechanical forces [24] to secreted proteins [25]. Different segments of *Drosophila* are specified using different sets of genes, starting with the mother co-ordinate genes. Further expression of gap, pair-rule, and finally segment polarity genes create the fully segmented *Drosophila* embryo [8] [9] [26-29]. In these segments, the antero-posterior and dorso-ventral axes are specified via transcription factors (TFs), such as *ventral nervous system defective* or *muscle segment homeobox* [30-33].

1.1.1 Neuronal lineages and specification

The diversity of neuronal morphologies is generated through specification of neuronal lineages using patterning programs [16] [17]. Different mechanisms specify neuronal cell fates such as position of the progenitor in the embryo [34] [35] or positive/negative feedback loops of receptor expression [36] (see Fig. 1.1). Usually cell fate decisions are irreversible and have been compared to marbles rolling down a hill falling into different ridges (see Fig. 1.1a) [18].

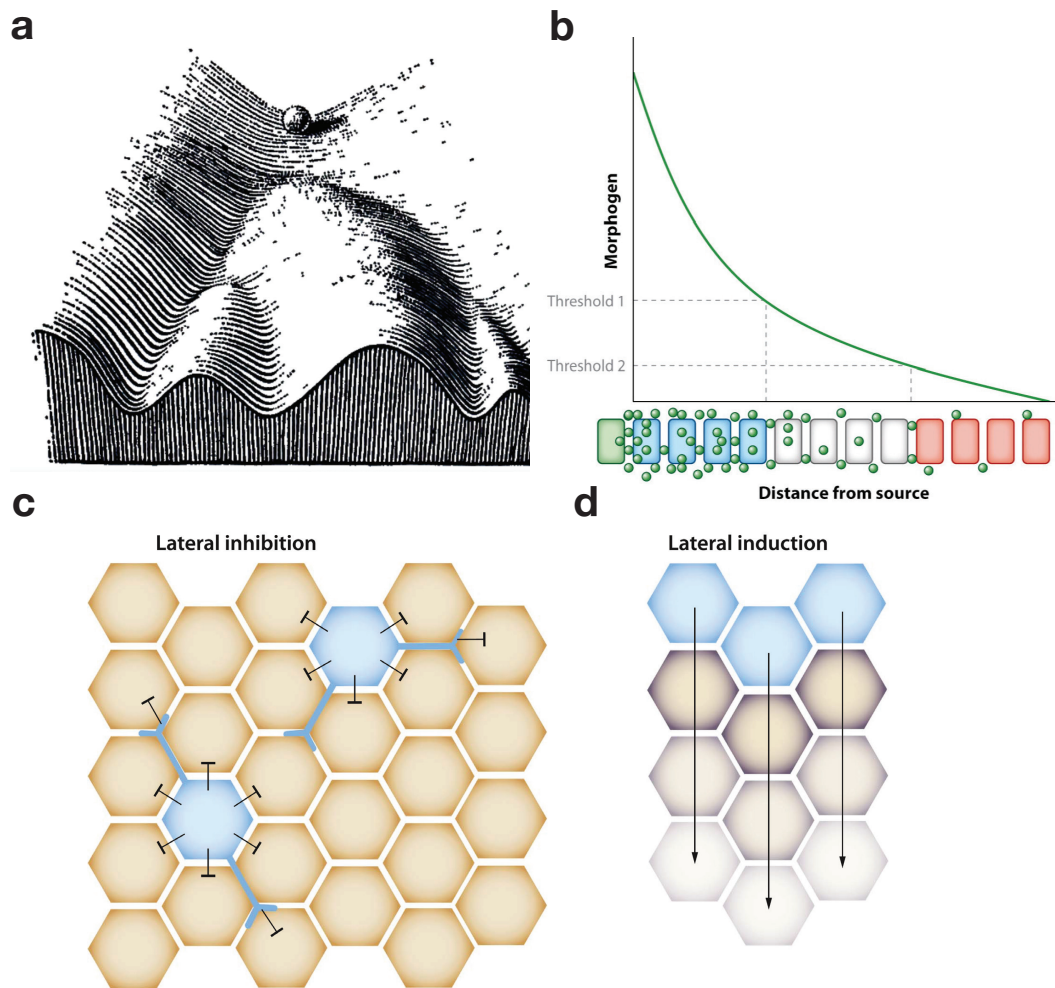


Figure 1.1: Developmental mechanisms in neuronal specification. **a** Waddington's epigenetic landscape [18]. **b** French flag model for the specification of discrete cell types from a concentration gradient. Morphogens are indicated as green balls, squares indicate cells. The green square secretes morphogens and blue, white, and red squares indicate the differentiation into different cell types [19]. **c** Mechanism of lateral inhibition. Hexagons represent cells, where blue cells are inhibiting the brown cells from assuming the same cell fate [20]. **d** Mechanism of lateral induction. Blue cells are inducing a cell type which then is propagated down in a contact-dependent way. Arrows indicate the direction of cell type induction. [20].

One prominent example to specify cell lineages are morphogens. These are secreted proteins that diffuse from a local source into the neuropil forming a concentration gradient [7, 19]. Morphogens are essential to create a gradient along a certain anatomical axis, which defines different cell types dependent on the respective morphogen concentration. However, this continuous gradient needs to be converted to discrete cell types. One possible mechanism has been famously called 'the French flag model' (Fig 1.1b) [34]. The release of the morphogen at one end of a developing tissue will gradually diffuse to the other side, thereby creating a concentration gradient. Since the concentration is different at every point, the French flag model suggests that different cells have different

concentration thresholds in their response to the morphogen. These thresholds then lead to a differentiation into certain cell lineages [18]. Such a mechanism has first been observed in *Drosophila* embryos where the *bicoid* protein forms a gradient along the antero-posterior axis [37] specifying the anterior development.

Another mechanism to induce cell fates depends on the competitive interaction between neighbouring neurons, termed lateral inhibition (Fig 1.1c-d). Here, all neurons have the same ground state, but through competition a founder cell is chosen in regular spatial intervals to pattern the whole tissue [20]. A prominent example is the specification of the ommatidium in the *Drosophila* retina, through the determination of R8 photoreceptors. *notch* expression leads to the specification of R8, which then secretes other proteins to induce the formation of other photoreceptors [38-40]. *notch* and *delta* are transmembrane proteins, but upon binding the intracellular domain of *notch* is cleaved. The cleaved part translocates to the nucleus and initiates transcription in combination with other transcriptional regulators, such as *Suppressor of Hairless* [41]. The specialisation of neurons is decided based on a competition between neighbouring cells. Cells express *delta* and *notch* proteins with the activation of *notch* leading to a decrease of expression of *delta*. *Delta* inhibits the *notch* activation. If one cell has a slightly higher expression of *notch* it will result in a positive feedback loop and increase its own *notch* production and subsequently inhibit the production in the neighbouring neurons.

The whole process from neuronal progenitor to fully differentiated neuron can take many cell divisions and intermediate progenitor states. Each state however needs to be defined. The specification into discrete states on a molecular level uses TFs as its determinants. These can be more specifically called temporal transcription factors [42-43]. They are expressed transiently during development and help to create the diversity of neurons which are all determined to assume a specific cell fate [15, 44].

1.1.2 Extrinsic cues guiding neuronal development

The genetic specification of neurons intrinsically prepares them to assume a certain morphology [16, 17]. However, dendrites and axons require extrinsic guidance cues to decide on their growth direction. Therefore, the extracellular space is made of many different guidance cues to bring the axons of the presynaptic neurons and dendrites of the postsynaptic neurons to the same location [45].

These cues can be separated into long-range and short-range guidance molecules. The short-range cues, likely cell surface molecules, are located on neighbouring cells or in the extracellular matrix [45]. In the *Drosophila* medulla these local cues are used to restrict axonal and dendritic growth of unicolunar neurons to single columns [46]. *Cadherin-N* [47, 48] has been shown to be important for restricting neurons to a single

column, which is necessary to generate columnar organisation. In addition, it is used for correct neuronal targeting, and circuit formation in the *Drosophila* optic lobe [46]. Contrary to local interactions, long-range cues create a structured global pattern in the neuropil. Morphogens [19] or cell surface molecules [49] create concentration gradients along different anatomical axes of the neuropil serving as guiding cues for neurons. These short- and long-range cues create a topographic map in the neuropil which enable growing dendrites and axons to orient themselves.

Topographic maps are important for neuronal function [50] and development [51, 52]. In the visual system, neurons, which are propagating information from neighbouring points in visual space, are also projecting to neighbouring columns in neuropils. This principle is called retinotopy. This is essential for computations, such as motion detection, which require input from neighbouring points in visual space [53, 54]. Topographic maps along the antero-posterior or dorso-ventral axes of visual space have formed to guide developing neurons to the right position [52, 55, 56].

1.2 Neuronal development

Neurons are highly asymmetric cells, receiving information at the dendrite and transmitting it to postsynaptic targets through the axon. Both, dendrites and axon, are established during development in a process called polarisation [57, 59, 60]. Right after the last cell division, neurons are only comprised of their cell body. Subsequently, they extend neurites to form their dendrite and axon. The growth modes during this step of development can be put into two categories: the targeting of neurites to a different brain region [61–63] and a more local and elaborate branching to realise the adult morphology [16, 58, 64, 65]. Both dendrites and axons can be found in either mode, although dendrites usually do not grow to a different brain region. This whole process requires many resources for neurons, such as proteins for the cytoskeleton serving as supporting structure [45, 66]. Additionally, the whole process of neuronal development is highly dependent on interactions with the extracellular space [57, 58, 62, 67–69]. Protein interactions are usually contact-dependent, as seen in the wide variety of cell surface molecules that play a role in the developmental process [17, 63, 70] (see Fig. 1.2). Aside from their role in guiding growth, cell surface molecules can be specific for either dendrite or axon and help to assign the respective compartment identity [57].

In the following, I focus on two topics of neuronal development: axon growth and guidance, and dendritic growth rules. These aspects of neuronal development constitute general principles of growth that apply to most, if not all, neurons.

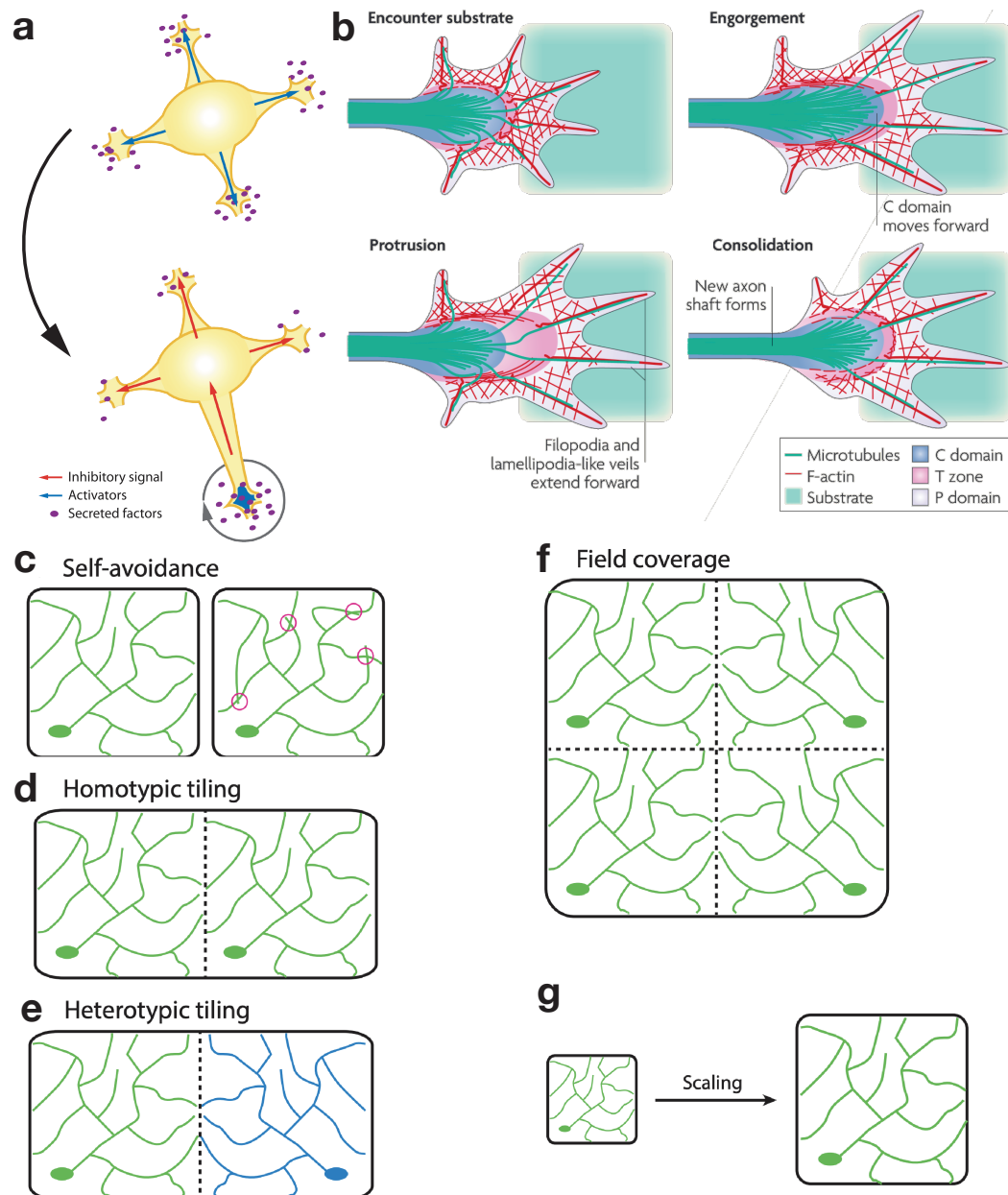


Figure 1.2: Neuronal growth mechanisms. **a** Specification of compartments through polarisation in a fully differentiated neuron, which is shown in yellow [57]. **b** Different states of a growth cone when it encounters a substrate to grow towards [45]. **c-g** Growth rules for developing dendrites with borders between dendritic fields shown as dashed lines [58].

1.2.1 Axon growth and guidance

As soon as neurites have been assigned their respective identity, axons grow to a target area. Guiding cues were first described in the context of axons preferentially growing on different surfaces [71 72]. The guiding process requires long-range migration via a growth cone (Fig 1.2b). The axonal growth cone is the driver of this process and decides through contact-dependent interactions with the external cues whether to grow further in a certain direction or to stop and form the axonal arbor [45 73]. The growth cone itself consists of two main structures: filopodia and lamellipodia. The more variable filopodia are small neurites extending from the end of the growth cone and are the protruding part. The lamellipodia are the structure connecting the filopodia to the axon shaft (see Fig 1.2b). It has been shown that different cytoskeletal proteins are involved in filopodia and lamellipodia. In the tip of the growth cone, filopodia and lamellipodia are mainly made of actin, whereas the axon shaft contains microtubules [74 76]. Through polymerisation of actin and microtubules, the growth cone sends protrusions to search the adjacent area for cues.

The external growth cues have respective partner proteins, which are receptors in the growth cone membrane. They transduce information to the growth cone concerning path decisions [77]. One prominent example is the *slit/robo* signaling pathway that guides midline crossings in the central nervous system (CNS) of axonal neurites [78 79]. *Slit* is an aversive cue that repels growth cones expressing the *robo* receptor. Here, the internal signaling occurs through the activation of guanine exchange factors, where guanine triphosphatase activates proteins and *rho guanine triphosphatase* regulators [6 80 81]. *Semaphorins* are another class of important proteins in this process [70 82], acting as either repellents or attractants depending on the binding partner [83].

1.2.2 Dendritic growth rules

Dendrites follow growth rules during morphogenesis, such as self-avoidance [84] or tiling [85] (see Fig 1.2c-g). At the same time, they grow efficiently without wasting resources on unnecessary branches [86]. Neurons must be able to detect the location of their own branches to avoid growing to the same area twice, which is regulated through self-avoidance (see Fig 1.2c). It is a contact-dependent mechanism, where dendrites from the same neuron express the same cell surface molecule and therefore repulse each other in a homophilic interaction [84]. Two main groups of proteins have been identified to be responsible for this process, the *Dscams* in *Drosophila* [87] and *protocadherins* [88] in mice. Both are cell surface molecules that have a variable extracellular but a shared intracellular domain. This can give rise to different splice variants, allowing the

sister branches from the same neuron to repel each other. *Dscam1* has been shown to have more than 38000 potential splice isoforms [89]. These are randomly determined within each cell, strongly reducing the probability of two neurons in close vicinity of each other having identical isoforms.

While *Dscam1* and *protocadherin* mediate the avoidance between dendritic branches of the same cell, neurons must also tile the neuropil to maintain the functional topographic map in downstream brain regions. Therefore, they recognize neuronal types with which overlapping should be avoided [90]. Tiling can occur within the same neuronal type (homotypic tiling, see Fig 1.2d) or with different neuronal types (heterotypic tiling, see Fig 1.2e) [58], and is driven by contact-dependent repulsion. Sometimes, however, dendrites still overlap if repulsion is not strong enough [91]. Tiling is observed to different degrees in many parts of the nervous system, while starburst amacrine cells in the retina overlap considerably [92], other retinal ganglion cells tile the visual space tightly [93].

With self-avoidance and tiling, the molecular mechanisms responsible for avoiding dendritic overlap have been studied quite well. However, dendrites still need to cover their receptive field (see Fig 1.2f). Especially in the visual system, the concept of the receptive field is well described as the area of visual space a neuron responds to [94-97].

Neurons that have branches throughout the whole span of their dendritic tree are called space-filling neurons [98, 99]. This type of neuron uses intrinsic and extrinsic cues, such as *Slit* and *Robo*, to grow into the right shape [100]. This mechanism is also often observed in tiling neurons [85].

Furthermore, it is not uncommon that the organisms continue to grow after neurons have reached their receptive field size. In this case, neurons need to increase their size in accordance with the growth of the organism (see Fig 1.2g) [58]. It means that they must grow without changing the relative distances between branches. This mechanism has been observed in the *Drosophila* larva, where the sensory neurons in the body wall need to increase in size to cover the same area from the first to the third instar larva [101].

1.3 Neuronal cell types

The comparison of neurons across individuals and species requires a systematic way of identifying cell types from the neuronal diversity [4, 102, 103]. To unambiguously identify neurons, it is necessary to establish clear metrics by which one can judge similarities or differences between them. In this section, I will discuss how neuronal cell types are defined through TFs, differential expression of other proteins, morphology and function.

1.3.1 Combinatorial transcription factor codes

TFs are a class of proteins often used for the classification of cells. They interact with the DNA and can turn transcription on or off. [104]. Their expression determines the cell lineage in progenitor cells [69] and leads to the functional and morphological characteristics of the fully differentiated neuron [105]. This function makes them an ideal family of proteins for classifying cell types. However, the number of cell types easily surpasses the number of TFs in the genome. Therefore, to regulate gene expression for every neuronal type, they have to work in a combinatorial manner [106, 107]. This allows to reuse TFs in different brain areas as the outcome is modulated based on other TFs being co-expressed.

The regulation of gene expression through multiple TFs has been termed 'gene regulatory network'. A simple explanation for the function of gene regulatory networks is the coordinated transcription through a network of positive and negative interactions of TFs. Gene regulatory networks are modular and necessary to determine a fully differentiated cell's morphology and function [108, 109]. Since TFs can have different roles during several developmental stages and act in gene regulatory networks [69], their individual function is hard to disentangle.

Still TFs can be broadly grouped into functional categories based on the molecular mechanisms they influence. Temporal TFs (Intro [1.1.1]) only appear transiently during development but are necessary to decide the cell fate [15]. Another group of TFs have been termed terminal selectors [105]. They control all genes necessary for the function and morphology of the specific cell type. This includes the expression of different groups of genes such as ion channels or cell surface molecules (CSMs). Specifically in neurons, morphological TFs play a large role, since they need to determine the elaborate structure of dendrites and axons. Morphological TFs influence projection pattern, dendritic elaboration and size among others [110].

To investigate the function of single TFs, it is important to find their DNA binding motifs. This binding motif consist of a sequence of nucleotides in the DNA. The position-weight matrix calculates the most probable binding motif for each nucleotide position based on TF-DNA interactions [111]. Depending on the binding region, the TF can either increase or decrease the chance of transcription by recruiting transcription initiation proteins [104]. The enhancer or promoter fragments, which allow TF binding, contain sequences for a few different TFs [112].

TFs are one of the main ways used to define a cell type, especially in the field of transcriptomics and genetics [107]. Nevertheless, the relevance of the TF expression for the cell type they are defining, influencing morphology or function, still needs to be investigated in more detail.

1.3.2 Protein expression

While TFs determine a specific cell type at a genetic level [105], other types of proteins are necessary to build certain morphologies or achieve specific neuronal activities. Therefore, proteins other than TFs are used to classify neurons. A class of proteins to identify cell types are ion channels present in the membrane, which define the neuronal activity of a neuron. They are permeable to different ions, such as sodium, potassium or chloride, and can have different properties for opening or closing depending on the membrane potential [113]. Additionally, they can be dependent on different neurotransmitter, such as acetyl-choline or glutamate [114].

G-protein coupled receptors (GPCRs) are also functionally relevant. They are not ion channels themselves, but through modifications, such as phosphorylation, they modulate the neuronal activity of a neuron, to be more easily excitable or have a higher threshold for action potentials [115]. GPCRs rely on a downstream signaling cascade, which can be different for each cell type and change the overall effect on the neuron.

Proteins can also specify neuronal morphologies, such as receptors guiding axons to a specific target locations in the brain [45]. Additionally, they are required to contain dendrites and axons within a specific layer or column of neuropils [5, 46].

1.3.3 Morphology

In the late 19th and early 20th century, Ramon y Cajal [3] used Golgi stainings to label single cells in brains and produced beautiful drawings of the morphologies he saw under the microscope. Through his painstaking work, he first showed the diverse, neuronal morphologies in brains of different animals.

Neurons can be grouped based on certain morphological characteristics, such as axonal projection patterns or dendritic stratification [102]. The differentiation between morphological types of neurons using the projection pattern are found in the olfactory system, where olfactory receptor neurons project to different glomeruli dependent on their olfactory receptor expression [116]. The layer of arborisation of the axon and dendrite can also be used to identify certain types of neurons. In the mammalian retina, neurons responding to light increments have their dendritic arbors in a different layer compared to neurons responding to light decrements. This separation of neuronal responses into different neuropil layers allows for the classification of neurons belonging to different circuits based on the layer of arborisation [117].

To classify neurons based on their morphology, it is important to define a set of morphometrics [118, 119]. These allow not only the precise description of the adult neurons but also help to characterize the growth process. With the help of new software

it becomes possible to extract many morphological features such as branch points, branch angles and others [120]. These allow for a more precise and quantitative morphological characterization of neurons.

Additionally, morphological characteristics for assigning cell types can also help to infer the function of neurons. Combined analysis of morphology and function revealed a correlation between the types of neurons classified based on morphology and function separately [121]. Altogether, neuronal morphology is used to classify neurons into types and subtypes helping to describe their development and function.

1.3.4 Function

There are certain requirements for neuronal responses, such as rhythmic activity or a fast response. Especially for escape behaviours, there are small groups of neurons with big axons, which have a high conductivity. They can transmit neuronal signals quickly and are able to elicit a fast and strong behavioural response [122, 123]. These neurons need to respond fast and strongly to activate the muscles as quickly as possible. Other neurons can have a variety of different activity patterns. These can range from bursting, where a neurons spikes repeatedly in short duration of time, or periodically [124]. They can have graded potentials without any spikes or action potentials, where both states, hyperpolarized and depolarized, can lead to a different signal transmission [125]. Grouping neurons based on these characteristics can help to compare neurons across different circuits and connect protein expression and morphology to function [4, 126].

1.3.5 Classifying neurons

With all characteristics of neurons listed, it should in theory be easy to classify neurons into types and subtypes based on the individual similarities in function, morphology, as well as TF and protein expression. However, neurons are more variable in gene expression [127] and morphology [128, 129]. Therefore, it is useful to combine different methods to get a more robust classification into neuronal types [4, 121]. Altogether, the combined analysis of different neuronal characteristics will allow for a better understanding of neuronal identity in the adult and developing brain [102].

1.4 Advancements in the field of *Drosophila* neuroscience and development

Research in neuroscience and development has hugely benefited from *Drosophila* as a model organism and the tools available in *Drosophila* research [130-132]. One major contribution is the genetic access to the genome, which made it possible to use binary expression systems such as the Gal4-UAS-System [131]. The native yeast protein and DNA

binding site are used to express a given effector under a specific enhancer fragment from the *Drosophila* genome [133]. This leads to the effector being expressed in cells where the enhancer fragment is activated, thereby confining the expression of the effector to a single cell type [134–138]. Tools such as RNA interference (RNAi) have been used to knockdown certain genes in cells of interest [139–141].

Many proteins have been engineered to visualize neuronal activity and morphology. In combination with cell type specific driver lines, these tools, such as calcium indicators [142–144] and fluorescent proteins [145–147], can be targeted precisely and allow for a rigorous investigation of neurons in *Drosophila*.

Beside their value for visualization, the ability to label specific cell types for extraction has allowed the development of RNA-seq techniques for, e.g., transcriptional profiling. These methods capture and sequence the messenger RNA (mRNA) of cells, which reveals all genes that were in the process of being translated to proteins. This provides a better understanding of their function and development from a transcriptional point of view [148, 149].

More recently, single cell RNA sequencing (scRNA-seq) methods using droplet-based techniques in a microfluidics device have allowed the transcriptomic profiling of hundreds to thousands of cells [150]. These techniques create water droplets in an oil suspension as a miniature reaction chamber. Each droplet contains all the necessary enzymes for the biochemical reaction (lysis and reverse transcription) combined with barcodes to identify single molecules of mRNA. This way scRNA-seq can detect transcriptomes of single cells relatively efficiently and at a low cost compared to previous techniques. The advancement in microfluidic techniques has been also applied to techniques such as the assay for transposase-accessible chromatin (ATAC-seq) to probe the accessibility of the genome [151–153] or chromatin immunoprecipitation (ChIP-seq) for investigating chromatin bound DNA [154–156]. Together, single-cell RNA, ChIP and ATAC-seq allow for an in-depth characterisation of the *Drosophila* transcriptome and epigenome and the data have been integrated in an international effort to get a comprehensive picture [157, 158].

Another ongoing global effort in the *Drosophila* research community is in the field of connectomics [159–161]. Its goal is to reconstruct the morphology of all neurons within the brain, identifying synaptic partners on a nanometer scale. The laborious process of generating data uses either scanning or transmission electron microscopy (EM). These methods label brain tissue using heavy metals to visualize cell membranes. The shorter wavelength of electrons give images a higher resolution compared to conventional light microscopy (LM). One prominent method for generating large three dimensional volumes is serial block-face scanning EM [162]. By acquiring the three dimensional structure of a sample with a resolution in the nanometer scale, it is possible to reconstruct

neuronal morphologies down to individual synapses and even synaptic vesicles. Through manual annotation and automated reconstruction, a large part of the brain has been reconstructed [161]. This ongoing effort has generated complete connectivity maps between neurons, and therefore allows to find the components of neural circuits [163–166].

Drosophila is also used extensively in behavioural research. Besides mainly sensory-based behaviours, such as the optomotor response [167, 168], *Drosophila* display an intricate mating ritual [169]. Among others, recent advancements in machine learning techniques have helped to automate the analysis of behavioural data [170, 171]. This allows for a more quantitative approach of behavioural analysis and can be combined with genetic screens for developmental defects [172].

In conclusion, genetic access combined with engineered proteins through cell typification and morphological reconstruction, together with machine learning supported analysis are advancing *Drosophila* research quickly. Integrating results from several methods, such as **scRNA-seq** and microscopy, can help to understand how the information contained in the DNA is translated into neuronal morphologies.

1.5 *Drosophila* vision as a model system for neurodevelopment

Drosophila has already been used quite extensively in the field of neurodevelopment. Investigations of developmental mechanisms in its visual system, for example, are linked to important discoveries, such as lateral inhibition (Fig. 1.1c-d) during the specification of photoreceptors in the ommatidium [40, 176, 177]. The optic lobe has also been leveraged to study layering and cellular migration [46, 69]. Altogether, *Drosophila* has proven itself a good model organism to discover universal molecular mechanisms in neurodevelopment [178, 179].

1.5.1 *Drosophila* visual system

Drosophila relies on its visual system for many things, including navigation, course control, and mating. The *Drosophila* visual system consists of a compound eye made up of 750 ommatidia arranged in a regular, hexagonal, pattern across the whole retina [180]. Each ommatidium contains eight photoreceptors (R1-8) of which R1-6 are responsible for spatial vision and R7/R8 are mainly used to perceive color [36, 181, 182]. They express different sets of rhodopsins to detect light in different spectral sections [183]. The spatial resolution of each ommatidium corresponds to around 5° of visual space [168]. Downstream of the photoreceptors lies the optic lobe, which consists of four neuropils, the lamina, medulla, lobula and lobula plate [3, 184] (Fig. 1.3a-b). There are two optic lobes in each fly, one on each side of the central brain, together containing 60% of all neurons in the *Drosophila* brain [185].

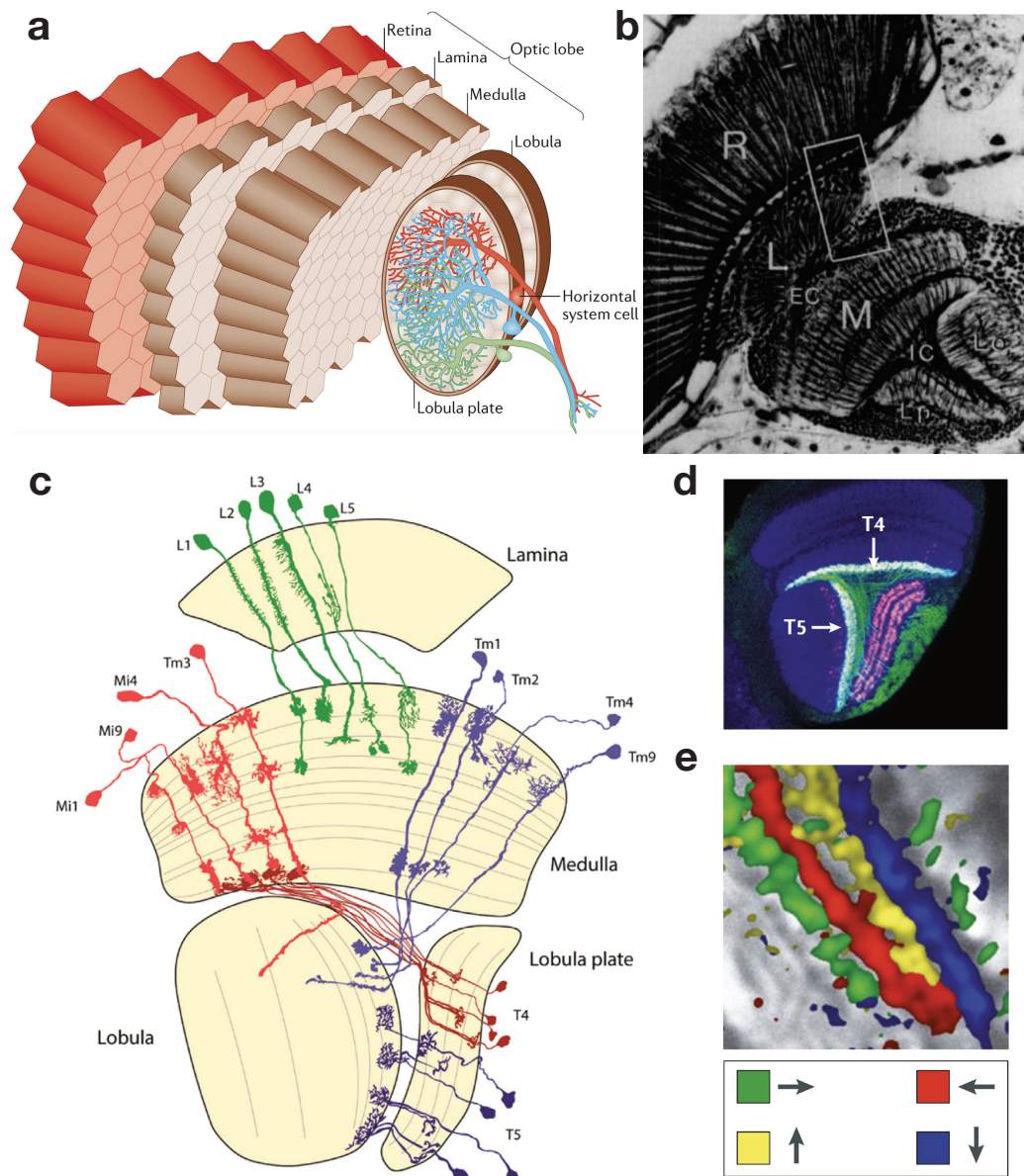


Figure 1.3: *Drosophila* optic lobe and neurons of the motion vision circuit. **a** Organisation of the optic lobe neuropils together with the retina [173]. **b** Horizontal section of the optic lobe with the optic chiasmata between the neuropils. R: retina, EC: external chiasm, L: lobula, M: medulla, IC: internal chiasm, Lo: lobula, Lp: lobula plate [174]. **c** Scheme of the optic lobe with the main neurons in the motion vision circuit [175]. **d** Confocal image of the T4 and T5 neurons located in the optic lobe showing dendrites in white, cell bodies and neurites in green, axons in red [173]. **e** Neuronal responses to the four cardinal directions (green: front-to-back, red: back-to-front, yellow: upwards, blue: downwards) of T4 and T5 subtypes measured in the lobula plate [173].

Retinotopy is preserved in all neuropils of the optic lobe [36, 186]. R1-6 send their axonal projections to the lamina and, through neural superposition, combine the same points of visual space within one lamina cartridge [186, 187]. L1-5 are five neuron types in the lamina, among others, that project to the medulla. [186] (Fig. 1.3c). L1 and L2 neurons have been shown to respond identically to visual stimuli, while they are glutamatergic and cholinergic, respectively. Therefore, the downstream neurons receive a sign-inverted signal from L1 and L2, creating parallel pathways responsive to brightness increments (ON) or brightness decrements (OFF) [188, 189]. In comparison, L3-5 have not been linked to a specific function. Some results suggest a role for L3 and L4 in motion processing [190, 191] while L5 has not been studied in detail.

Retinotopy reverses in the antero-posterior axis between the lamina and the medulla in the external chiasm of the optic lobe (Fig. 1.3b) [174, 186]. Here, the L neurons of the lamina transmit information to the opposite anatomical position in the medulla. While the lamina does not show a separation in layers, the medulla is composed of layers and columns. Columns follow the same structure as the lamina cartridges, and are arranged in a hexagonal pattern [186]. They are however elongated in the dorso-ventral axis, giving them an irregular shape in the neuropil (Fig. 1.4d) [166, 192]. Furthermore, the medulla is separated into ten layers (M1-10). These are defined through a set of molecular markers, and are most likely a product of neuronal arborisation patterns. The medulla contains far more neurons than the lamina [186]. Additionally, it is cone shaped and therefore has smaller columns in M10 compared to M1 (Fig. 1.4d) [48, 56, 166]. From the medulla, neurons project to the lobula, lobula plate or both.

The lobula complex, consisting of lobula and lobula plate, contain the neurons that project into the central brain [186]. Both are also separated into columns and layers [46], with the lobula being split into six (Lo1-6) and the lobula plate into four layers (Lp1-4) [186]. The information processed in these structures is already of a higher complexity and does not only contain information about brightness [169, 193, 194]. Two important computations performed by the lobula complex are object detection [193] and optic flow estimation [195]. Lobula columnar neuron, LC11, has been identified as an object detector, which project from the lobula to the central brain [196]. The neurons detecting flow fields are located in the lobula plate, and are called lobula plate tangential cells [197-199]. Altogether, the optic lobes provide preprocessed input to the brain and play a role in behaviours such as course control, object fixation, landing and escape response as well as courtship behaviour [123, 169, 173, 200, 201].

1.5.2 Computation of motion

One of the most important brain functions of every sighted animal is the computation of motion. Studies in the mid 50s proposed a number of prominent ideas that have since been refined. The Hassenstein-Reichart [53] and the Barlow-Levick [54] detectors were among the first models suggested, and they are still relevant today. The model implements three main requirements: first, the motion detector needs to receive input from at least two different but neighbouring points in visual space. Second, the inputs need to be filtered differently in time. Last, the signals need to interact non-linearly to amplify the signal in the preferred direction compared to the null direction [202, 203]. The motion detector acts as a coincidence detector, performing either a multiplication in the case of the Hassenstein-Reichart or a division in the case of the Barlow-Levick detector. For both detector models, this leads to a larger output when the visual pattern is moving along the detector's preferred direction than its null direction [204]. More recently, it was shown that T4 and T5 cells use both mechanisms, i.e. amplification and suppression, leading to an increased direction selectivity [205]. This leads us to the question of how these models are implemented at the cellular level.

1.5.3 Motion vision circuit

With motion vision being important for flight in *Drosophila*, it has been studied intensively [173]. Its function is essential as it plays a role in many different computations such as optic flow or object detection. It is split into two parallel pathways: the ON and the OFF pathway [188]. They mainly receive visual input from the L1 or L2 neurons, respectively. The first neurons that selectively respond to one direction of motion are called T4 and T5 for the ON and OFF pathway, respectively [206]. They are local motion detectors and the key neurons in the circuit. They are divided into four subtypes (*a-d*; Fig 1.4a) based on function and anatomy, where each subtype responds to one of the cardinal directions (*a*: front-to-back, *b*: back-to-front, *c*: upwards, *d*: downwards) [163, 206, 207]. Anatomically, they have their cell bodies next to the lobula plate and are monopolar [186].

T4 neurons project a neurite into M10 of the medulla, and T5 into layer 1 of the lobula (Lo1) to form their dendrites (Fig 1.3d) [186]. Then, a neurite is sent to the lobula plate to arborise in one of its four layers dependent on the subtype. T4/T5 subtypes *a* are located in layer 1 of the lobula plate, with subtypes *b-d* in corresponding layers 2-4 [207]. None of the input cells to T4 and T5 are directionally selective. Therefore, T4 and T5 are the first neurons in the visual pathway to respond in a direction-selective way to motion [190, 191, 208-210]. EM reconstructions of T4 and T5 have provided the identity of all synaptic partners at the dendrite (Fig 1.4a-c) [163, 166]. For T4 neurons, the inputs

come from medulla cell types Mi1, Mi4, Mi9, Tm3, TmY15, CT1 and C3. T5 neurons are postsynaptic to lobula neurons Tm1, Tm2, Tm4, Tm9, Tm23, TmY15, CT1, and LT33 (Fig 1.4a) [166]. Additionally, there are synapses between T4 neurons within the same subtypes, and the same is true for T5 neurons [166].

Since the signal in the axon is already direction selective, the computation of motion happens in the dendrite of T4 and T5 neurons (Fig 1.3e) [206]. To fully understand the computation, the precise position of synapses from input neurons have been mapped along the T4 and T5 dendrites [163, 166]. Notably, they compartmentalize into the proximal, central and distal area of the dendrite (Fig 1.4b-c) [166, 211]. In order to combine the algorithmic models with the biological implementation, different input neurons have been theorized to have a specific function within the motion detector based on their response properties [210]. More recently, experiments investigating Mi9 neurons have shown their function in sharpening direction selectivity of T4 neurons through a release of inhibition combined with the excitatory response of Mi1 neurons [212]. These results demonstrate the possibility to assign clear roles for input neurons to T4 and T5 motivating further research in the area to fully understand the neuronal computation of motion detection on a biophysical level [163, 166, 205, 212-214].

1.5.4 Local motion detectors in *Drosophila*

T4 and T5 neurons are the central part of the motion vision circuit, since they are the first neurons that selectively respond to one direction of motion. Concerning their dendritic field size, T4 dendrites cover an area of around 25 μ m in the dorso-ventral and 20 μ m in the antero-posterior axis, based on EM reconstructions, with medulla columns being around 5 μ m wide [163]. As T4/T5 are local motion detectors, there is one of each subtype in every column in their respective neuropil, M10 and Lo1, reaching a total number of around 6000 T4/T5 neurons per optic lobe [215]. There is a strong correlation between function and morphology within T4 and T5 subtypes: the dendrite's preferred direction of motion along the retinotopy of the respective neuropil is opposite to the orientation of the dendrite (Fig 1.4a) [163]. Along this dendritic direction, the dendrites are compartmentalized (Fig 1.4c) [166, 211]. This compartmentalization (Introduction 1.5.3) is the same for all subtypes along their respective dendritic orientation (Fig 1.4b-c). This means that the inputs, which are mostly columnar and available at every position, will only form synapses with T4 and T5 dendrites in the correct compartment. Additionally, T4 and T5 neurons overlap with their neighbours from the same type ignoring the tiling principles of dendrites completely [163, 166, 207].

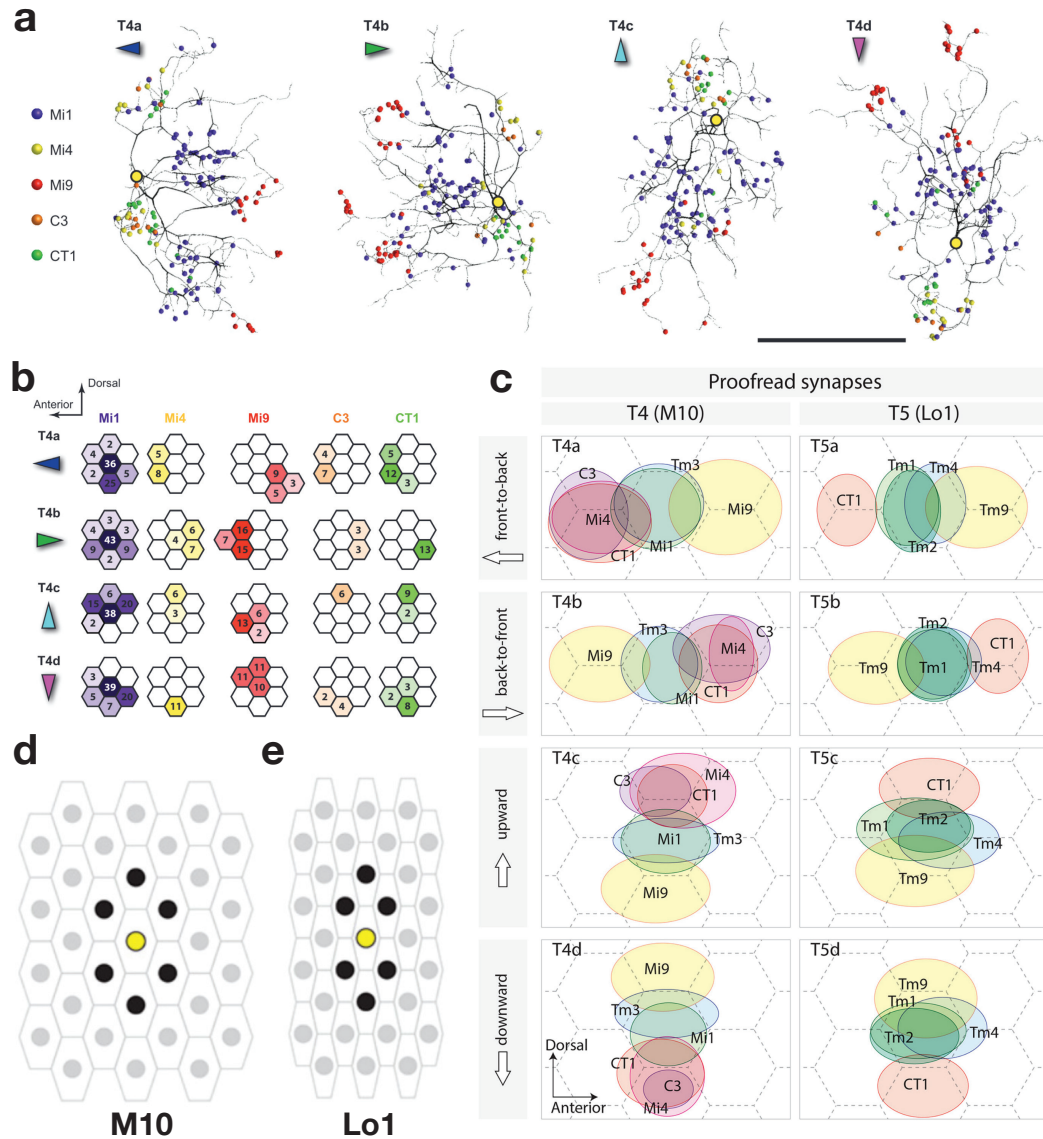


Figure 1.4: Synaptic connectivity and grid of T4 and T5 neurons. **a** Examples of reconstructed T4 dendrites for each subtype. Synapses of specific input neurons are labelled in different colours according to their position in the EM reconstructions. Entry points are labelled in yellow with a black outline. Arrows indicate their preferred direction of motion [163, 166]. **b** Number of synapses in each column innervated by T4 dendrites with the deeper shapes representing higher numbers of synapses [163]. **c** Distribution of synapses along the dendrite of T4 and T5 neurons by different presynaptic partners [166]. **d-e** Anisotropic column grid in the M10 and Lo1, respectively. Yellow point marks the central column of the dendritic field of T4 and T5. Black points show the neighbouring columns [166].

1.5.5 T4/T5 development

The cell lineages of T4 and T5 neurons originate in the inner proliferation center of the optic lobe [216, 217]. *a/b* and *c/d* subtypes are separated through the expression of *decapentaplegic* activated by *wingless*. These lineages first produce the C2/C3 and T2/T3 neurons [218]. Then the induction of *atonal* determines the progenitors of T4/T5 neurons [219]. They follow two *notch*-dependent divisions, neurons are first separated into *a* or *b* and *c* or *d* subtypes. In the last division, T4a and T5a are born from the same progenitor, with *b-d* subtypes showing the same pattern [52]. Therefore, from a cell lineage point of view, T4a and T5a are more closely related than T4a and T4b. The fully differentiated T4 and T5 then start to project their neurites first into M10 of the medulla or Lo1 in the lobula, respectively. This happens in waves, where each wave consists of neurites in one row along the dorso-ventral axis [52]. After arborising the dendrite in their respective location, T4 and T5 neurons project back into the corresponding lobula plate layer depending on their subtype and retinotopic position.

1.6 Motivation for the choice of model system

Neuronal development is a complicated process. *Drosophila* as a model system, and especially the motion vision circuit, lead to important discoveries concerning the functional specificity and morphological characteristics of adult T4 and T5 (see Introduction 1.5.3, 1.5.4). Additionally, their function in the adult shows a strong correlation with anatomy. Their morphology is highly relevant for establishing the specificity in synaptic wiring of T4 and T5 dendrites (Fig 1.4) [163, 166].

Studies in neuronal development so far have not investigated dendritic development in great detail. T4 and T5 neurons provide the opportunity to study dendritic growth in a system with only a few but important differences. These neurons are interesting from a developmental point of view for several reasons. Firstly, they are genetically accessible. Secondly, they have been extensively characterised in the adult. Thirdly, all subtypes receive synaptic input from the same types of neurons in a spatially distinct order dependent on their subtype. This order is the same across either T4 or T5 subtypes in the egocentric view but not in the allocentric view. Lastly, the main differences between subtypes of T4 and T5 neurons are their dendritic orientation and axon position in the lobula plate. Therefore, differences in their transcriptomic profile could potentially directly translate into effector genes responsible for their morphological differences.

In conclusion, T4 and T5 neurons in the motion vision circuit of *Drosophila* are a well established system in the adult. Accordingly, they were selected for this work to study dendrite development in general and how TFs specifically influence the direction of dendritic growth during development.

2

MANUSCRIPTS

2.1 Manuscript 1

Title: A combinatorial code of transcription factors specifies subtypes of visual motion-sensing neurons in *Drosophila*

Authors: Nikolai Hörmann^{1,3,*}, Tabea Schilling¹, Aicha Haji Ali¹, Etienne Serbe¹, Christian Mayer², Alexander Borst¹ and Jesús Pujol-Martí^{1,*}

1: Department of Circuits – Computation – Models, Max Planck Institute of Neurobiology, 82152 Martinsried, Germany.

2: Laboratory of Neurogenomics, Max Planck Institute of Neurobiology, 82152 Martinsried, Germany.

3: Graduate School of Systemic Neurosciences, Ludwig-Maximilians-Universität München, 82152 Martinsried, Germany

*: Authors for correspondence: hoermann@neuro.mpg.de; pujolmarti@neuro.mpg.de

Author contributions: Conceptualization: **N.H.**, T.S., A.B., J.P.-M.; Methodology: **N.H.**, T.S., C.M., J.P.-M.; Software: **N.H.**, C.M.; Investigation: **N.H.**, T.S., A.H.A., E.S., J.P.-M.; Writing (original draft): J.P.-M.; Writing (review and editing): **N.H.**, T.S., C.M., A.B., J.P.-M.; Visualization: **N.H.**, T.S., J.P.-M.; Supervision: A.B., J.P.-M.; Funding acquisition: A.B. (order according to author list)

Personal contributions in detail:

For this manuscript, I helped to design the study. I also established and performed the sample preparation and the method of single cell RNA sequencing in the lab. Further, I analysed the single cell RNA sequencing data in R using the Seurat package with the help of C.M.. Additionally, I performed experiments collecting fixed immunohistochemistry data of T4 neurons during different developmental stages and reconstructed single neurons using the Amira software. I wrote Python code to analyse the morphology and compare the similarity between dendrites for identification. Lastly, I wrote part of the manuscript and reviewed as well as edited it over several iterations.

RESEARCH ARTICLE

A combinatorial code of transcription factors specifies subtypes of visual motion-sensing neurons in *Drosophila*

Nikolai Hörmann^{1,*}, Tabea Schilling¹, Aicha Haji Ali¹, Etienne Serbe¹, Christian Mayer², Alexander Borst¹ and Jesús Pujol-Martí^{1,*}

ABSTRACT

Direction-selective T4/T5 neurons exist in four subtypes, each tuned to visual motion along one of the four cardinal directions. Along with their directional tuning, neurons of each T4/T5 subtype orient their dendrites and project their axons in a subtype-specific manner. Directional tuning, thus, appears strictly linked to morphology in T4/T5 neurons. How the four T4/T5 subtypes acquire their distinct morphologies during development remains largely unknown. Here, we investigated when and how the dendrites of the four T4/T5 subtypes acquire their specific orientations, and profiled the transcriptomes of all T4/T5 neurons during this process. This revealed a simple and stable combinatorial code of transcription factors defining the four T4/T5 subtypes during their development. Changing the combination of transcription factors of specific T4/T5 subtypes resulted in predictable and complete conversions of subtype-specific properties, i.e. dendrite orientation and matching axon projection pattern. Therefore, a combinatorial code of transcription factors coordinates the development of dendrite and axon morphologies to generate anatomical specializations that differentiate subtypes of T4/T5 motion-sensing neurons.

KEY WORDS: *Drosophila*, Dendrite development, Motion vision, Neuronal subtypes, Combinatorial code, Grain

INTRODUCTION

A central question in developmental neuroscience is how different neuronal cell types acquire the diverse morphologies and connectivities that support their distinct functions within complex neural circuits. The T4/T5 neuronal population of the *Drosophila* visual system provides a unique model for the study of this process. All T4/T5 neurons must acquire common morphological properties that set them apart from other visual interneurons and are important for their function as local motion sensors (Maisak et al., 2013; Shinomiya et al., 2015; Schilling et al., 2019). However, among the T4/T5 neurons, distinct subtypes with anatomical specializations relevant for the detection of motion along different directions must be specified (Fischbach and Dittrich, 1989; Maisak et al., 2013). Here, we examine the genetic programmes that control the

development of subtype-specific morphologies in postmitotic T4/T5 neurons.


In *Drosophila*, visual information from ~800 retinal ommatidia is processed in distinct neuropils (lamina, medulla, lobula and lobula plate), each consisting of retinotopically arranged columns. All neuropils except the lamina are further divided into synaptic layers (Fischbach and Dittrich, 1989; Bausenwein et al., 1992). The dendrites of T4 and T5 neurons are the first stage within the visual processing pathway in which directional motion information is extracted (Maisak et al., 2013; Behnia et al., 2014; Fisher et al., 2015; Serbe et al., 2016; Arenz et al., 2017). T4 dendrites arborise in layer 10 of the medulla and selectively respond to ON (bright edge) motion, whereas T5 dendrites arborise in layer 1 of the lobula and only respond to OFF (dark edge) motion (Maisak et al., 2013).

Each T4 and T5 dendrite extends across approximately eight neuropil columns to receive signals from various presynaptic partners that relay information from neighbouring points in the visual space (Haag et al., 2016; Shinomiya et al., 2019). Both T4 and T5 neurons exist in four subtypes of equal numbers (a, b, c and d) (Pinto-Teixeira et al., 2018), each with the dendrite oriented preferentially along one of four directions within the respective neuropil (Takemura et al., 2013). In accordance with their distinct dendrite morphologies, the four T4/T5 subtypes respond to either front-to-back, back-to-front, upward or downward motion (Maisak et al., 2013). Therefore, the directional tunings of the four T4/T5 subtypes appear to be strictly linked to their dendrite orientations (Fig. 1A). In addition, the four T4/T5 subtypes exhibit distinct axon projection patterns. Axons from T4/T5 neurons of the same subtype exclusively innervate one of the four lobula plate layers (Fig. 1A) (Fischbach and Dittrich, 1989; Shinomiya et al., 2019). The segregation of T4/T5 axons into four layers, each encoding motion in a different cardinal direction, provides the anatomical basis for subsequent processing steps performed by downstream neurons that are relevant for motion-driven behaviours, e.g. the integration of opposing motions in the visual field (Mauss et al., 2015; Klapoetke et al., 2017).

Recent studies have uncovered the developmental genetic programmes that take place in T4/T5 neuron progenitors to specify T4/T5 neurons into the four subtypes (Apitz and Salecker, 2018; Pinto-Teixeira et al., 2018). During the differentiation of postmitotic T4/T5 neurons, these programmes must be translated into the expression of effector genes ensuring that four subgroups of T4/T5 neurons develop dendrites oriented along four different directions in common extracellular environments. In addition, the development of a specific dendrite orientation must be strictly coupled to the placement of the axon terminal in a specific lobula plate layer in order to relay specific qualities of directional motion to correct downstream neurons (Fig. 1A). Until now, only one gene [*optomotor-blind* (*omb*); also known as *bifid*] has been proposed to act in differentiating T4/T5c and T4/T5d to distinguish their axons from those of T4/T5a and T4/T5b neurons (Apitz and Salecker,

¹Department of Circuits – Computation – Models, Max Planck Institute of Neurobiology, 82152 Martinsried, Germany. ²Laboratory of Neurogenetics, Max Planck Institute of Neurobiology, 82152 Martinsried, Germany.

*Authors for correspondence (hoermann@neuro.mpg.de; pujolmarti@neuro.mpg.de)

 N.H., 0000-0002-5952-6889; J.P.-M., 0000-0001-9500-7106

This is an Open Access article distributed under the terms of the Creative Commons Attribution License (<https://creativecommons.org/licenses/by/4.0>), which permits unrestricted use, distribution and reproduction in any medium provided that the original work is properly attributed.

Handling Editor: François Guillemot

Received 11 November 2019; Accepted 20 March 2020

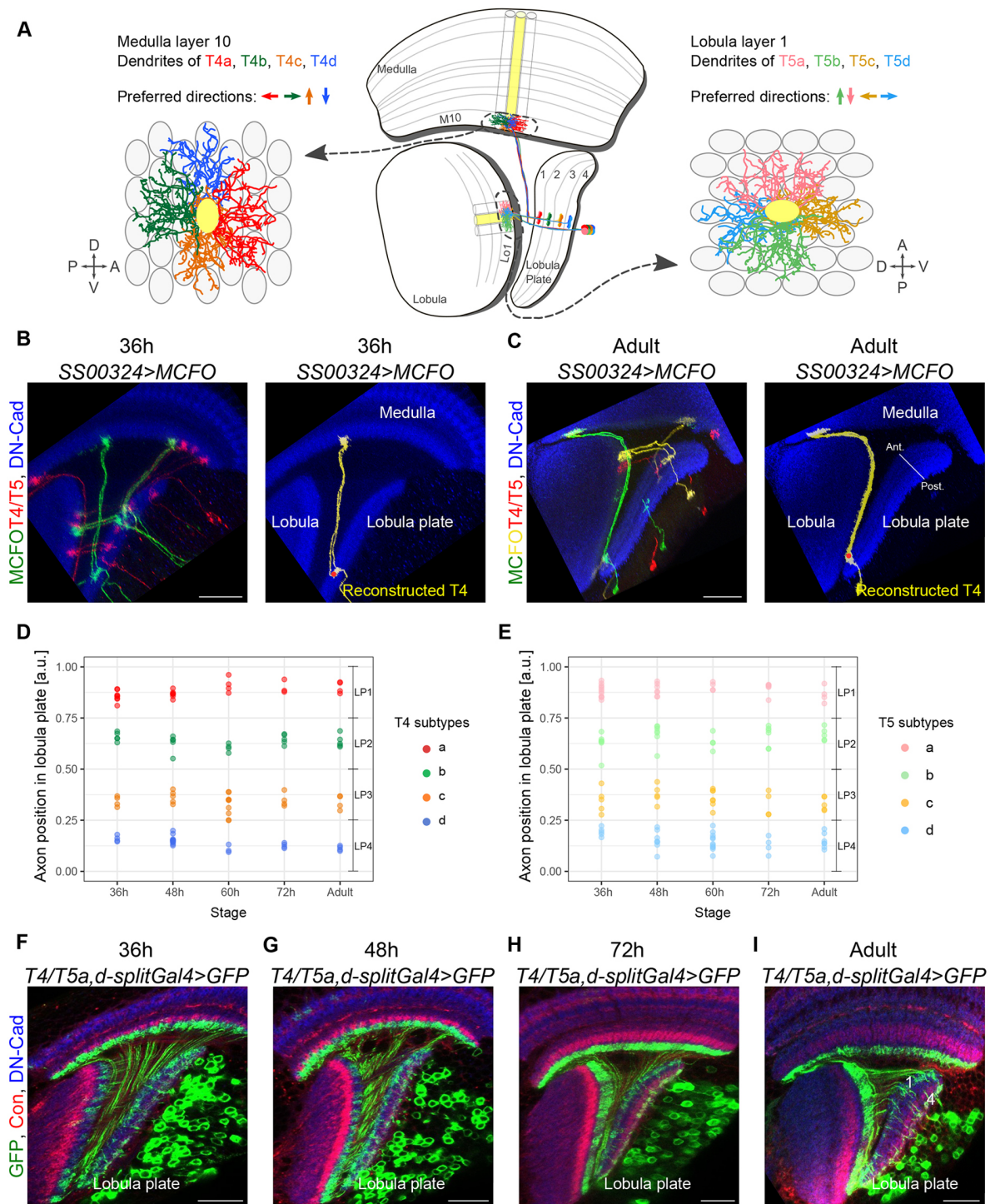


Fig. 1. Developing T4 and T5 subtypes can be identified by the positions of their axons in the lobula plate. (A) Schematic of adult optic lobe (horizontal view, central panel) highlighting the morphologies of the four T4/T5 subtypes (a, b, c and d). Each of the four lobula plate layers (1-4) receives axons from only one T4/T5 subtype. Left and right panels show frontal views of medulla layer 10 and lobula layer 1. Four T4 and T5 dendrites (each of one subtype) enter a single medulla and lobula column (in yellow) to extend along four distinct directions. Arrows indicate the dendrites' preferred directions of motion. A, P, D and V: anterior, posterior, dorsal and ventral (visual field coordinates). (B,C) Optic lobes at 36 h APF and at the adult stage showing individual T4 and T5 neurons labelled with different fluorescent proteins using the MCFO approach. A digitally reconstructed T4 neuron is shown for each of the stages. The red dot marks the axon's first branching point, which was used to calculate the relative position in the lobula plate occupied by the axon. Anti-DN-Cadherin (DN-Cad) labels the neuropils. (D,E) Relative positions in the lobula plate occupied by axons of single T4 ($n=104$) and T5 ($n=122$) neurons at different developmental stages (36-72 h APF), and at the adult stage. LP1-4 refers to the regions that correspond to the lobula plate layers 1-4 at the adult stage. Each T4 and T5 neuron was classified into one of the four subtypes based on the position of the lobula plate occupied by its axon. a.u., arbitrary units. (F-I) At the adult stage, the *T4/T5a,d-splitGal4* driver line labels T4/T5a,d neurons with axons innervating lobula plate layers 1 and 4 (I). From 36 to 72 h APF (F-H), this line labels T4/T5 neurons with axons in lobula plate regions that correspond to the lobula plate layers 1 and 4 at the adult stage. Anti-Connectin (Con) labels layers 3 and 4 of the lobula plate. Scale bars: 20 μ m.

2018). Therefore, the following questions have remained elusive so far: (1) how do axons of T4/T5a and T4/T5b or axons of T4/T5c and T4/T5d become distinct from each other?; (2) how do the four T4/T5 subtypes acquire their four different dendrite orientations?; and (3) how is dendrite orientation matched to axon projection layer within each subtype?

Here, we first analysed the dendrite growth patterns of the four T4/T5 subtypes. The dendrites of all T4/T5 subtypes grow simultaneously during a ~36 h-window of pupal development to acquire the oriented arbours that define their adult morphology. To investigate the underlying molecular mechanisms, we used single cell RNA sequencing (scRNA-seq) to profile the transcriptomes of T4/T5 subtypes at five stages that cover the period of dendrite growth. Our analysis revealed that each T4/T5 subtype is defined by a unique combination of cell-membrane proteins, as well as by a unique combination of two to three transcription factors that is stable for most of the dendrite growth period. To test whether such transcription factor combinations control the development of subtype-specific dendrite orientations, we manipulated them in specific T4/T5 subtypes. Overexpressing the transcription factor Grain (normally expressed only in T4/T5b and T4/T5c neurons) in all developing T4/T5 subtypes resulted in neurons with dendrite orientations specific to either T4/T5b or T4/T5c subtypes. Therefore, Grain is sufficient to invert the orientation of developing dendrites in T4/T5a and T4/T5d subtypes to generate dendrites typical of T4/T5b and T4/T5c subtypes, respectively. In addition, *grain*-overexpressing neurons with T4/T5b and T4/T5c dendrite orientations also project their axons to layers of the lobula plate normally innervated by T4/T5b and T4/T5c subtypes, respectively. Conversely, *grain* loss of function in all developing T4/T5 neurons resulted in neurons with morphologies characteristic of either T4/T5a or T4/T5d subtypes. We conclude that Grain, in combination with subtype-specific sets of transcription factors, coordinates dendrite and axon development in T4/T5b and T4/T5c to differentiate their morphologies from those of T4/T5a and T4/T5d.

RESULTS

Directed dendrite growth of the four T4 and T5 neuron subtypes occurs simultaneously

We first sought to investigate when and how each T4/T5 subtype acquires its defining dendrite orientation. We stochastically labelled individual T4 and T5 neurons with different combinations of fluorescent proteins using the MultiColor FlpOut (MCFO) approach (Nern et al., 2015) together with the *SS00324-splitGal4* line that drives expression specifically in all T4/T5 neurons (Schilling and Borst, 2015). This allowed us to digitally reconstruct a total of 226 T4 and T5 neurons at four stages of pupal development [36, 48, 60 and 72 h after puparium formation (APF)] and in adult flies (Fig. 1B,C). After measuring the positions within the lobula plate in which the axon terminals of adult T4 and T5 neurons enter, we found four clusters of T4 and four clusters of T5 neurons (Fig. 1D,E). These clusters represent the four T4 and T5 subtypes (a, b, c and d), with axons innervating the four lobula plate layers and with four distinct dendrite orientations (Fig. 1A) (Fischbach and Dittrich, 1989; Takemura et al., 2013). Similarly, four axon-position-based clusters of T4 and T5 neurons were found in every examined developmental stage (Fig. 1D,E). Once established, the positions occupied by T4 and T5 axon terminals in the lobula plate did not appear to change, as a driver line labelling T4/T5 neurons with axons in layers 1 and 4 of the lobula plate at the adult stage also labelled T4/T5 neurons innervating the corresponding regions of the lobula plate at earlier stages of development (Fig. 1F-I). Therefore, the T4 and the T5 subtypes can

be reliably identified from 36 h APF onwards by the position of their axons in the lobula plate.

Next, we measured the dendrite volume of every reconstructed T4/T5 neuron and examined changes during development in the different T4/T5 subtypes. The four T4/T5 subtypes grew their dendrites at similar rates between 36 and 72 h APF. Afterwards, between 72 h APF and the adult stage, all T4/T5 dendrites underwent a reduction in volume (Fig. 2A,B). Two different mechanisms to develop oriented dendrites are compatible with these observations: (1) T4/T5 dendrites might undergo a symmetrical overgrowth of branches towards all directions (36-72 h APF) followed by a period in which branches with wrong orientations are eliminated (72 h APF-adult stage); or, alternatively, (2) the dendritic branches of each T4/T5 neuron might grow in specific directions during the period of dendrite growth (36-72 h APF). To distinguish between these possibilities, we examined the dendrite orientation of developing T4 neurons by quantifying the 2D distribution of branches around the dendrite's first branching point. Adult T4 dendrites, either imaged by confocal microscopy or reconstructed from electron microscopy data (Takemura et al., 2017), showed subtype-specific dendrite orientations that fitted with those originally reported (Takemura et al., 2013) (Fig. S1). The quantification of T4 dendrite orientations at 36 and 72 h APF revealed that subtype-specific orientations arose between those two developmental stages (Fig. 2C-J). Collectively, these results indicate that the four T4/T5 subtypes acquire their characteristic dendrite orientations through simultaneous processes of directed growth that span a ~36 h window of development, and that subsequent dendrite pruning does not play a major role in shaping dendrite orientation.

Each of the four T4 and T5 subtypes has a unique transcriptional profile during dendrite growth

The dendrites of the four T4 subtypes grow simultaneously within layer 10 of the medulla, and thus they share a common extracellular environment. The same holds true for the dendrites of the four T5 subtypes in layer 1 of the lobula. We hypothesised that, in order to develop different dendrite orientations, the four T4/T5 subtypes must rely on intrinsic molecular asymmetries such that their dendrites respond differentially to extrinsic cues available to all of them. Recent studies have profiled the transcriptomes of T4/T5 neurons at the adult stage. These studies either were not suitable for the analysis of T4/T5 subtype-specific transcriptomes (Pankova and Borst, 2016; Davie et al., 2018; Konstantinides et al., 2018) or explored gene expression differences only between two subtype-pairs at the adult stage (Davis et al., 2020), likely missing genes underlying the development of the morphologies defining the four T4/T5 subtypes.

To overcome these limitations, we profiled the transcriptomes of single T4/T5 neurons collected at four equally spaced developmental stages during dendrite growth (36, 48, 60 and 72 h APF), as well as a preceding stage (24 h APF). For each stage, we dissected brains containing all T4/T5 neurons labelled by membrane-targeted GFP expressed by the line *SS00324-splitGal4*. Single cell suspensions were prepared and GFP⁺ T4 and T5 cells were sorted by fluorescence-activated cell sorting (FACS). Next, we performed scRNA-seq based on droplet microfluidics (10x Chromium) (Fig. 3A). Cells were sequenced to a mean depth of 26,153 reads per cell, and a median of 1627 genes were detected per cell. After filtering to remove low-quality cells, we obtained the transcriptomes of ~44 K high-quality cells, with the number of cells per stage ranging between 5051 (60 h APF) and 11,716 (72 h APF). Two biological replicates were obtained for each developmental stage and batch-corrected using canonical correlation analysis in Seurat v3 (Stuart et al., 2019). Next, we implemented

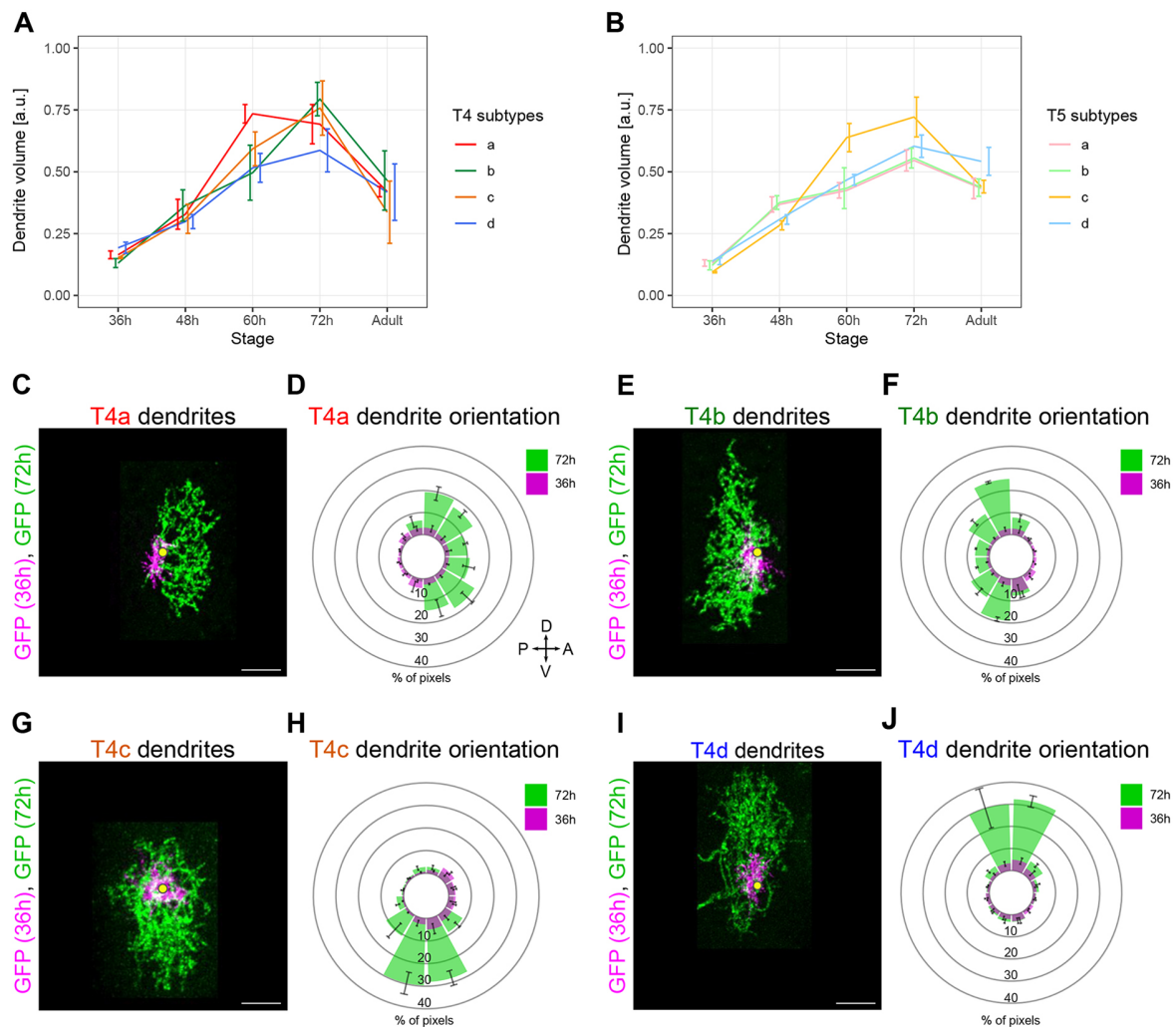


Fig. 2. Directed dendrite growth of the four T4 and T5 subtypes occurs simultaneously. (A,B) Volumes from T4 ($n=104$) and T5 ($n=122$) dendrites of the four subtypes at different developmental stages, and at the adult stage. Data are mean \pm s.e.m. a.u., arbitrary units. (C,E,G,I) Overlay of two different T4a, T4b, T4c or T4d dendrites imaged at 36 and 72 h APF ($n=4$ per subtype and stage). Scale bars: 5 μ m. (D,F,H,J) Average dendrite orientation of the four T4 subtypes at 36 and 72 h APF ($n=4$ per subtype and stage). Polar histograms show the 2D distribution of fluorescent pixels around the dendrite's first branching point. The number of pixels at 36 h APF was normalised to the number of pixels at 72 h APF to visualise dendrite size changes. Data are mean \pm s.e.m.

dimensionality reduction and unsupervised clustering methods based on principal component analysis (PCA) and the Louvain algorithm (Seurat v3). For each developmental stage, we manually assigned clusters either to T4 or T5 types based on known marker genes such as *TfAP-2* (Davis et al., 2020). We found that four clusters can be grouped reliably into each type (Fig. 3B; Fig. S2).

Based on the previously reported subtype-specific marker genes *omb* and *dachshund* (*dac*) (Apitz and Salecker, 2018), we assigned clusters to one of the following subtype-pairs: T4a,b; T5a,b; T4c,d; or T5c,d (Fig. 3B; Fig. S2). To identify novel marker genes discriminating the clusters within each pair, we performed a differential gene-expression analysis (Fig. 3C; Fig. S2). The results revealed that one cluster from each pair consistently showed differential co-expression of *beat-IV*, *CG34353* and *grain*. We examined the expression patterns of these genes *in vivo* with transgenic lines and antibody staining and found that they constituted specific markers of T4/T5b and T4/T5c neurons (Fig. 3E-I). Taken together, the use of three known and three newly characterised T4/T5 neuron subtype-specific marker genes was sufficient to assign all eight single cell clusters to four T4 and

four T5 subtypes in every examined developmental stage (Fig. 3B; Fig. S2). Consistently, the integration of scRNA-seq datasets across all developmental stages, using the integration tool from Seurat v3, grouped all cell types in agreement with our manual cluster assignment at each stage (Fig. 3D).

Analysis of gene expression patterns reveals combinatorial codes potentially controlling the development of the four T4/T5 dendrite orientations

Transcription factors act as intrinsic determinants of dendrite shape, in part by controlling the expression of cell-membrane proteins relevant for sensing extrinsic cues (Puram and Bonni, 2013; Dong et al., 2015; Lefebvre et al., 2015; Prigge and Kay, 2018). The discovery of transcriptionally different groups of T4/T5 neurons that match morphologically distinct T4/T5 subtypes during dendrite growth allowed us to search for candidate genes that control subtype-specific dendrite orientations. To identify differentially expressed genes, we ran differential expression tests separately for each developmental dataset. We required genes to have a twofold change to be considered differentially expressed. We found seven

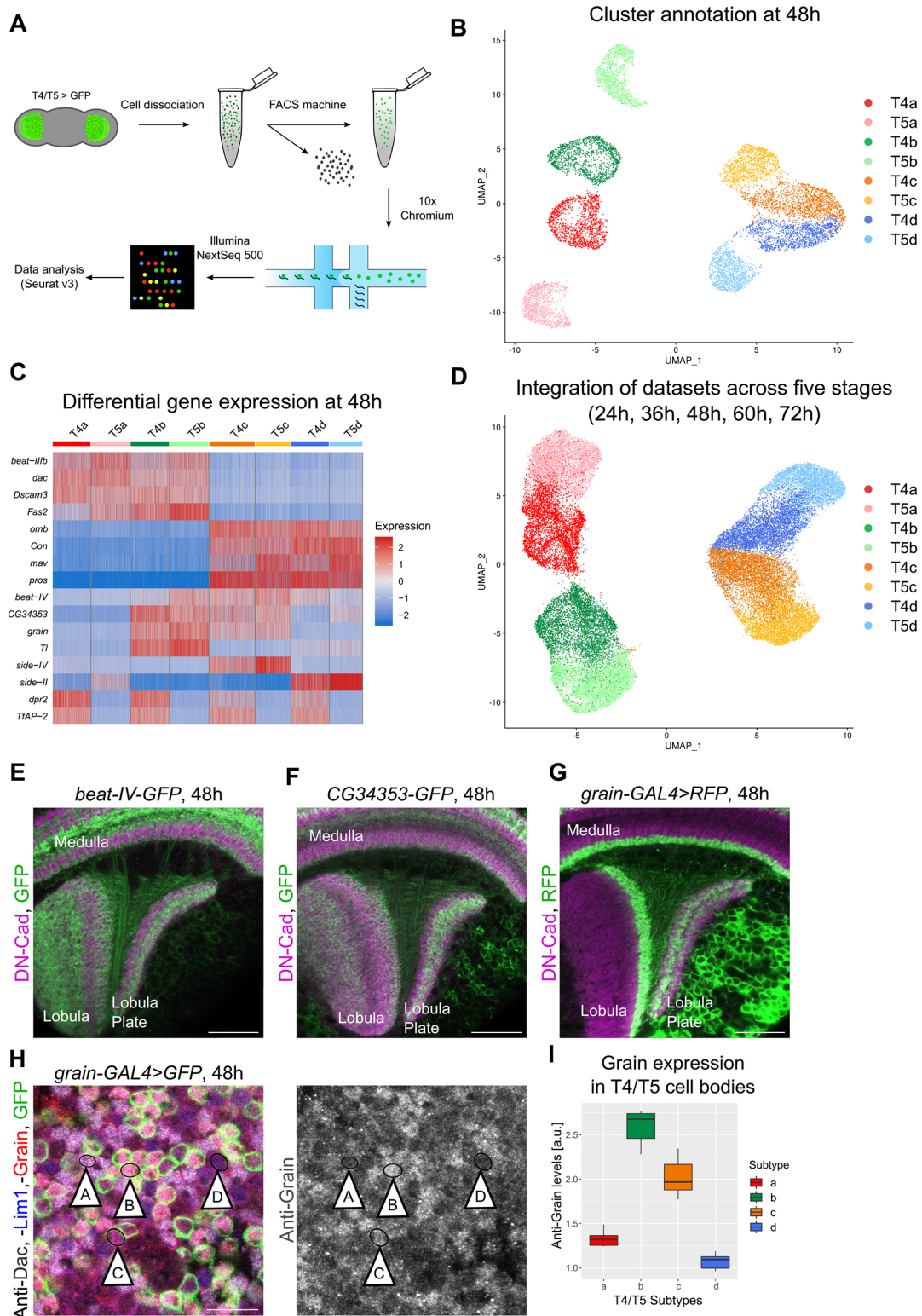


Fig. 3. See next page for legend.

genes encoding for transcription factors and 62 genes encoding for cell-membrane proteins (excluding neurotransmitter/neuropeptide receptors, ion channels and transporters) that were differentially expressed between the transcriptionally distinct groups of T4/T5 neurons at any of the examined stages. Further analysis of gene

expression patterns revealed that 22 out of the 69 genes (32%) had either higher expression levels in all T4 subtypes than in all T5 subtypes, or vice versa, at some point during development (e.g. *TfAP-2* and *CG14340*) or with subtype-specific expression patterns only in T4 or T5 neurons (e.g. *dpr3* and *DIP- θ*) (Fig. 4A; Fig. S3A).

Fig. 3. Each T4 and T5 subtype has a unique transcriptional profile during dendrite growth. (A) Schematic of scRNA-seq protocol. (B) Visualization of T4/T5 neurons sequenced at 48 h APF using UMAP after dimensionality reduction by PCA and unsupervised clustering based on the Louvain algorithm. Dots represent single cells and are arranged according to transcriptome similarity. We assigned clusters to either T4 or T5 based on *TfAP-2* expression, and to T4/T5a,b, T4/T5c,d or T4/T5b,c based on *dac*, *omb* or *grain* expression. (C) Heat map showing the expression levels of the 16 genes differentially expressed between the single cell clusters of T4 and T5 subtypes found in every developmental stage. Columns represent cells and were grouped based on cluster identities. Genes (rows) were manually ordered based on similarity of subtype-specific expression patterns. (D) Integration of scRNA-seq datasets across all developmental stages (24, 36, 48, 60, 72 h APF). Cells were previously assigned to four T4 and T5 subtypes at each developmental stage as described in B. (E-G) At 48 h APF, *beat-IV-GFP* and *CG34353-GFP* MiMIC lines (endogenous GFP-tagging of proteins), and the *grain-Gal4* driver line label specifically T4/T5 neurons with axons in the regions of the lobula plate corresponding to adult lobula plate layers 2 and 3 (innervated by T4/T5b,c neurons). (H) Anti-Lim1 and Anti-Dac immunostainings mark T4/T5a-d and T4/T5a,b cell bodies, respectively. *grain-Gal4* labels T4/T5b,c neurons. The combination of these markers allowed the identification of T4/T5 cell bodies of the four subtypes at 48 h APF (arrowheads, A, B, C and D). Anti-Grain immunostaining signal is enriched specifically in cell bodies of T4/T5b,c (*grain-Gal4*⁺). (I) Quantification of anti-Grain immunostaining in T4/T5 cell bodies of the four subtypes at 48 h APF supports that *grain* is specifically expressed in T4/T5b,c neurons ($n=4$ optic lobes). The end of the whiskers represent the minimum and maximum values. a.u., arbitrary units. Scale bars: 20 μ m (E-G); 10 μ m (H).

We hypothesised that these genes probably play a role in defining properties of T4 versus T5 neurons.

The other 47 out of the 69 genes (68%) exhibited subtype-specific expression patterns and dynamics that were remarkably similar between T4 and T5 neurons (Fig. 4B-G; Fig. S3A), thus positing them as candidates for controlling subtype-specific traits shared between T4 and T5 neurons, like the four dendrite orientations. We attempted to narrow down this list of 47 candidate genes by further exploring their expression dynamics. We found six genes differentially expressed between T4/T5 subtypes only during the last phase of dendrite growth (60-72 h APF) (e.g. *zld* and *fz2*) (Fig. 4G, Fig. S3A). This period coincides with the onset of synaptogenesis in the *Drosophila* central nervous system (Chen et al., 2014; Muthukumar et al., 2014), suggesting an involvement of these genes in this process. Another ten genes exhibited subtype-specific expression patterns that switched over time (e.g. *kuz* and *Lac*) (Fig. S3A). Because such discontinuous and/or late subtype-specific expression patterns during dendrite growth are unlikely to contribute to the development of four dendrite orientations, we discarded these genes.

The resulting list of 31 candidate genes potentially controlling the development of the four dendrite orientations contained only one gene that was exclusively expressed in a single T4/T5 subtype (*side-IV*) (Fig. S3A,B). Within the remaining genes, some genes were clearly co-expressed in several subtypes, although not necessarily at the same levels. For example, we found genes specific to T4/T5a,b (*Dscam3*), T4/T5c,d (*robo3*), T4/T5b,d (*Tl*), T4/T5a,d (*side-II*), T4/T5b,c,d (*beat-IV*) and T4/T5a,c,d (e.g. *kek1*) (Fig. S3B). These results indicate that the four T4/T5 subtypes are defined by combinatorial codes of gene expression that might underlie the development of the four different dendrite orientations.

Grain acts as part of two combinations of transcription factors controlling the dendrite orientations and matching axon projection patterns of two T4/T5 subtypes

Combinatorial codes of transcription factors control the development of subtype-specific traits in postmitotic neurons

(Allan and Thor, 2015; Hobert and Kratsios, 2019). Only five transcription factors were present in our list of 31 candidate genes potentially controlling the development of the four T4/T5 dendrite orientations: *dac*, *omb*, *abrupt* (*ab*), *prospero* (*pros*) and *grain*. Consistent with our scRNA-seq analysis, a previous study found that *dac* and *omb* were expressed in postmitotic developing T4/T5a, b and T4/T5c,d neurons, respectively (Fig. 4B,E) (Apitz and Salecker, 2018). Our scRNA-seq analysis further revealed that *ab* was enriched in T4/T5a,b (Fig. 4C), whereas *pros* was enriched in T4/T5c,d (Fig. 4F). Because of their expression patterns (T4/T5a,b versus T4/T5c,d), the combination of these four transcription factors alone were not sufficient to divide T4/T5 neurons into four subtypes (T4/T5a-d). Interestingly, *grain* was expressed only in T4/T5b,c neurons (Fig 3; Fig. 4D). Therefore, the combination of a T4/T5a,b- (*dac* or *ab*), a T4/T5c,d- (*omb* or *pros*) and a T4/T5b,c- (*grain*) specific transcription factor represents a minimal set of genes to encode the identity of the four T4/T5 subtypes. Remarkably, the subtype-specific expression pattern of each of these transcription factors is stable for most of the period of T4/T5 dendrite growth (Fig. 4H-J). Altogether, these observations suggest that the unique and stable combination of transcription factors that defines each T4/T5 subtype during development controls its specific morphology.

A prediction of this hypothesis would be that changing the code of transcription factors that a T4 or a T5 neuron expresses during development should result in a conversion of subtype-specific properties, i.e. dendrite orientations and axon projection patterns. For example, ectopic expression of *grain* in T4/T5a (normally *Dac*⁺/*Ab*⁺/*Grain*⁻) and T4/T5d (normally *Omb*⁺/*Pros*⁺/*Grain*⁻) should result in neurons with morphological properties of T4/T5b (*Dac*⁺/*Ab*⁺/*Grain*⁺) and T4/T5c (*Omb*⁺/*Pros*⁺/*Grain*⁺) subtypes. To test this hypothesis, we overexpressed *grain* in all postmitotic developing T4/T5 neurons by means of the *R42F06-Gal4* line (Maisak et al., 2013), which drives expression in maturing T4/T5 neurons before dendrite growth and axon segregation (Fig. S4A-C). This condition generated no defects in the neuropil- and layer-specific innervation of T4 and T5 dendrites. However, two, rather than four, layers of T4/T5 axons were visible in the lobula plate (Fig. 5A,B). A recent study reported similar results using different reagents and ruled out that this anatomical defect is caused by neuronal apoptosis, and proposed that the overexpression of *grain* affects T4/T5 neurons such that their axons cannot segregate to form four layers without affecting their dendrites (Kurmangaliyev et al., 2019). Alternatively, changes in T4/T5 axon projection patterns upon *grain* overexpression might result from an identity conversion of T4/T5a,d into T4/T5b,c neurons. To differentiate between these possibilities, we overexpressed *grain* in individual developing T4 and T5 neurons of all subtypes and labelled them by means of mosaic analysis with a repressible cellular marker (MARCM) and *R42F06-Gal4* (Fig. 5C,D). In control MARCM experiments, T4 and T5 neurons of all subtypes (axons in four lobula plate layers and four dendrite orientations) were found (Fig. 5E-M; Fig. S5A-C). By contrast, in *grain* overexpression MARCM experiments, we only found T4 and T5 neurons with axons in either lobula plate layer 2 or 3, which are normally innervated by T4/T5b or T4/T5c subtypes, respectively (Fig. 5N; Fig. S5D). Remarkably, *grain*-overexpressing T4 and T5 neurons that innervated either lobula plate layer 2 or 3 showed corresponding dendrite orientations of T4/T5b or T4/T5c subtypes (Fig. 5O-S; Fig. S5E,F). In addition, T4 and T5 neurons overexpressing *grain* did not show defects in morphological properties that are common to all T4/T5 subtypes, i.e. the restriction of dendrites and axons to single neuropil layers (Fig. 5; Fig. S5).

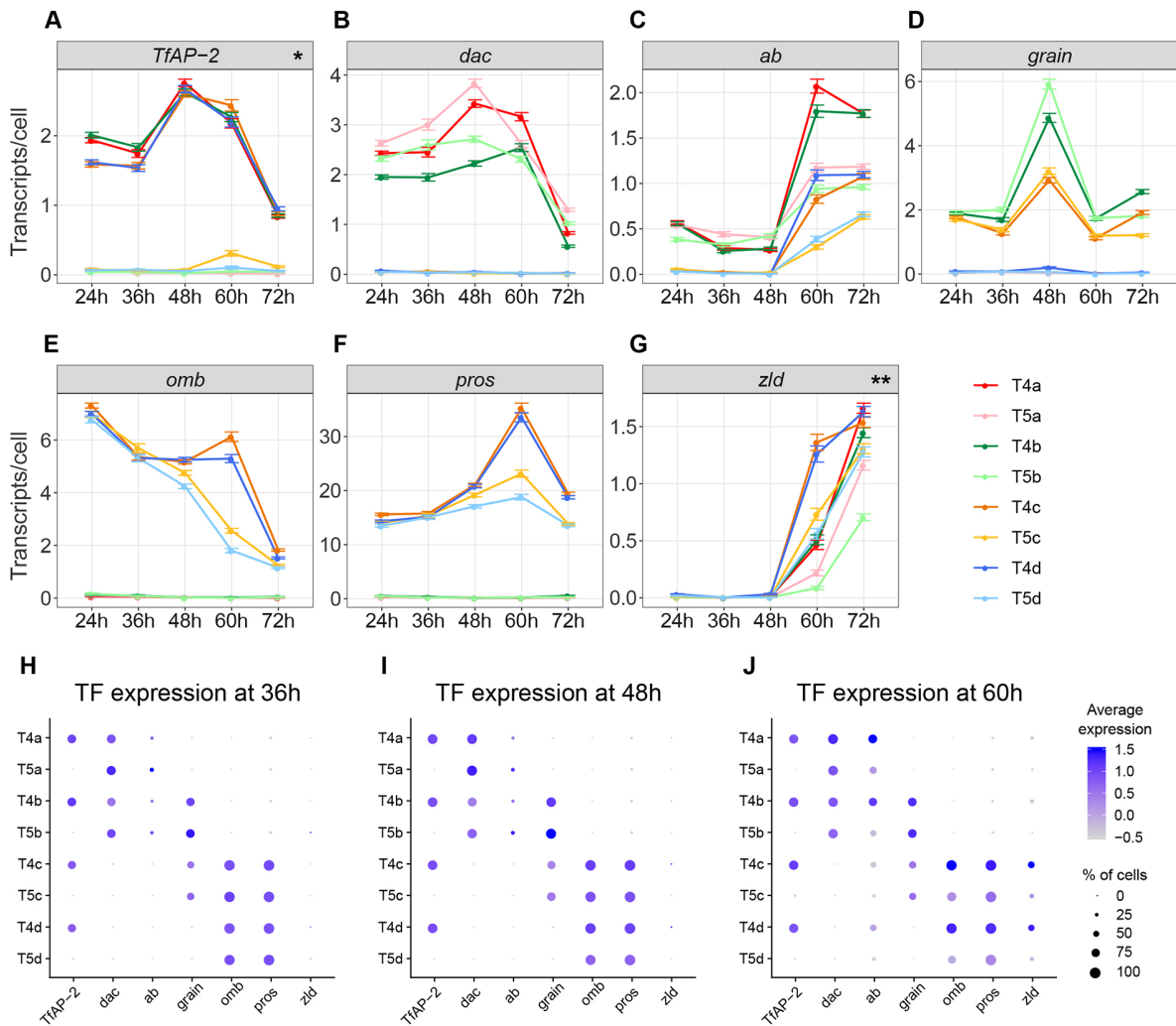


Fig. 4. A combinatorial code of transcription factors defines the four T4/T5 subtypes during dendrite growth. (A-G) Subtype-specific expression patterns and dynamics of transcription factors that are differentially expressed between subtypes of T4/T5 neurons. y-axis shows the count of transcripts per cell (mean \pm s.e.m.). x-axis shows developmental stage (h APF). *Higher expression in all T4 subtypes than in all T5 subtypes. **Differential expression between T4/T5 subtypes only during the last phase of dendrite growth (60-72 h APF). (H-J) Dot plots showing the mean scaled expression levels (colour-coded) of each transcription factor (TF) in the different T4/T5 subtypes at 36, 48 and 60 h APF. Dot sizes represent the percentage of cells in which the transcription factor was detected. Transcription factors were manually ordered based on the similarity of subtype-specific expression patterns.

Three lines of evidence ruled out the possibility that T4/T5a,d-selective death might cause the presence of exclusively T4/T5b,c neurons in the adult upon *grain* overexpression. First, we found no difference in the number of single-labelled T4 and T5 neurons between control and *grain* overexpression MARCM experiments (Fig. S6A). Second, a single neuroblast precursor of T4/T5 neurons always produces four neurons, either T4a/T5a/T4b/T5b or T4c/T5c/T4d/T5d, that project to the same retinotopic position (Fig. S6B) (Pinto-Teixeira et al., 2018). In MARCM experiments with *grain* overexpression, we also found clones of four T4/T5 neurons projecting to the same retinotopic position, and thus originating from the same neuroblast. However, these clones consisted of either T4b/T5b/T4b/T5b or T4c/T5c/T4c/T5c neurons ($n=3/3$ clones of four T4/T5 neurons) (Fig. S6C). Third, *grain* overexpression with the *T5d-splitGal4* line, which drives expression in T5d neurons before dendrite growth and axon segregation (Fig. S4D; Fig. S6D), produced changes in axon projection patterns consistent with T5d transformation into T5c neurons (Fig. S6E). These experiments demonstrate that *grain* overexpression in developing T4/T5a and

T4/T5d neurons transforms them into T4/T5b and T4/T5c neurons, respectively, based on their dendrite orientations and axon projection patterns.

Finally, we tested whether *grain* loss of function in T4/T5b (normally $Dac^+/Ab^+/Grain^+$) and T4/T5c (normally $Omb^+/Pros^+/Grain^+$) results in neurons with morphological properties of T4/T5a ($Dac^+/Ab^+/Grain^-$) and T4/T5d ($Omb^+/Pros^+/Grain^-$) subtypes. To this end, we first performed a knockdown of *grain* in all developing T4/T5 neurons with RNAi and the *R39H12-Gal4* line, which drives expression in T4/T5 neurons of all subtypes from the late third instar (L3) larval stage onwards (Schilling et al., 2019). This resulted in adult T4/T5 neurons with dendrites that showed no defects in their neuropil- and layer-specific innervation but with axons that failed to form four layers in the lobula plate (Fig. 6A,B). Next, we employed MARCM to express *grain-RNAi* in individual maturing T4 neurons with the *R39H12-Gal4* line and to further analyse their morphology in adult brains (Fig. 6C,D). In *grain-RNAi* MARCM experiments, most T4 neurons innervated either lobula plate layer 1 or 4 and showed dendrite orientations of T4/T5a or T4/T5d subtypes,

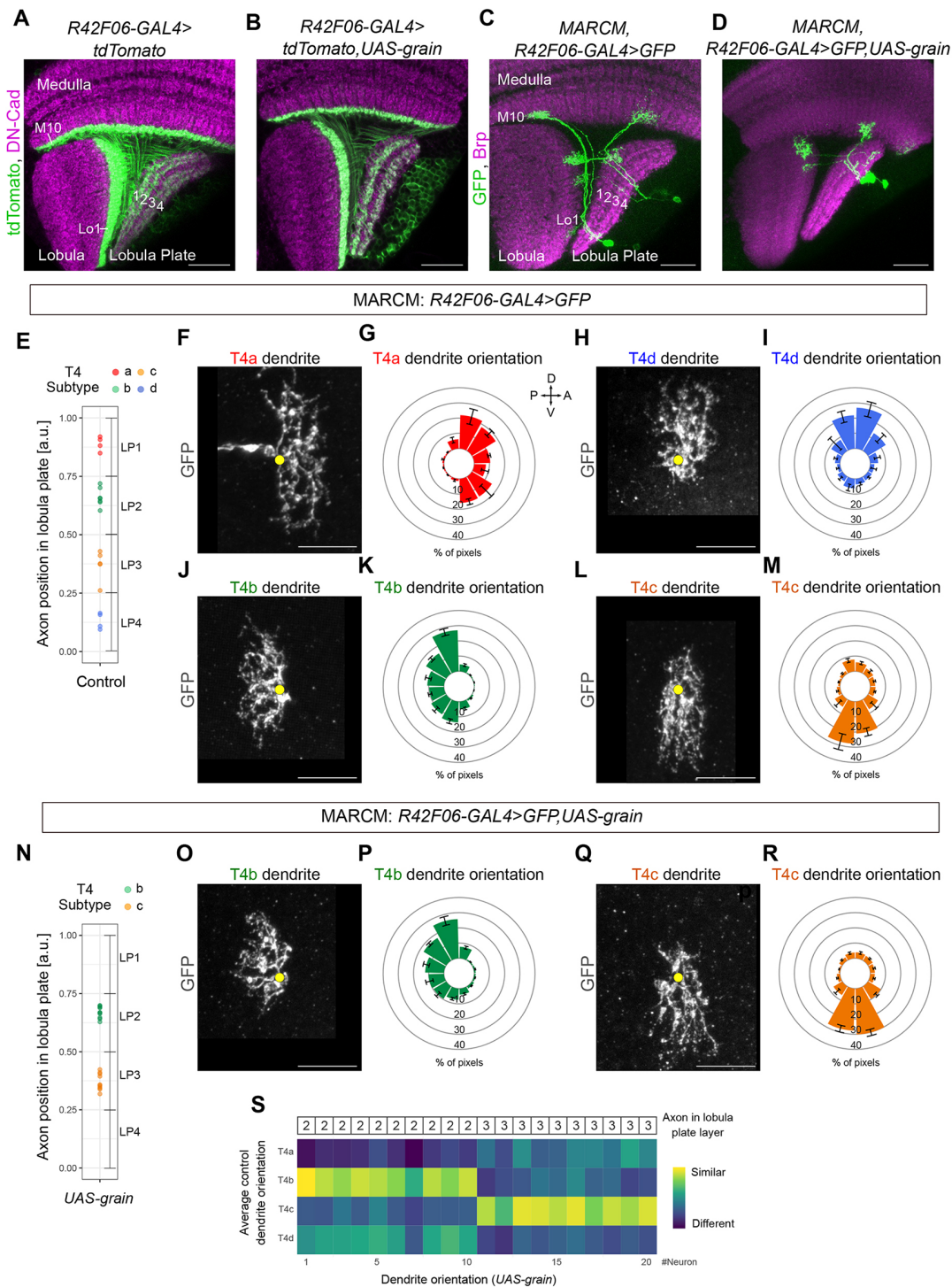


Fig. 5. *grain* overexpression in developing T4 neurons results in adult optic lobes with only T4b,c neurons. (A,B) Adult control T4/T5 neurons and adult T4/T5 neurons overexpressing *grain* by means of the *R42F06-Gal4* line. (C,D) Adult single-labelled T4 and T5 neurons from either control or *grain* overexpression MARCM experiments. (E) Positions in the lobula plate occupied by axon terminals of single control T4 neurons labelled by MARCM ($n=20$). Each T4 neuron was classified into one of the four subtypes based on its axon position in the lobula plate (T4a: $n=4$, T4b: $n=7$, T4c: $n=5$, T4d: $n=4$). (F-M) Dendrite orientations of control T4 neurons of the four subtypes classified based on axon position. Data are mean \pm s.e.m. (N) Positions in the lobula plate occupied by axon terminals of single, *grain*-overexpressing T4 neurons labelled by MARCM ($n=20$). *grain*-overexpressing T4 neurons project axons only to either lobula plate layer 2 ($n=10$) or lobula plate layer 3 ($n=10$). (O-R) Dendrite orientations of *grain*-overexpressing T4 neurons classified as T4b ($n=10$) or T4c ($n=10$) based on axon position. The dendrite orientations of these neurons are indistinguishable from those of wild-type T4b and T4c neurons (J-M). (S) Matrix showing colour-coded similarity indexes between the dendrite orientations of individual *grain*-overexpressing T4 neurons ($n=20$, manually ordered along the horizontal axis based on the innervated layer of the lobula plate) and the average dendrite orientations of the four control T4 subtypes (vertical axis). Yellow dots in F,H,J,L,O,Q mark the first branching point of the dendrite. a.u., arbitrary units. Data are mean \pm s.e.m. Scale bars: 20 μ m (A-D); 5 μ m (F,H,J,L,O,Q).

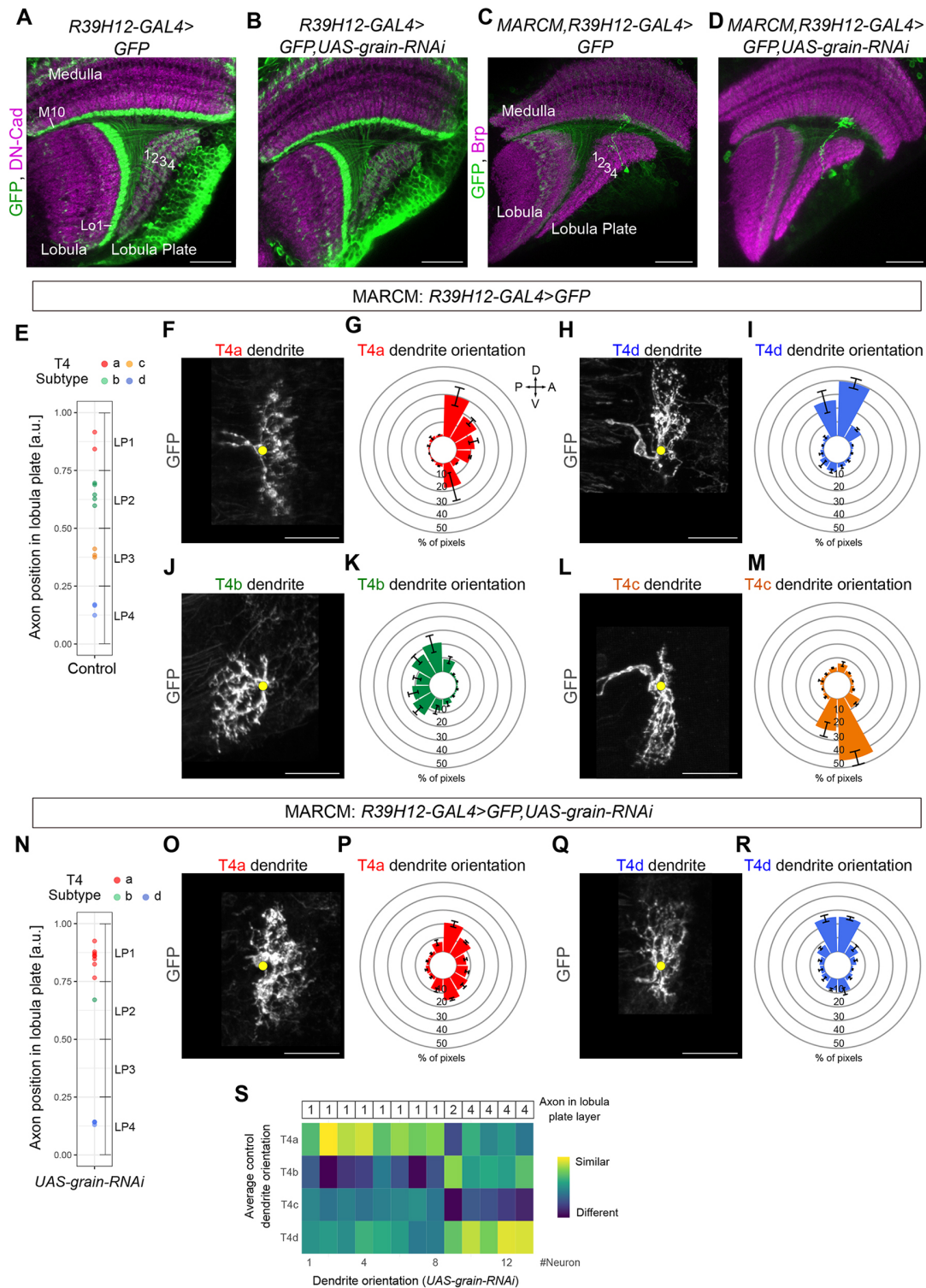


Fig. 6. *grain* loss of function in developing T4 neurons results in adult optic lobes with mainly T4a,d neurons. (A,B) Adult control T4/T5 neurons and adult T4/T5 neurons expressing *grain-RNAi* with the *R39H12-Gal4* line. (C,D) Adult single-labelled T4 neurons from either control or *grain-RNAi* MARCM experiments. (E) Positions in the lobula plate occupied by axon terminals of single, control T4 neurons labelled by MARCM ($n=13$). Each T4 neuron was classified into one of the four subtypes based on its axon position in the lobula plate (T4a: $n=2$, T4b: $n=5$, T4c: $n=3$, T4d: $n=3$). (F-M) Dendrite orientations of control T4 neurons of the four subtypes classified based on axon position. Data are mean±s.e.m.. (N) Positions in the lobula plate occupied by axon terminals of single T4 neurons expressing *grain-RNAi* and labelled by MARCM ($n=13$). Most T4 neurons with *grain* knockdown project axons to either lobula plate layer 1 ($n=8$) or lobula plate layer 4 ($n=4$). (O-R) Dendrite orientations of T4 neurons with *grain* knockdown classified as T4a ($n=8$) or T4d ($n=4$) based on axon position. The dendrite orientations of these neurons are indistinguishable from those of wild-type T4a and T4d neurons (F-I). (S) Matrix showing colour-coded similarity indexes between the dendrite orientations of individual T4 neurons expressing *grain-RNAi* ($n=13$, manually ordered along the horizontal axis based on the innervated layer of the lobula plate) and the average dendrite orientations of the four control T4 subtypes (vertical axis). Yellow dots in F,H,J,L,O,Q mark the first branching point of the dendrite. a.u., arbitrary units. Data are mean±s.e.m. Scale bars: 20 μm (A-D); 5 μm (F,H,J,L,O,Q).

respectively, which is consistent with a transformation of T4/T5b,c into T4/T5a,d upon *grain* loss of function (Fig. 6E-S). Collectively, our data indicate that Grain acts as part of two different combinations of transcription factors, one of them differentiating T4/T5b from T4/T5a and the other one differentiating T4/T5c from T4/T5d morphologies.

DISCUSSION

The development of neuronal morphology relies on the interplay between cell-intrinsic factors, i.e. genetic programmes, and extracellular cues, e.g. growth factors (Sanes and Zipursky, 2010; Melnattur and Lee, 2011; Dong et al., 2015). In this study, we investigated the genetic programmes underlying the acquisition of the different morphologies defining the four T4/T5 subtypes, which are essential for detecting visual motion along the four cardinal directions. Our work reveals that the development of T4/T5 subtype-specific morphologies relies on a postmitotic combinatorial code of transcription factors. In particular, Grain acts together with different transcription factors in T4/T5b and T4/T5c subtypes to coordinate dendrite and axon morphogenesis in order to differentiate their morphologies from those of T4/T5a and T4/T5d, respectively. The coordinated regulation of different aspects of neuron morphogenesis by the same set of transcription factors might provide a general strategy to ensure the establishment of precise neuron wiring patterns during development (Enriquez et al., 2015; Santiago and Bashaw, 2017; Schilling et al., 2019). Furthermore, the combinations of transcription factors controlling the development of subtype-specific properties do not appear to regulate morphological properties that are common to all T4/T5 subtypes, i.e. the restriction of dendrites and axons to single neuropil layers. The acquisition of these morphological properties is controlled postmitotically by two transcription factors of the Sox family, SoxN and Sox102F (Contreras et al., 2018; Schilling et al., 2019). Therefore, distinct sets of transcription factors control differentially subtype-specific properties and properties that are shared by all T4/T5 subtypes, shedding light on the developmental strategies that ensure that each neuron acquires its complete morphological signature.

How do the expression patterns of T4/T5 postmitotic transcription factors arise during development? *SoxN* and *Sox102F* expression in all T4/T5 subtypes arises from temporal patterning of the neuroblasts that are precursors of T4/T5 neurons (Apitz and Salecker, 2015; Schilling et al., 2019). Spatial patterning of the neuroepithelium that generates T4/T5-producing neuroblasts results in the specific expression of *omb* in neuroblasts that are precursors of T4/T5c,d neurons. The expression of *omb* is further relayed to postmitotic developing T4/T5c,d neurons, in which it represses *dac* expression (Apitz and Salecker, 2018). In addition, each *Omb*⁻ neuroblast (precursor of T4/T5a,b), as well as each *Omb*⁺ neuroblast (precursor of T4/T5c,d), divides to produce two ganglion mother cells, only one of which has Notch activity. Only ganglion mother cells with Notch activity generate T4/T5a and T4/T5d neurons (Pinto-Teixeira et al., 2018). The transcriptional programmes downstream of this Notch-dependent fate decision remain elusive. Notch activity has been shown to repress *grain* in the aCC motoneuron of the *Drosophila* embryo (Garces and Thor, 2006). In agreement with this, *grain* is not expressed in T4/T5a,d neurons originating from ganglion mother cells with Notch activity. Together, these observations suggest that the specific expression of *grain* in postmitotic T4/T5b,c neurons could result from the Notch-dependent fate decision occurring during the final division of T4/T5-producing neuroblasts. Future studies will need to investigate

how the T4/T5 subtype-specific expression of *grain*, as well as of *ab* and *pros*, is achieved during development.

Our data revealed that only one transcription factor, Grain, defines T4/T5b,c neurons during development. By contrast, T4/T5a,b and T4/T5c,d are each defined by two transcription factors: *Dac* and *Ab* are co-expressed in T4/T5a,b, whereas *Omb* and *Pros* are co-expressed in T4/T5c,d. These transcription factors with overlapping expression patterns might play redundant roles. Alternatively, they might be specialised to control different aspects of development. Systematic manipulations of the expression patterns of these transcription factors will be needed to address these possibilities, as well as to further elucidate how they act in a combinatorial manner to determine the different morphologies of the four T4/T5 neuron subtypes.

Transcription factors control dendrite growth, in part by controlling the expression of genes relevant for sensing extrinsic cues. We found many cell-membrane proteins with T4/T5 subtype-specific expression patterns that might result from the action of the combinatorial code of transcription factors that we uncovered here. In agreement with the results of a recent publication (Kurmangaliyev et al., 2019), the vast majority of cell-membrane proteins with subtype-specific expression patterns in T4 neurons exhibited the same expression patterns and dynamics in T5 neurons. These mostly included receptors, ligands, regulators of various signalling pathways, and cell-adhesion molecules, some of which have been shown to be involved in axon guidance, dendrite patterning and/or synaptic specificity in *Drosophila* (Keleman et al., 2002; Furrer et al., 2007; Zarin et al., 2014; Ward et al., 2015; Tadros et al., 2016; Li et al., 2017; Barish et al., 2018; Xu et al., 2018). We hypothesise that those cell-membrane proteins with stable subtype-specific expression patterns during, at least, the first phase of dendrite growth are the most likely candidates to regulate the development of the four dendrite orientations in a combinatorial way. However, they might also control other subtype-specific properties, e.g. axon projection patterns and connectivity with distinct postsynaptic neurons. Collectively, our data indicate that the four T4 and T5 subtypes share combinations of transcription factors and downstream effector genes that might control the development of four dendrite orientations. Yet, T4 dendrites grow in the medulla and T5 dendrites grow in the lobula. One exciting possibility is that both neuropils share extrinsic cues conveying directional information to the dendrites of T4 and T5 neurons, which might also be used as universal guideposts by other neuronal cell types that must develop oriented dendrites (Ting et al., 2014).

The dendrites of all T5 subtypes extend across the same number of neuropil columns to connect to the same set of presynaptic functionally distinct neurons signalling luminescence changes from neighbouring points in the visual space, but in a spatial order that is subtype specific. The same holds true for the dendrites of all T4 subtypes (Shinomiya et al., 2019). As a simplified example, T4a connects to Mi4 in column 1, Mi1 in column 2 and Mi9 in column 3, whereas T4b connects to Mi9 in column 1, Mi1 in column 2 and Mi4 in column 3. What could the minimal set of developmental instructions look like to ensure such a specific wiring? Interestingly, the dendrites of the four T4 and T5 subtypes all show a clear and distinct orientation with respect to the extrinsic coordinates of the neuropil that they occupy. The dendrites' intrinsic coordinates define three compartments: proximal, medial and distal. With respect to these intrinsic coordinates, the wiring of all T4 and T5 subtypes is identical. In the above example, both T4a and T4b connect to Mi4 on the proximal, to Mi1 on the medial and to Mi9 on the distal part of their dendrite. Thus, once the compartmentalization of synapses from

different inputs along their dendrites is controlled by cell-intrinsic mechanisms (Lefebvre et al., 2015), the decisive point that differentiates between the subtypes is how they distinctly orient their dendrite. By growing their dendrites along different extrinsically defined directions, they could all apply the same genetic programmes to connect to a set of input neurons. This would lead to a spatial arrangement of synaptic inputs that is different for each subtype with respect to the extrinsic coordinates of the neuropil, thus supporting the detection of motion across four different directions but identical within the intrinsic coordinates of the neurons' dendrite.

We envisage that the manipulation of the genetic programmes controlling dendrite orientation in T4/T5 neurons will allow us to address these ideas systematically. Studying how the four T4/T5 neuron subtypes acquire their morphologies provides a great opportunity to link development, anatomy and function in a neuronal type that performs a computation that is conserved across visual systems (Mauss et al., 2017), which might uncover universal blueprints of neural wiring.

MATERIALS AND METHODS

Fly strains

Flies were raised at 25°C and 60% humidity on standard cornmeal agar medium at 12 h light/dark cycle, except for RNAi experiments, in which offspring were moved from 25°C to 29°C at late larval or early pupal stages. At pupal stages, female and male brains were analysed. At adult stages, only female brains were analysed. The following fly strains were used as driver lines: *SS00324-splitGal4 (R59E08-AD attP40; R42F06-DBD attP2)* (Schilling and Borst, 2015), *T4/T5a,d-splitGal4, grain-Gal4* [Bloomington Drosophila Stock Center (BDSC), 42224], *R42F06-Gal4* (BDSC, 41253), *T5d-splitGal4* and *R39H12-Gal4* (BDSC, 50071). The *T4/T5a,d-splitGal4* driver line was generated by combining the *R35A10-AD* (BDSC, 70193), and *R39H12-DBD* (BDSC, 69444) hemidriver lines (Dionne et al., 2018). The *T5d-splitGal4* driver line was generated by combining the *R35A10-AD* (BDSC, 70193) and *R42H07-DBD* (BDSC, 69609) hemidriver lines. The following fly strains were used as reporter lines: *MCFO-1* (BDSC, 64085), *UAS-myr::GFP* (BDSC, 32198), *UAS-mCD8::GFP* (BDSC, 32188), *UAS-mCD8::GFP* (BDSC, 32187), *UAS-myr::tdTomato* (BDSC, 32222) and *UAS-mCD8::RFP* (BDSC, 32229). To examine the expression of *beat-IV* and *CG34353* genes *in vivo*, we used the *beat-IV-GFP* (BDSC, 66506) and *CG34353-GFP* (BDSC, 60534) MiMIC lines (Venken et al., 2011). The *UAS-grain2* line was used for *grain* overexpression experiments (a gift from J. C. G. Hombria, Universidad Pablo de Olavide, Seville, Spain) (Brown and Castelli-Gair Hombria, 2000). The *UAS-grain-RNAi* line (Vienna Drosophila Stock Center, shRNA-330376) was used for *grain* loss-of-function experiments. *grain* overexpression MARCM experiments were carried out by crossing virgin female *hs-Flp tub-Gal80 FRT19A; UAS-mCD8::GFP; R42F06-Gal4* (a gift from F. Pinto-Teixeira, New York University Abu Dhabi, Abu Dhabi, United Arab Emirates) to male *FRT19A; UAS-grain2/Sp. grain-RNAi* MARCM experiments were performed by crossing virgin female *hs-Flp tub-Gal80 FRT19A; UAS-mCD8::GFP; R39H12-Gal4 UAS-mCD8::GFP* to male *FRT19A; UAS-grain-RNAi/Sp. L3* larvae and early pupae resulting from these crosses were heatshocked for 15–20 min in a 37°C water bath. Adult females with and without *Sp* were used as control and experimental groups, respectively.

Antibodies and immunolabelling

The following primary antibodies were used in this study: rabbit anti-GFP (1:500, Torrey Pines Biolabs, TP401), chicken anti-GFP (1:500, Rockland, 600901215S), rabbit anti-DsRed (1:500, Clontech Laboratories, 632496), rabbit anti-HA (1:300, Cayman Chemical, 162200), rat anti-FLAG (1:200, Novus Biologicals, NBP-1-06712), chicken anti-V5 (1:500, Bethyl Laboratories, A190-118A), rat anti-DN-Cadherin (1:50, Developmental Studies Hybridoma Bank, AB528121), mouse anti-Connexin (1:50, Developmental Studies Hybridoma Bank, AB10660830), mouse anti-Bruchpilot (1:20, Developmental Studies Hybridoma Bank, AB2314866), rat anti-Elav (1:50, Developmental Studies Hybridoma Bank, Rat-Elav-7E8A10),

mouse anti-Dachshund (1:20, Developmental Studies Hybridoma Bank, AB528190), rabbit anti-Lim1 (1:500, a gift from C. Desplan, New York University, New York, USA) and rat anti-Grain (1:200, a gift from A. Garcès) (Garcès and Thor, 2006). Secondary antibodies used in this study were as follows (used at 1:400): Alexa Fluor 488-conjugated goat anti-rabbit (Invitrogen, A11034), Alexa Fluor 488-conjugated goat anti-chicken (Invitrogen, A10262), Alexa Fluor 488-conjugated goat anti-mouse (Thermo Fisher, A28175), Alexa Fluor 488-conjugated goat anti-rat (Invitrogen, A11006), Alexa Fluor 568-conjugated goat anti-rabbit (Life Technologies, A11011), Alexa Fluor 568-conjugated goat anti-mouse (Invitrogen, A11004), Alexa Fluor 633-conjugated goat anti-mouse (Life Technologies, A21050) and Alexa Fluor 680-conjugated goat anti-rat (Invitrogen, A21096).

For immunolabelling, brains were dissected in cold PBS and fixed in 4% paraformaldehyde (containing 0.1% Triton X-100) at room temperature for 23 min. Afterwards, they were washed three times with PBT (PBS containing 0.3% Triton X-100) and blocked with 10% normal goat serum in PBT at room temperature for 2 h. Brains were incubated with primary antibodies diluted in PBT containing 5% normal goat serum for 24–48 h at 4°C. After being washed five times with PBT, brains were incubated with secondary antibodies diluted in PBT containing 5% normal goat serum for 24–48 h at 4°C. Brains were then washed five times with PBT and once with PBS, before being mounted in SlowFade Gold Antifade Mountant (Thermo Fisher Scientific).

Confocal imaging, and image processing and visualisation

Imaging was performed with a Leica SP8 laser scanning confocal microscope equipped with 488-, 561- and 633-nm lasers, and using a 40× or 63× objective. Deconvolution of confocal data (Figs 1,2; Fig. S1) was performed with Huygens Deconvolution software (Scientific Volume Imaging) using default parameters. Image processing and measurements were performed with the Fiji software package (Schindelin et al., 2012). Three-dimensional visualization of confocal data (Fig. S6B,C), neuron reconstructions and measurements (Figs 1,2) were performed with Amira software (Zure Institute Berlin, Thermo Fisher Scientific). Vaa3D software (Allen Institute for Brain Science) was also used for 3D visualization of confocal data (Fig. S5). All figures were prepared using Inkscape software.

In *grain-RNAi* MARCM experiments (Fig. 6), both control and experimental brains showed leaky GFP expression in most of the T4/T5 neurons. However, some brains contained single-labelled T4 and/or T5 cells expressing GFP at much higher levels than the rest of the T4/T5 neurons, which indicated the absence of the *tub-Gal80* transgene and the high expression of *UAS* transgenes in these cells. In both control and experimental brains, only T4 neurons with the highest GFP expression (showing saturated fluorescent signals with laser power of 10%, gain of 100% and pinhole of 0.6) were selected for imaging. In this way, we aimed to image and analyse only those T4 neurons with the highest expression of *UAS-grain-RNAi*. All control and experimental brains were immunolabelled and mounted in parallel following the same protocols.

Quantification of Grain levels in T4/T5 cell bodies

Relative expression levels of Grain in T4/T5 cell bodies of different subtypes (Fig. 3H,I) were quantified as follows: For each optic lobe, we used Fiji to measure the mean fluorescence intensity (anti-Grain channel) from approximately 60 manually segmented T4 and T5 cell bodies (Lim⁺) in single optical sections. We classified each cell body into one of the four T4/T5 subtypes based on anti-Dac staining and *grain-Gal4* expression (GFP⁺). For each T4/T5 subtype, we obtained the average of Grain fluorescence per cell body and divided it by the mean fluorescence intensity (in the anti-Grain channel) of ten surrounding cell bodies that were not from T4/T5 neurons (Lim⁻). Calculations were performed using Microsoft Excel Software and plots were constructed using Python 3.6. In box-and-whisker plots, the end of the whiskers represent the minimum and maximum values.

Morphological characterization of T4 and T5 neuron subtypes

We digitally reconstructed individual T4 and T5 neurons from deconvolved confocal image stacks (Figs 1,2) using the magic wand tool of Amira's

segmentation editor, followed by surface model generation. For each neuron, the range of pixel intensities used by the magic wand tool was adjusted manually in the display and masking area. In order to classify each reconstructed T4 and T5 cell into one of the four subtypes (Fig. 1D,E), we used the relative position of the axon terminal in the lobula plate, which was quantified as follows: the distance between the axon's first branching point and the most posterior edge of the lobula plate along the anteroposterior axis was measured in a single optical section with Fiji. This value was normalised by the total length of the lobula plate along the anteroposterior axis at the proximodistal position occupied by the axon's first branching point. The numbers 0 and 1 represent the most posterior and the most anterior edges of the lobula plate, respectively. We followed a very similar procedure to classify single-labelled T4 and T5 cells in MARCM experiments (Fig. 5; Fig. S5; Fig. 6), with the only difference being that we used the position of the first axonal bouton to calculate the relative position of the axon terminal in the lobula plate.

The dendrite of each digitally reconstructed T4 and T5 was segmented using the brush tool of Amira's segmentation editor, and dendrite volume (Fig. 2A,B) was determined using the material statistics tool of Amira. For comparisons of dendrite volumes across developmental stages, the dendrite volume of each dendrite was normalised to the dendrite volume with the highest value.

To quantify T4 dendrite orientation (Figs 2,5,6; Fig. S1), we imaged dendrites only in frontally oriented regions of the medulla, in which the anteroposterior and dorsoventral axes were recognisable. For each dendrite, we first defined the dendrite's first branching point and made a maximal z projection of the whole dendrite in Fiji. Next, we used a custom-written Python script to manually set a threshold in the image to remove background noise, and to calculate a vector from the dendrite's first branching point to every fluorescent pixel. The angles of the calculated vectors were binned in 12 bins, values were normalised to the total number of vectors, and polar histograms were plotted. A similarity index between the dendrite orientation of a *grain*-overexpressing (or a *grain-RNAi* expressing) T4 neuron and the average dendrite orientation of a control T4 subtype (Fig. 5S; Fig. 6S) was calculated as follows: the values of equivalent bins in the two polar histograms were subtracted, and all the resulting absolute values were summed. Therefore, the higher the value was (dark blue in Fig. 5S; Fig. 6S), the more different the dendrite orientations of the two neurons were. By contrast, the lower the value was (yellow in Fig. 5S; Fig. 6S), the more similar the dendrite orientations of the two neurons were. Calculations were performed using Microsoft Excel and Rstudio, and plots were constructed using Rstudio.

Sample preparation and single cell RNA-sequencing

Drosophila pupae of the line *SS00324-Gal4* recombined with *UAS-mCD8::GFP*, were collected at 0 h APF and kept in an incubator at 25°C at 60% humidity. Pupae were put on ice for 15 min before the desired developmental stage and then dissected in Schneider's insect medium (Sigma-Aldrich, S0146) with 10% fetal bovine serum (complete Schneider's medium). The dissociation protocol was modified from a previous study (Harzer et al., 2013). Pupae were dissected for a total of 1 h and washed three times with complete Schneider's medium before an incubation for 30 min at 30°C with a mix of papain (5 units), Liberase TM (0.13 Wu) and complete Schneider's medium in a total volume of 210 μ l. Afterwards, they were washed three times with complete Schneider's medium before dissociating the cell bodies by pipetting up and down 15 times with a 200 μ l pipette. Next, GFP⁺ cell bodies were isolated from the samples using a BD Aria III cell sorter. Propidium iodine was added as a dead cell marker to remove apoptotic cells. The sorted cells were immediately counted with a haemocytometer and loaded in the 10x Chromium Controller. We aimed to recover between 5000 and 10,000 cells per reaction, dependent on the concentration of the cell suspension. The libraries were prepared as instructed by the 10x Genomics protocol. We used the v. 3 Kit for all reactions. All sequencing runs were performed on an Illumina NextSeq 500 Sequencing System (SY-415-1001) by the next-generation sequencing facility at the Max Planck Institute (MPI) of Biochemistry. The libraries were sequenced with a NextSeq 500/550 High Output Kit v2.5 (75 cycles or 150 cycles, Illumina, 20024906/20024907).

Single cell RNA-sequencing analysis

The data were preprocessed using the Cell Ranger software v3 (10x Genomics) and aligned to the Ensemble 97 *Drosophila melanogaster* genome. GFP, Gal4 DBD and Gal4 AD (Addgene sequences: #26220, #17574, #26233, #26234) were added to the reference genome and annotation file. The output files of Cell Ranger were loaded into R and analysed with the R package Seurat v3.1.0.9007 (development version). The datasets were manually filtered based on the number of counts per cell and the number of features per cell (Table S1). Genes were only considered if they were expressed in at least three cells and cells with fewer than 200 unique molecular identifiers (UMIs, molecular tags to detect unique mRNA transcripts) were excluded. Furthermore, we removed all cells in which more than 10% of all counts could be allocated to either genes coding for mitochondrial or heatshock proteins (Table S2). These genes are an indicator of a cellular stress response, which can change the transcription profile of affected neurons (Morrow and Tanguay, 2003). The genes were identified by searching the list of detected genes for 'mt:' and 'Hsp'. Gender-specific gene expression can also drive substantial transcriptomic variation that can mask biological signal. To mitigate this effect, we used an approach similar to that proposed in a previous study (Mayer et al., 2018). A gender score for each cell was calculated using a supervised analysis with known gender specific markers (Amrein and Axel, 1997; Mayer et al., 2018). To remove misleading sources of variation, we regressed out the number of UMIs, genes detected per cell, the gender score, as well as the percentages of mitochondrial, heatshock and ribosomal proteins expressed using the SCTransform function in Seurat v3. SCTransform was also used to normalise the expression values. To batch correct the two datasets acquired for each developmental stage, we used the integration tools from Seurat v3. We set the number of variable genes to 10,000 in the SCTransform and the SelectIntegrationFeatures functions. Subsequently, we applied the PrepSCTIntegration and FindIntegrationAnchors functions before combining the datasets with IntegrateData from Seurat v3. The adjusted expression levels were saved in the 'integrated' assay of the Seurat object, which was used for the following analysis. After PCA, we used the first 15 principal components (PCs) and a resolution parameter of 0.8 for the clustering of all datasets with the Louvain algorithm. We qualitatively identified and removed clusters that were not T4/T5 neurons or had a different transcriptome because of the cellular stress response, by manually excluding cell clusters that had an unusually high percentage of heatshock and mitochondrial counts (Table S2), as well as clusters with low expression of T4/T5-specific markers (SoxN, Sox102F, Lim1) (Pankova and Borst, 2016; Davie et al., 2018; Konstantinides et al., 2018; Davis et al., 2020). Thus, we were able to discard cells that added noise to the datasets. For the resulting datasets, we first defined the 2000 most variable genes for every developmental stage followed by PCA and clustering, as before, with adjusted parameters (Table S2). The number of PCs used for the clustering was determined manually using the elbow method based on the value of the standard deviation of every PC. We visualised the integrated datasets using uniform manifold approximation and projection (UMAP) and annotated the clusters according to known markers. In order to validate the similarity of clusters between stages, we integrated the datasets from each developmental stage using the CCA alignment tool from Seurat v3. The variable genes were set to 2000 and we used ten PCs for dimensionality reduction and visualization (Fig. 3D).

Differential gene expression analysis

In order to find differentially expressed genes (DEGs) between T4/T5 subtypes, we performed a pairwise comparison of the annotated clusters using the FindMarkers function of Seurat v3 for all developmental stages separately after the clusters were annotated. We used the 'RNA' assay with high thresholds (min.pct=0.5, min.diff.pct=0.5, logfc=2) in order to only find genes that were specific for each cluster. Of the 159 DEGs identified at any of the five developmental stages (Table S3), 16 DEGs passed the thresholds at all stages. For visualization of these genes, we used the 'integrated' assay for the heat map (Fig. 3C; Fig. S2). In order to compare the expression of genes, we switched to the 'RNA' assay, as it contains the number of UMIs assigned to each gene, without any normalisation

(Fig. 4A-G; Fig. S3A). Dot plots were obtained using the DotPlot function of Seurat v3 and the 'SCT' assay, which calculated the average expression of each gene in each cluster and represented it by a colour scale. The size of the dots was determined by the percentage of cells expressing the respective gene (Fig. 4H-J, Fig. S3B).

Identification of transcription factors and cell-membrane proteins in the list of 159 DEGs

In order to identify transcription factors in the list of 159 DEGs, we obtained a list of 651 *Drosophila* transcription factors from the Animal Transcription Factor Database v. 3.0 (bioinfo.life.hust.edu.cn/AnimalTFDB/) (Hu et al., 2019). To identify cell-membrane proteins (excluding neurotransmitter/neuropeptide receptors, ion channels and transporters), we manually inspected the function annotation of each gene in FlyBase (release FB2019_04) (Thurmond et al., 2019). A few genes that were not annotated in FlyBase as cell-membrane proteins were considered as cell-membrane proteins based on previous work (Li et al., 2017).

Acknowledgements

We are grateful to J. C. G. Hombria, F. Pinto-Teixeira, C. Desplan, A. Garcès, the Bloomington *Drosophila* Stock Center, the Vienna *Drosophila* Stock Center and the Developmental Studies Hybridoma Bank for flies and antibodies. We also thank M. Oster (Imaging Facility, MPI of Biochemistry), R. Kim, R. Gautsch, M. Driessen (NGS core facility, MPI of Biochemistry) and A. Yeroslaviz (Cox lab, MPI of Biochemistry) for assistance with scRNA-seq experiments and analysis; M. Sauter for technical assistance with optic lobe dissections; R. Kasper (Imaging Facility, MPI of Neurobiology) for technical assistance with confocal imaging; A. Mauss and L. Groschner for carefully reading the manuscript; M. Drews and F. Richter for helping with programming; and the members of the A. Borst department for discussions.

Competing interests

The authors declare no competing or financial interests.

Author contributions

Conceptualization: N.H., T.S., A.B., J.P.-M.; Methodology: N.H., T.S., C.M., J.P.-M.; Software: N.H., C.M.; Investigation: N.H., T.S., A.H.A., E.S., J.P.-M.; Writing - original draft: J.P.-M.; Writing - review & editing: N.H., T.S., C.M., A.B., J.P.-M.; Visualization: N.H., T.S., J.P.-M.; Supervision: A.B., J.P.-M.; Funding acquisition: A.B.

Funding

This work was supported by the Max Planck Society (Max-Planck-Gesellschaft). Deposited in PMC for immediate release.

Data availability

Raw sequencing data (fastq-files) are freely available from NCBI Gene Expression Omnibus under accession number GSE147987. Code is freely available from GitHub (github.com/borstlab/TF_code_paper).

Supplementary information

Supplementary information available online at <http://dev.biologists.org/lookup/doi/10.1242/dev.186296.supplemental>

Peer review history

The peer review history is available online at <https://dev.biologists.org/lookup/doi/10.1242/dev.186296.reviewer-comments.pdf>

References

- Allan, D. W. and Thor, S. (2015). Transcriptional selectors, masters, and combinatorial codes: regulatory principles of neural subtype specification. *Wiley Interdiscip. Rev. Dev. Biol.* **4**, 505-528. doi:10.1002/wdev.191
- Amrein, H. and Axel, R. (1997). Genes expressed in neurons of adult male *Drosophila*. *Cell* **88**, 459-469. doi:10.1016/S0092-8674(00)81886-3
- Apitz, H. and Salecker, I. (2015). A region-specific neurogenesis mode requires migratory progenitors in the *Drosophila* visual system. *Nat. Neurosci.* **18**, 46-55. doi:10.1038/nn.3896
- Apitz, H. and Salecker, I. (2018). Spatio-temporal relays control layer identity of direction-selective neuron subtypes in *Drosophila*. *Nat. Commun.* **9**, 2295. doi:10.1038/s41467-018-04592-z
- Arenz, A., Drews, M. S., Richter, F. G., Ammer, G. and Borst, A. (2017). The temporal tuning of the *Drosophila* motion detectors is determined by the dynamics of their input elements. *Curr. Biol.* **27**, 929-944. doi:10.1016/j.cub.2017.01.051
- Barish, S., Nuss, S., Strunilin, I., Bao, S., Mukherjee, S., Jones, C. D. and Volkan, P. C. (2018). Combinations of DIPs and Dprs control organization of olfactory receptor neuron terminals in *Drosophila*. *PLoS Genet.* **14**, e1007560. doi:10.1371/journal.pgen.1007560
- Bausenwein, B., Dittrich, A. P. M. and Fischbach, K.-F. (1992). The optic lobe of *Drosophila melanogaster*. II. Sorting of retinotopic pathways in the medulla. *Cell Tissue Res.* **267**, 17-28. doi:10.1007/BF00318687
- Behnia, R., Clark, D. A., Carter, A. G., Clandinin, T. R. and Desplan, C. (2014). Processing properties of ON and OFF pathways for *Drosophila* motion detection. *Nature* **512**, 427-430. doi:10.1038/nature13427
- Brown, S. and Castelli-Gair Hombria, J. (2000). *Drosophila* grain encodes a GATA transcription factor required for cell rearrangement during morphogenesis. *Development* **127**, 4867-4876.
- Chen, Y., Akin, O., Nern, A., Tsui, C. Y. K., Pecot, M. Y. and Zipursky, S. L. (2014). Cell-type-specific labeling of synapses in vivo through synaptic tagging with recombination. *Neuron* **81**, 280-293. doi:10.1016/j.neuron.2013.12.021
- Contreras, E. G., Palominos, T., Glavic, A., Brand, A. H., Sierralta, J. and Oliva, C. (2018). The transcription factor SoxD controls neuronal guidance in the *Drosophila* visual system. *Sci. Rep.* **8**, 13332. doi:10.1038/s41598-018-31654-5
- Davie, K., Janssens, J., Koldere, D., De Waegeneer, M., Pech, U., Kreft, L., Aibar, S., Makhzami, S., Christiaens, V., Bravo González-Blas, C. et al. (2018). A single-cell transcriptome atlas of the aging *Drosophila* brain. *Cell* **174**, 982-998.e920. doi:10.1016/j.cell.2018.05.057
- Davis, F. P., Nern, A., Picard, S., Reiser, M. B., Rubin, G. M., Eddy, S. R. and Henry, G. L. (2020). A genetic, genomic, and computational resource for exploring neural circuit function. *eLife* **9**, e50901. doi:10.7554/eLife.50901
- Dionne, H., Hibbard, K. L., Cavallaro, A., Kao, J.-C. and Rubin, G. M. (2018). Genetic reagents for making split-GAL4 lines in *Drosophila*. *Genetics* **209**, 31-35. doi:10.1534/genetics.118.300682
- Dong, X., Shen, K. and Bülow, H. E. (2015). Intrinsic and extrinsic mechanisms of dendritic morphogenesis. *Annu. Rev. Physiol.* **77**, 271-300. doi:10.1146/annurev-physiol-021014-071746
- Enriquez, J., Venkatasubramanian, L., Baek, M., Peterson, M., Aghayeva, U. and Mann, R. S. (2015). Specification of individual adult motor neuron morphologies by combinatorial transcription factor codes. *Neuron* **86**, 955-970. doi:10.1016/j.neuron.2015.04.011
- Fischbach, K.-F. and Dittrich, A. P. M. (1989). The optic lobe of *Drosophila melanogaster*. I. A Golgi analysis of wild-type structure. *Cell Tissue Res.* **258**, 441-475. doi:10.1007/BF00218858
- Fisher, Y. E., Silies, M. and Clandinin, T. R. (2015). Orientation selectivity sharpens motion detection in *Drosophila*. *Neuron* **88**, 390-402. doi:10.1016/j.neuron.2015.09.033
- Furrer, M.-P., Vasenkova, I., Kamiyama, D., Rosado, Y. and Chiba, A. (2007). Slit and Robo control the development of dendrites in *Drosophila* CNS. *Development* **134**, 3795-3804. doi:10.1242/dev.02882
- Garcés, A. and Thor, S. (2006). Specification of *Drosophila* aCC motoneuron identity by a genetic cascade involving even-skipped, grain and zfh1. *Development* **133**, 1445-1455. doi:10.1242/dev.02321
- Haag, J., Arenz, A., Serbe, E., Gabbiani, F. and Borst, A. (2016). Complementary mechanisms create direction selectivity in the fly. *eLife* **5**, e17421. doi:10.7554/eLife.17421
- Harzer, H., Berger, C., Conder, R., Schmauss, G. and Knoblich, J. A. (2013). FACS purification of *Drosophila* larval neuroblasts for next-generation sequencing. *Nat. Protoc.* **8**, 1088-1099. doi:10.1038/nprot.2013.062
- Hoebert, O. and Kratsios, P. (2019). Neuronal identity control by terminal selectors in worms, flies, and chordates. *Curr. Opin. Neurobiol.* **56**, 97-105. doi:10.1016/j.conb.2018.12.006
- Hu, H., Miao, Y.-R., Jia, L.-H., Yu, Q.-Y., Zhang, Q. and Guo, A.-Y. (2019). AnimalTFDB 3.0: a comprehensive resource for annotation and prediction of animal transcription factors. *Nucleic Acids Res.* **47**, D33-D38. doi:10.1093/nar/gky822
- Keleman, K., Rajagopalan, S., Cleppien, D., Teis, D., Paiha, K., Huber, L. A., Technau, G. M. and Dickson, B. J. (2002). Comm sorts robo to control axon guidance at the *Drosophila* midline. *Cell* **110**, 415-427. doi:10.1016/S0092-8674(02)00901-7
- Klapoetke, N. C., Nern, A., Peek, M. Y., Rogers, E. M., Breads, P., Rubin, G. M., Reiser, M. B. and Card, G. M. (2017). Ultra-selective looming detection from radial motion opponency. *Nature* **551**, 237-241. doi:10.1038/nature24626
- Konstantinides, N., Kapuralin, K., Fadil, C., Barboza, L., Satija, R. and Desplan, C. (2018). Phenotypic convergence: distinct transcription factors regulate common terminal features. *Cell* **174**, 622-635.e613. doi:10.1016/j.cell.2018.05.021
- Kurmangaliyev, Y. Z., Yoo, J., LoCascio, S. A. and Zipursky, S. L. (2019). Modular transcriptional programs separately define axon and dendrite connectivity. *eLife* **8**, e50822. doi:10.7554/eLife.50822
- Lefebvre, J. L., Sanes, J. R. and Kay, J. N. (2015). Development of dendritic form and function. *Annu. Rev. Cell Dev. Biol.* **31**, 741-777. doi:10.1146/annurev-cellbio-100913-013020
- Li, H., Watson, A., Olechwiec, A., Anaya, M., Sorooshyari, S. K., Harnett, D. P., Lee, H.-K., Vielmetter, J., Fares, M. A., Garcia, K. C. et al. (2017).

- Deconstruction of the beaten Path-Sidestep interaction network provides insights into neuromuscular system development. *eLife* **6**, e28111. doi:10.7554/eLife.28111
- Maisak, M. S., Haag, J., Ammer, G., Serbe, E., Meier, M., Leonhardt, A., Schilling, T., Bahl, A., Rubin, G. M., Nern, A. et al.** (2013). A directional tuning map of *Drosophila* elementary motion detectors. *Nature* **500**, 212-216. doi:10.1038/nature12320
- Mauss, A. S., Pankova, K., Arenz, A., Nern, A., Rubin, G. M. and Borst, A.** (2015). Neural circuit to integrate opposing motions in the visual field. *Cell* **162**, 351-362. doi:10.1016/j.cell.2015.06.035
- Mauss, A. S., Vlasits, A., Borst, A. and Feller, M.** (2017). Visual circuits for direction selectivity. *Annu. Rev. Neurosci.* **40**, 211-230. doi:10.1146/annurev-neuro-072116-031335
- Mayer, C., Hafemeister, C., Bandler, R. C., Machold, R., Batista Brito, R., Jaglin, X., Allaway, K., Butler, A., Fishell, G. and Satija, R.** (2018). Developmental diversification of cortical inhibitory interneurons. *Nature* **555**, 457-462. doi:10.1038/nature25999
- Melnattur, K. V. and Lee, C.-H.** (2011). Visual circuit assembly in *Drosophila*. *Dev. Neurobiol.* **71**, 1286-1296. doi:10.1002/dneu.20894
- Morrow, G. and Tanguay, R. M.** (2003). Heat shock proteins and aging in *Drosophila melanogaster*. *Semin. Cell Dev. Biol.* **14**, 291-299. doi:10.1016/j.semcdb.2003.09.023
- Muthukumar, A. K., Stork, T. and Freeman, M. R.** (2014). Activity-dependent regulation of astrocyte GAT levels during synaptogenesis. *Nat. Neurosci.* **17**, 1340-1350. doi:10.1038/nn.3791
- Nern, A., Pfeiffer, B. D. and Rubin, G. M.** (2015). Optimized tools for multicolor stochastic labeling reveal diverse stereotyped cell arrangements in the fly visual system. *Proc. Natl. Acad. Sci. USA* **112**, E2967-E2976. doi:10.1073/pnas.1506763112
- Pankova, K. and Borst, A.** (2016). RNA-Seq transcriptome analysis of direction-selective T4/T5 neurons in *Drosophila*. *PLoS ONE* **11**, e0163986. doi:10.1371/journal.pone.0163986
- Pinto-Teixeira, F., Koo, C., Rossi, A. M., Neric, N., Bertet, C., Li, X., Del-Valle-Rodriguez, A. and Desplan, C.** (2018). Development of concurrent retinotopic maps in the fly motion detection circuit. *Cell* **173**, 485-498.e411. doi:10.1016/j.cell.2018.02.053
- Prigge, C. L. and Kay, J. N.** (2018). Dendrite morphogenesis from birth to adulthood. *Curr. Opin. Neurobiol.* **53**, 139-145. doi:10.1016/j.conb.2018.07.007
- Puram, S. V. and Bonni, A.** (2013). Cell-intrinsic drivers of dendrite morphogenesis. *Development* **140**, 4657-4671. doi:10.1242/dev.087676
- Sanes, J. R. and Zipursky, S. L.** (2010). Design principles of insect and vertebrate visual systems. *Neuron* **66**, 15-36. doi:10.1016/j.neuron.2010.01.018
- Santiago, C. and Bashaw, G. J.** (2017). Islet coordinately regulates motor axon guidance and dendrite targeting through the frazzled/DCC receptor. *Cell Rep.* **18**, 1646-1659. doi:10.1016/j.celrep.2017.01.041
- Schilling, T. and Borst, A.** (2015). Local motion detectors are required for the computation of expansion flow-fields. *Biol. Open* **4**, 1105-1108. doi:10.1242/bio.012690
- Schilling, T., Ali, A. H., Leonhardt, A., Borst, A. and Pujol-Marti, J.** (2019). Transcriptional control of morphological properties of direction-selective T4/T5 neurons in *Drosophila*. *Development* **146**, dev169763. doi:10.1242/dev.169763
- Schindelin, J., Arganda-Carreras, I., Frise, E., Kaynig, V., Longair, M., Pietzsch, T., Preibisch, S., Rueden, C., Saalfeld, S., Schmid, B. et al.** (2012). Fiji: an open-source platform for biological-image analysis. *Nat. Methods* **9**, 676-682. doi:10.1038/nmeth.2019
- Serbe, E., Meier, M., Leonhardt, A. and Borst, A.** (2016). Comprehensive characterization of the major presynaptic elements to the *Drosophila* OFF motion detector. *Neuron* **89**, 829-841. doi:10.1016/j.neuron.2016.01.006
- Shinomiya, K., Takemura, S.-Y., Rivlin, P. K., Plaza, S. M., Scheffer, L. K. and Meinertzhagen, I. A.** (2015). A common evolutionary origin for the ON- and OFF-edge motion detection pathways of the *Drosophila* visual system. *Front. Neural Circuits* **9**, 33. doi:10.3389/fncir.2015.00033
- Shinomiya, K., Huang, G., Lu, Z., Parag, T., Xu, C. S., Aniceto, R., Ansari, N., Cheatham, N., Lauchie, S., Neace, E. et al.** (2019). Comparisons between the ON- and OFF-edge motion pathways in the *Drosophila* brain. *eLife* **8**, e40025. doi:10.7554/eLife.40025
- Stuart, T., Butler, A., Hoffman, P., Hafemeister, C., Papalexi, E., Mauck, W. M., III, Hao, Y., Stoeckius, M., Smibert, P. and Satija, R.** (2019). Comprehensive integration of single-cell data. *Cell* **177**, 1888-1902.e1821. doi:10.1016/j.cell.2019.05.031
- Tadros, W., Xu, S., Akin, O., Yi, C. H., Shin, G. J., Millard, S. S. and Zipursky, S. L.** (2016). Dscam proteins direct dendritic targeting through adhesion. *Neuron* **89**, 480-493. doi:10.1016/j.neuron.2015.12.026
- Takemura, S.-Y., Bharioke, A., Lu, Z., Nern, A., Vitaladevuni, S., Rivlin, P. K., Katz, W. T., Olbris, D. J., Plaza, S. M., Winston, P. et al.** (2013). A visual motion detection circuit suggested by *Drosophila* connectomics. *Nature* **500**, 175-181. doi:10.1038/nature12450
- Takemura, S.-Y., Nern, A., Chklovskii, D. B., Scheffer, L. K., Rubin, G. M. and Meinertzhagen, I. A.** (2017). The comprehensive connectome of a neural substrate for 'ON' motion detection in *Drosophila*. *eLife* **6**, e24394. doi:10.7554/eLife.24394
- Thurmond, J., Goodman, J. L., Strelets, V. B., Attrill, H., Gramates, L. S., Marygold, S. J., Matthews, B. B., Millburn, G., Antonazzo, G., Trovisco, V. et al.** (2019). FlyBase 2.0: the next generation. *Nucleic Acids Res.* **47**, D759-d765. doi:10.1093/nar/gky1003
- Ting, C.-Y., McQueen, P. G., Pandya, N., Lin, T.-Y., Yang, M., Reddy, O. V., O'Connor, M. B., McAuliffe, M. and Lee, C.-H.** (2014). Photoreceptor-derived activin promotes dendritic termination and restricts the receptive fields of first-order interneurons in *Drosophila*. *Neuron* **81**, 830-846. doi:10.1016/j.neuron.2013.12.012
- Venken, K. J. T., Schulze, K. L., Haelterman, N. A., Pan, H., He, Y., Evans-Holm, M., Carlson, J. W., Levis, R. W., Spradling, A. C., Hoskins, R. A. et al.** (2011). MiMIC: a highly versatile transposon insertion resource for engineering *Drosophila melanogaster* genes. *Nat. Methods* **8**, 737-743. doi:10.1038/nmeth.1662
- Ward, A., Hong, W., Favaloro, V. and Luo, L.** (2015). Toll receptors instruct axon and dendrite targeting and participate in synaptic partner matching in a *Drosophila* olfactory circuit. *Neuron* **85**, 1013-1028. doi:10.1016/j.neuron.2015.02.003
- Xu, S., Xiao, Q., Cosmanescu, F., Sergeeva, A. P., Yoo, J., Lin, Y., Katsamba, P. S., Ahlsen, G., Kaufman, J., Linaval, N. T. et al.** (2018). Interactions between the Ig-Superfamily Proteins DIP-alpha and Dpr6/10 Regulate Assembly of Neural Circuits. *Neuron* **100**, 1369-1384.e1366. doi:10.1016/j.neuron.2018.11.001
- Zarin, A. A., Asadzadeh, J., Hokamp, K., McCartney, D., Yang, L., Bashaw, G. J. and Labrador, J.-P.** (2014). A transcription factor network coordinates attraction, repulsion, and adhesion combinatorially to control motor axon pathway selection. *Neuron* **81**, 1297-1311. doi:10.1016/j.neuron.2014.01.038

Figure S1

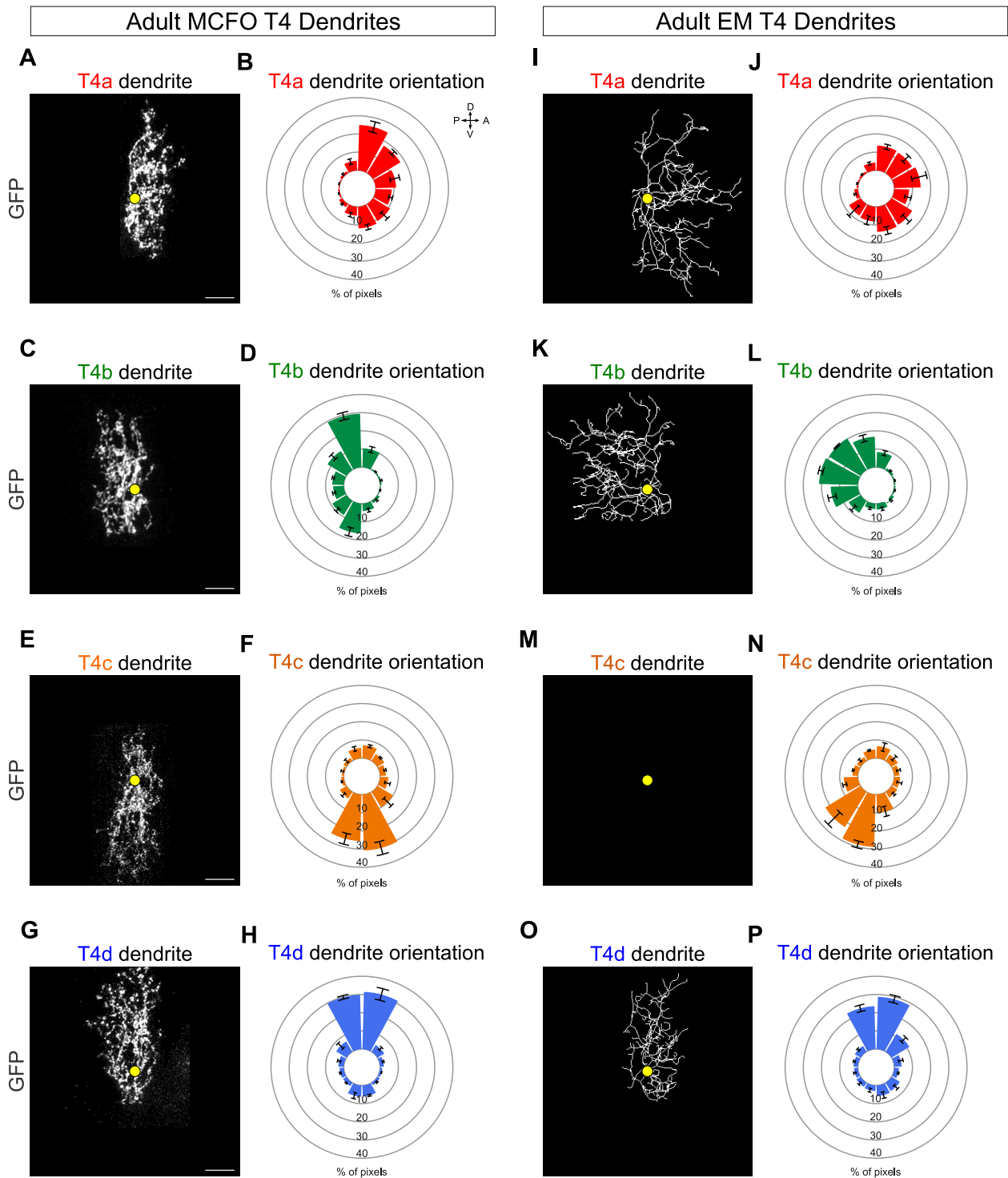


Figure S1. Quantification of dendrite orientation in the four T4 subtypes imaged by confocal microscopy or reconstructed from electron microscopy data.

(A-H) Examples of adult T4a, T4b, T4c and T4d dendrites imaged with confocal microscopy after labelling by means of the MCFO and the *SS00324-splitGal4*. Yellow dots mark the dendrite's first branching point. Scale bars: 5 μ m. Quantifications of dendrite orientation are shown as polar histograms with the 2D distribution of fluorescent pixels (indicative of the presence of dendritic branches) around the dendrite's first branching point (N=4 dendrites per subtype). A, P, D, V: Anterior, Posterior, Dorsal, Ventral (visual field coordinates). Mean \pm SEM are shown.

(I-P) Examples of adult T4a, T4b, T4c and T4d dendrites reconstructed from electron microscopy (EM) data (Takemura et al., 2017). Yellow dots mark the dendrite's first branching point. Quantifications of dendrite orientation are shown as in (A-H) (N=4 dendrites per subtype).

Figure S2

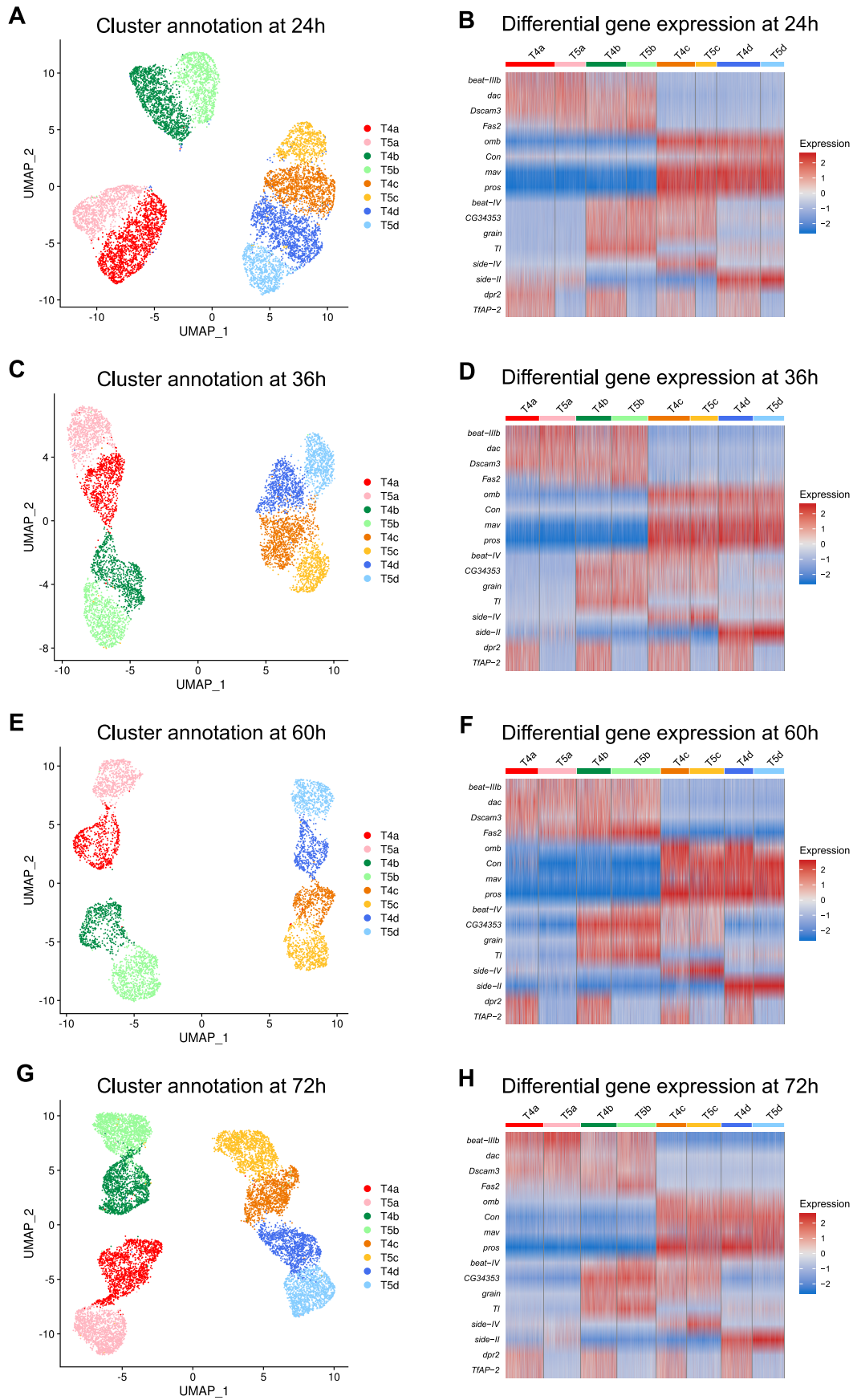
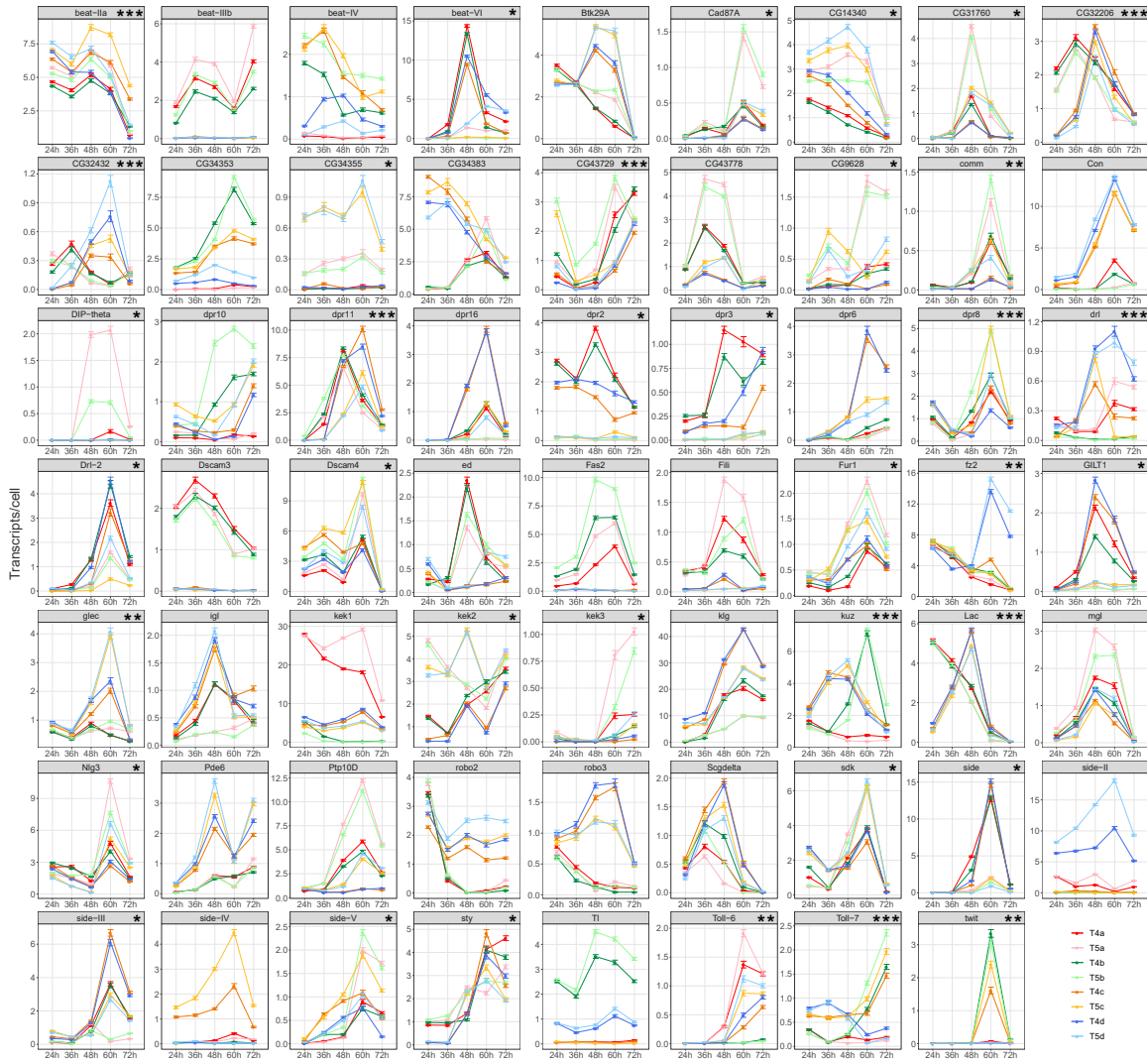


Figure S2. Eight transcriptionally distinct groups of T4/T5 neurons correspond to the four subtypes of T4 and T5 neurons at 24, 36, 60 and 72h APF.

(A-H) Visualizations of T4/T5 neurons sequenced either at 24, 36, 60 or 72h APF (A,C,E,G) using UMAP after dimensionality reduction by PCA and unsupervised clustering based on the Louvain algorithm. Each dot is a single cell. Cells are arranged according to transcriptome similarity. We manually assigned clusters to either T4 or T5 based on *TfAP-2* expression. Clusters were assigned to either T4/T5a,b or T4/T5c,d based on *dac* and *omb* expression. We assigned clusters to either T4/T5b,c or T4/T5a,d based on *grain* expression. Eight single-cell clusters were matched to the four T4 subtypes (T4a-d) and to the four T5 subtypes (T5a-d) in every examined developmental stage. Heat maps (B,D,F,H) show the expression levels of the 16 genes found to be differentially expressed between the single-cell clusters of T4 and T5 subtypes in every developmental stage examined. Each column corresponds to a cell and each row corresponds to a gene. Cells are grouped based on cluster identities. Genes were manually ordered based on visual inspection of subtype-specific expression patterns.

Figure S3

A



B

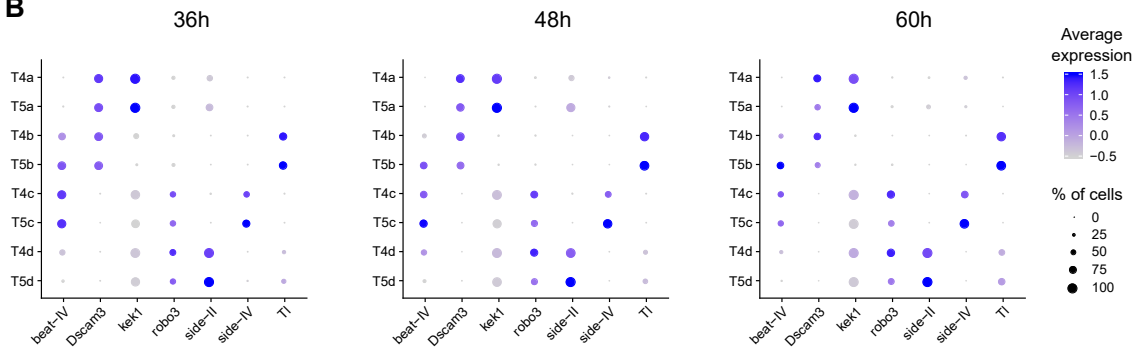


Figure S3. Expression patterns of cell-membrane proteins differentially expressed between T4/T5 subtypes.

(A) Subtype-specific expression patterns and dynamics of all genes encoding for cell-membrane proteins that were found differentially expressed between T4/T5 subtypes. Y axis shows the count of transcripts per cell (mean \pm SEM). X axis shows developmental stage (h APF). Genes were arranged alphabetically. *: Genes with either higher expression levels in all T4 than in all T5 subtypes, or vice versa, or with subtype-specific expression patterns only in T4 or T5 neurons. **: Genes differentially expressed between T4/T5 subtypes only during the last phase of dendrite growth (60-72h APF). ***: Genes with subtype-specific expression patterns that switch over time.

(B) Dot plots showing the mean scaled expression levels (colour-coded) of some cell-membrane proteins in the different T4/T5 subtypes at 36, 48 and 60h APF. Dot sizes represent the percentage of cells in which the gene was detected. Genes were arranged alphabetically.

Figure S4

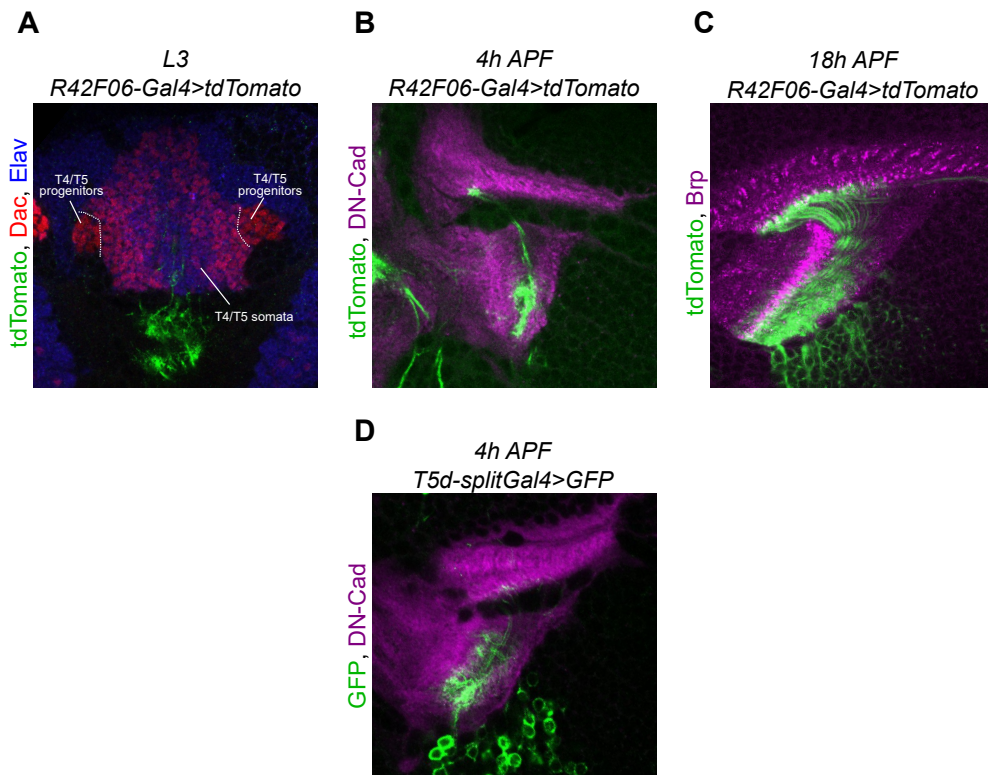


Figure S4. Characterization of *enhancer-Gal4* driver lines used for *grain* overexpression in T4/T5 neurons.

(A) The *R42F06-Gal4* line labels only a very few maturing T4/T5 neurons in the late L3 larval optic lobe. Neuronal cell bodies were marked with anti-Elav. T4/T5 neuron progenitors (Dac+/Elav-) are not labelled by the *R42F06-Gal4* line.

(B,C) T4/T5 neurons expressing tdTomato under the control of *R42F06-Gal4* in pupal optic lobes at 4h and 18h APF. The *R42F06-Gal4* expression pattern follows the maturation wave of T4/T5 neurons (Pinto-Teixeira et al., 2018). Anti-DN-Cadherin (DN-Cad) and anti-Bruchpilot (Brp) label the neuropils.

(D) Early pupal optic lobe (4h APF) showing T5 neurons expressing GFP by means of the *T5d-splitGal4* driver line.

Figure S5

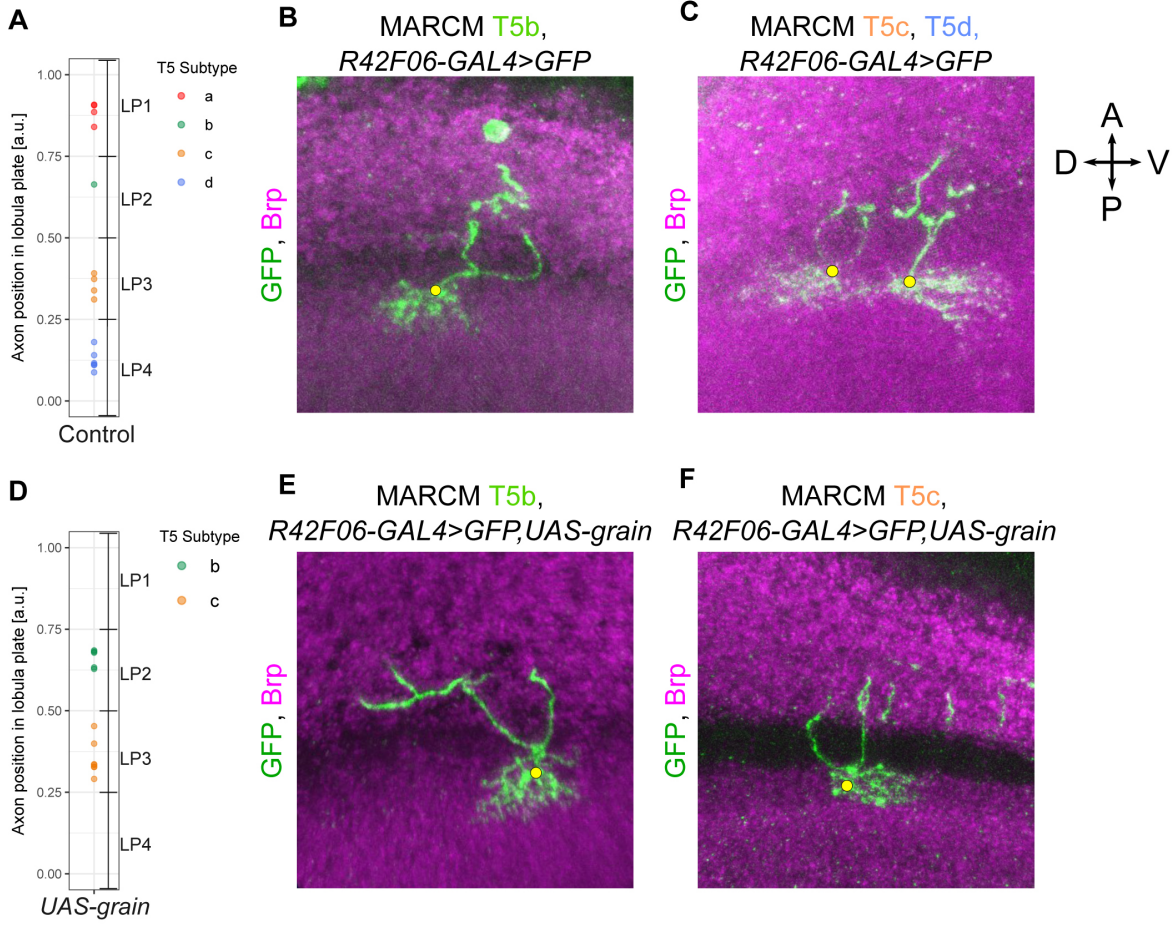


Figure S5. *Grain* overexpression in developing T5 neurons results in adult optic lobes with only T5b,c neurons.

(A) Positions in the lobula plate occupied by axon terminals of single, control T5 neurons labelled by MARCM (N=15). Each T5 neuron was classified into one of the four subtypes based on the lobula plate layer occupied by its axon (T5a: N=4, T5b: N=1, T5c: N=4, T5d: N=6).

(B) 3D visualization of the dendrite from a control T5b neuron (axon in lobula plate layer 2) labelled by MARCM. Yellow dot marks the dendrite's first branching point. Anti-Bruchpilot (Brp) labels the neuropils. A, P, D, V: Anterior, Posterior, Dorsal, Ventral (visual field coordinates).

(C) 3D visualization of the dendrites from a control T5d (left, axon in lobula plate layer 4) and a control T5c (right, axon in lobula plate layer 3) labelled by MARCM.

(D) Positions in the lobula plate occupied by axon terminals of single, *grain*-overexpressing T5 neurons labelled by MARCM (N=12). *Grain*-overexpressing T5 neurons project axons to either lobula plate layer 2 (N=5) or lobula plate layer 3 (N=7).

(E,F) 3D visualizations of the dendrites from *grain*-overexpressing T5b (axon in lobula plate layer 2) and T5c (axon in lobula plate layer 3) labelled by MARCM. The dendrite orientations of these neurons are indistinguishable from those of T5b and T5c wild-type neurons (B,C). The orientation of T5 dendrites was qualitatively assessed by visual inspection.

Figure S6

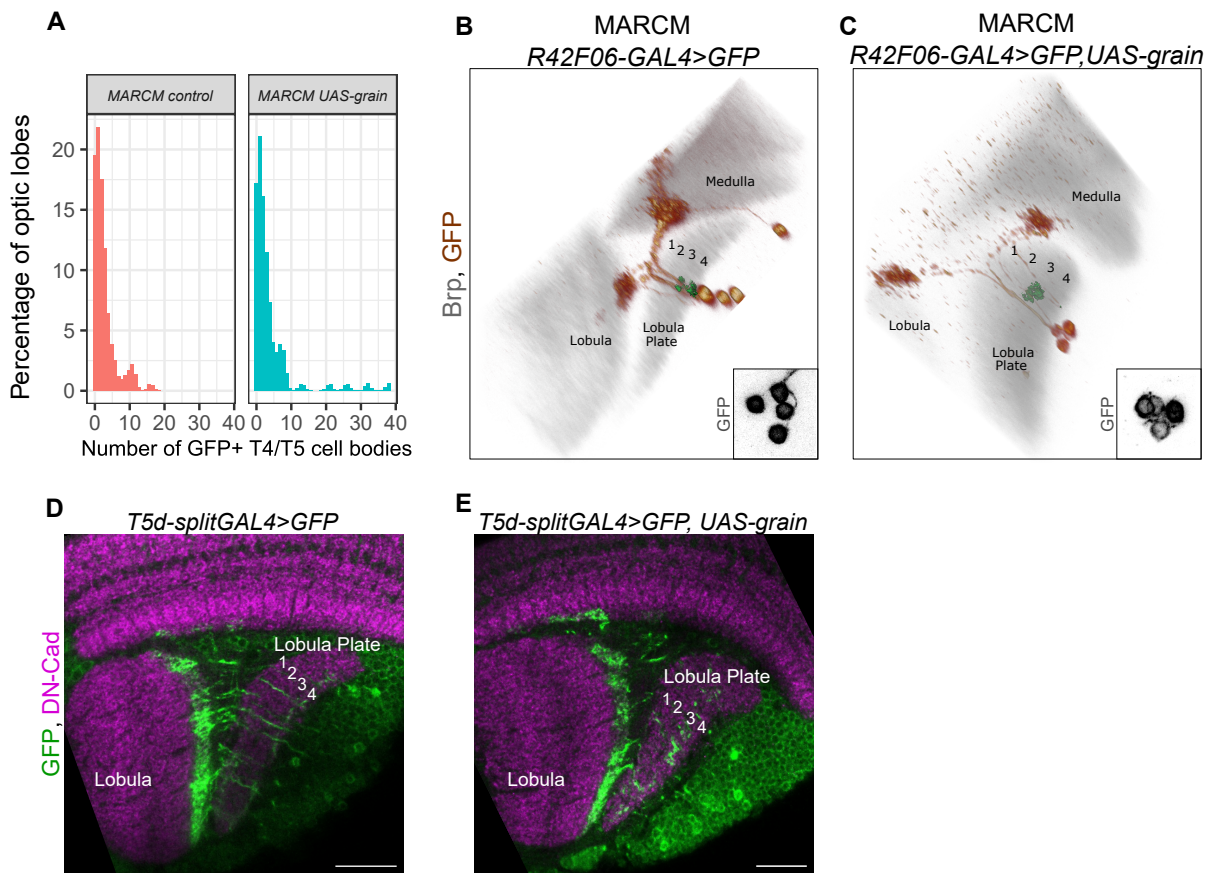


Figure S6. *Grain* overexpression in developing T4/T5 neurons does not cause specific cell death of T4/T5a,d subtypes.

(A) Histograms showing the percentages of optic lobes (Y Axis) found with different numbers of GFP⁺ T4 and T5 cell bodies (X Axis) in control MARCM experiments and in *grain* overexpression MARCM experiments.

(B) 3D visualization of two T4 and two T5 neurons labelled in a control MARCM experiment, and projecting dendrites and axons to the same retinotopic position of the medulla, lobula and lobula plate. The inset shows the cell bodies of these neurons. The axon terminals of the four neurons (in green, digitally reconstructed) were located in layers 3 and 4 of the lobula plate. These T4c,T5c,T4d,T5d neurons represent a four-cell clone produced by a single neuroblast (Pinto-Teixeira et al., 2018).

(C) 3D visualization of two T4 and two T5 neurons labelled in a *grain* overexpression MARCM experiment, and projecting dendrites and axons to the same retinotopic position of the medulla, lobula and lobula plate. Their cell bodies are shown in the inset. The axon terminals of the four neurons (in green, digitally reconstructed) were located only in layer 3 of the lobula plate. These T4c,T5c,T4c,T5c neurons represent a four-cell clone produced by a single neuroblast.

(D) The *T5d-splitGal4* line labels mainly T5 neurons with axons in layer 4 of the lobula plate (T5d subtype) at the adult stage. Anti-DN-Cadherin (DN-Cad) labels the neuropils.

(E) T5 neurons are still present at the adult stage upon overexpression of *grain* with the *T5d-splitGal4* line. T5 neurons have axons in layer 3 of the lobula plate in this condition, consistent with T5d transforming into T5c subtype after gaining *grain* expression.

Table S1. Output information from the cellranger pipeline and additional information concerning the filtering for every dataset.

[Click here to Download Table S1](#)

Table S2. Parameters used for different steps of the scRNA-seq analysis.

[Click here to Download Table S2](#)

Mitochondrial Genes:

mt:ND2, mt:tRNA:Trp-TCA, mt:tRNA:Tyr-GTA, mt:Col, mt:Coll, mt:ATPase8, mt:ATPase6, mt:Colll, mt:tRNA:Gly-TCC, mt:ND3, mt:tRNA:Ala-TGC, mt:ND5, mt:ND4, mt:ND4, mt:ND6, mt:Cyt-b, mt:ND1, mt:tRNA:Leu-TAG, mt:lrrRNA, mt:srRNA, mt:ori, mt:tRNA:Ile-GAT, mt:tRNA:Cys-GCA, mt:tRNA:Lys-CTT, mt:tRNA:Arg-TCG, mt:tRNA:Ser-TGA, mt:tRNA:Val-TAC

Heat Shock Proteins:

Hsp70Aa, Hsp70Ab, Hsp70Ba, Hsp70Bbb, Hsp70Bb, Hsp70Bc, Hsp68, Hsp83, Hsp67Bc, Hsp26, Hsp67Ba, Hsp23, Hsp27, Hsp60A, Hsp60D

Male-specific Genes:

lncRNA:roX1, lncRNA:roX2

Differentially Expressed Genes:

5-HT1A, AANAT1, ab, Adk1, ana, app, AstC-R2, beat-Ila, beat-IIIb, beat-IV, beat-VI, bi, bnb, Btk29A, Ca-alpha1T, Cad87A, Ccn, CG10384, CG11191, CG11319, CG12643, CG13739, CG14340, CG15236, CG15765, CG1688, CG17124, CG17716, CG17839, CG2016, CG2082, CG2269, CG30015, CG31221, CG31324, CG31637, CG31676, CG31690, CG31760, CG32204, CG32206, CG32333, CG32432, CG33143, CG33543, CG33639, CG34347, CG34353, CG34355, CG34377, CG34383, CG3655, CG42339, CG42541, CG42817, CG4341, CG43427, CG43729, CG43778, CG43902, CG45263, CG4546, CG6006, CG6959, CG7991, CG8861, CG9331, CG9628, CG9932, cmpy, comm, Con, dac, DIP-theta, dpr10, dpr11, dpr16, dpr2, dpr3, dpr6, dpr8, drl, Drl-2, Dscam3, Dscam4, ed, Fas2, Fili, fred, Frq1, Fur1, fz2, Gadd45, GILT1, glec, Grd, grn, hig, Hs3st-A, igl, jus, kek1, kek2, kek3, klg, kuz, Lac, lncRNA:CR44978, mAChR-B, mav, mgl, mspo, Nlg3, nolo, Nost, NPFR, Oatp26F, Octalpha2R, Octbeta2R, osp, Pde1c, Pde6, Pgant2, pHCl-1, pros, Ptp10D, PVRAP, px, rad, RapGAP1, Rgk2, robo2, robo3, sano, Scgdelta, sdk, Sf3b6, Shawl, side, side-II, side-III, side-IV, side-V, SKIP, SLO2, Slob, SPR, sty, Svil, Tet, TfAP-2, Tl, Toll-6, Toll-7, Trim9, TrissinR, twit, twz, zld

Table S3. Genes used for filtering the datasets and genes identified during the differential gene expression analysis.

2.2 Manuscript 2

Title: Topographic maps differently influence growth patterns in subtypes of *Drosophila* direction-selective neurons

Authors: Aicha Haji Ali^{1,2,†}, **Nikolai Hörmann**^{1,2,†,*}, Nikolas Drummond¹, Cemre Coskun^{1,2}, Melisa Özmen¹, Jesús Pujol-Martí¹ and Alexander Borst¹

1: Department of Circuits – Computation – Models, Max Planck Institute of Neurobiology, 82152 Martinsried, Germany.

2: Graduate School of Systemic Neurosciences, Ludwig-Maximilians-Universität München, 82152 Martinsried, Germany

†: These authors contributed equally

*: Author for correspondence: nikolai.hoermann@bi.mpg.de

Author contributions: Conceptualization: **N.H.**, A.H.A, J.P.M., A.B., Data curation: A.H.A., **N.H.**, Formal Analysis: A.H.A, **N.H.**, N.D., C.C., M.Ö., Funding acquisition: A.B., Investigation: A.H.A., **N.H.**, J.P.M., C.C., M.Ö., Methodology: **N.H.**, A.H.A, N.D., Project administration: **N.H.**, A.H.A, Resources: A.B., Software: **N.H.**, A.H.A, N.D., Supervision: A.B., J.P.M, Validation: **N.H.**, A.H.A, N.D., Visualization: A.H.A, **N.H.**, N.D., Writing original draft: **N.H.**, A.H.A, Writing review and editing: **N.H.**, A.H.A, N.D., C.C., M.Ö., J.P.M., A.B., (order according to contribution)

Personal contributions in detail:

For this manuscript, I built the microscope and established *ex vivo* time lapse imaging in the lab. I performed experiments collecting time lapse imaging data of growing T4 neurons. I conducted control experiments using immunohistochemistry of different stages during development. Furthermore, I contributed major part to the software of the preprocessing pipeline. I lead the study design, coordinated the project to a big extend and was part of data curation. I wrote the original draft and reviewed as well as edited it over several iterations.

Topographic maps differently influence dendritic growth patterns in subtypes of *Drosophila* direction-selective neurons

Aicha Haji Ali^{1,2†}, Nikolai Hörmann^{1,2*†}, Nikolas Drummond¹, Cemre Coskun^{1,2}, Melisa Özmen¹, Jesús Pujol-Martí¹ and Alexander Borst¹

¹Circuits-Computation-Models, Max Planck Institute for Biological Intelligence, Martinsried, Germany.

²Graduate School of Systemic Neurosciences, Ludwig-Maximilians-Universität, München, Germany.

*Corresponding author. E-mail: nikolai.hoermann@bi.mpg.de;

†These authors contributed equally to this work.

Abstract

The complex morphological patterning of dendrites during development depends on a combination of contact-dependent interactions between extrinsic and intrinsic proteins as well as signaling molecules. In this work we use the *Drosophila* motion-sensing neurons (T4) as a model for dendritic development. There are 4 subtypes (*a*, *b*, *c*, and *d*) of T4 neurons which each respond preferentially to one of the four cardinal directions. Their dendrites are directional and oriented opposite to their preferred direction of motion. To investigate the dendritic pattern formation, we used an *ex vivo* time lapse imaging approach to observe single T4 dendrites during development. We first established a quantitative framework utilizing a set of metrics for the morphological characterisation of adult T4 dendrites to precisely describe their structure. By applying this set of metrics to developing T4 dendrites, we found them to be indistinguishable at 36 hours after pupa formation (hAPF). At around 48 hAPF, our results clearly identify horizontal (*a*, *b*) and vertical (*c*, *d*) subtypes. Additionally, we could further separate the horizontal subtypes into *a* and *b* based on their directional growth at 57 hAPF. The different subtypes show varying growth patterns which indicate an elongation of the topographical map in the dorso-ventral direction of the neuropil. Finally, the growth pattern of horizontal subtypes follows a sequential order from the proximal to the distal synaptic compartments of T4 dendrites which might be based on the synaptic wiring following the synaptotrophic hypothesis.

Introduction

Dendrites have some of the most complex branching structures observed in nature [1]. Additionally, the developmental process to build dendrites is highly variable when comparing the branches of neurons from the same cell type across individual animals [2]. Nevertheless, neuronal circuits formed by variable dendrites and axons are still able to perform the same computations in different animals, indicating a robust process underlying neuronal development and dendrite formation [3].

The studies of dendritic development so far have discovered basic growth rules such as tiling, space filling and self-avoidance [4–7]. The mechanism behind self-avoidance, especially, has been well studied, showing that the genes responsible in different species have large varieties of splice isoforms, such as *Drosophila Dscam1*. It mediates the repulsion upon homophilic interaction between *Dscam1* transmembrane proteins [8].

Proprioceptive sensory neurons in *Drosophila* larvae showed that transcription factors, such as *hamlet*, can change the general shape of the dendrite to have more branches if *hamlet* is not expressed or less branches, if it is [9]. Other proteins, such as *Dlic* controlling vesicle transport or *Rab5*, a phosphatase, have also been shown to influence the branching pattern of dendrites [10].

The process of dendritic development is highly dynamic with filopodia growing and retracting constantly [11–13]. Recent studies in the *Drosophila* larvae have advanced our understanding in dendritic branching during development. They showed how proprioceptive sensory dendrites form larger branches first and afterwards add smaller ones to fill the space in between to reach their mature shape [12]. With this current research some basic principles of dendritic development have been uncovered. However, the influence of topographic maps in the context of dendritic development and patterning have not been understood so far.

In this work we are utilising the first motion-sensing neurons (T4) in *Drosophila melanogaster* to investigate how the anisotropic columnar shape of the medulla layer 10 (M10) influences directional growth patterns. T4 cells are located in the optic lobes of *Drosophila* (Fig.1A). More specifically, they have their dendrites in M10 and can be divided into four subtypes based on gene expression [14, 15], function [16] and morphology [17, 18]. Functionally, they each respond to one of the cardinal directions, which is their preferred direction of motion [16]. Accordingly, their axons arborise in one of the four layers of the lobula plate, depending on the subtype (Fig.1A).

T4 subtypes are already genetically identifiable right after the last division of their progenitor ganglion mother cell at the L3 stage of development. Afterwards, they send out neurites to the medulla in waves along the dorso-ventral axis to innervate M10. The waves of neurites arrive in a temporal gradient from anterior to posterior [19]. In the retinotopic map of the medulla, the dendrites grow in the direction opposite to their preferred direction as shown in electron microscopy (EM) reconstructions [17]. This finding has been further strengthened by the distribution of synapses from different presynaptic partners in

distinct compartments, proximal, central and distal, which is aligned with the dendritic orientation [20]. In order to compute the direction of motion, a single T4 cell needs to integrate input from these three compartments [17, 18, 21, 22].

From a developmental point of view, the motion vision circuit in *Drosophila* presents multiple challenges. The dendrites do not tile as previously observed in neurons [6, 12]. Instead they have substantially overlapping receptive fields. The subtypes each need to grow towards one of the four cardinal directions in the same extracellular space, while their branches form synapses with different presynaptic partners dependent on the dendritic compartment [17, 18, 20]. At the same time all of the inputs are available in every column [17, 18]. Altogether, the correlation of dendritic orientation with the T4 subtype allows for the investigation the effect of the M10 topographic map on dendritic growth patterns during development.

To address this question, we provide a framework to analyse light microscopy (LM) data of fixed samples and *ex vivo* time-lapse imaging data in a quantitative manner. We use it to describe the growth patterns in T4 neurons of *Drosophila*. First, we define a set of metrics that describe the adult dendrite. We show that T4 subtypes in the adult are similar in shape and size. Their directionality, however, is quite different and can be used as the main characteristic to distinguish between them. Second, we use two-photon time-lapse imaging to follow the dendritic development of individual T4 neurons in the pupa brain. We show that the method adapted from a previous study [23] can follow the growth of dendrites for at least 20 hours. Next, we could separate the dendrites into the horizontal and vertical subtypes based on elongation. Horizontal subtypes could be further subdivided into T4a and T4b based on their directionality. Horizontal and vertical subtypes show different growth patterns which could be linked to the shape of the receptive field and the anisotropic topographic map of M10 arranged in a hexagonal pattern.

Results

Morphological characteristics of adult T4 neurons

In order to describe the growth pattern of T4 neurons, the first direction-selective neurons in the *Drosophila* visual system, we defined a set of quantitative metrics that describe the dendrites in the adult. For this reason, we collected images of single T4 neurons. The z-projections of individual T4 neurons from each subtype (Fig.1B) show the general structure of the dendritic tree. The entry point (see Materials and Methods 2) was assigned manually and labels the first branching point of the neurite entering the medulla. The images were pre-processed (see Materials and Methods 2) and rotated to have the same anatomical coordinates. We first measured size descriptors of the dendrite such as the volume (Fig.1C). While it is variable across dendrites it did not show a clear difference between subtypes. Next, we determined convex hull area based on the z-projection (Fig.1D). This metric estimates dendritic growth by measuring the area covered within M10. While subtypes T4c and

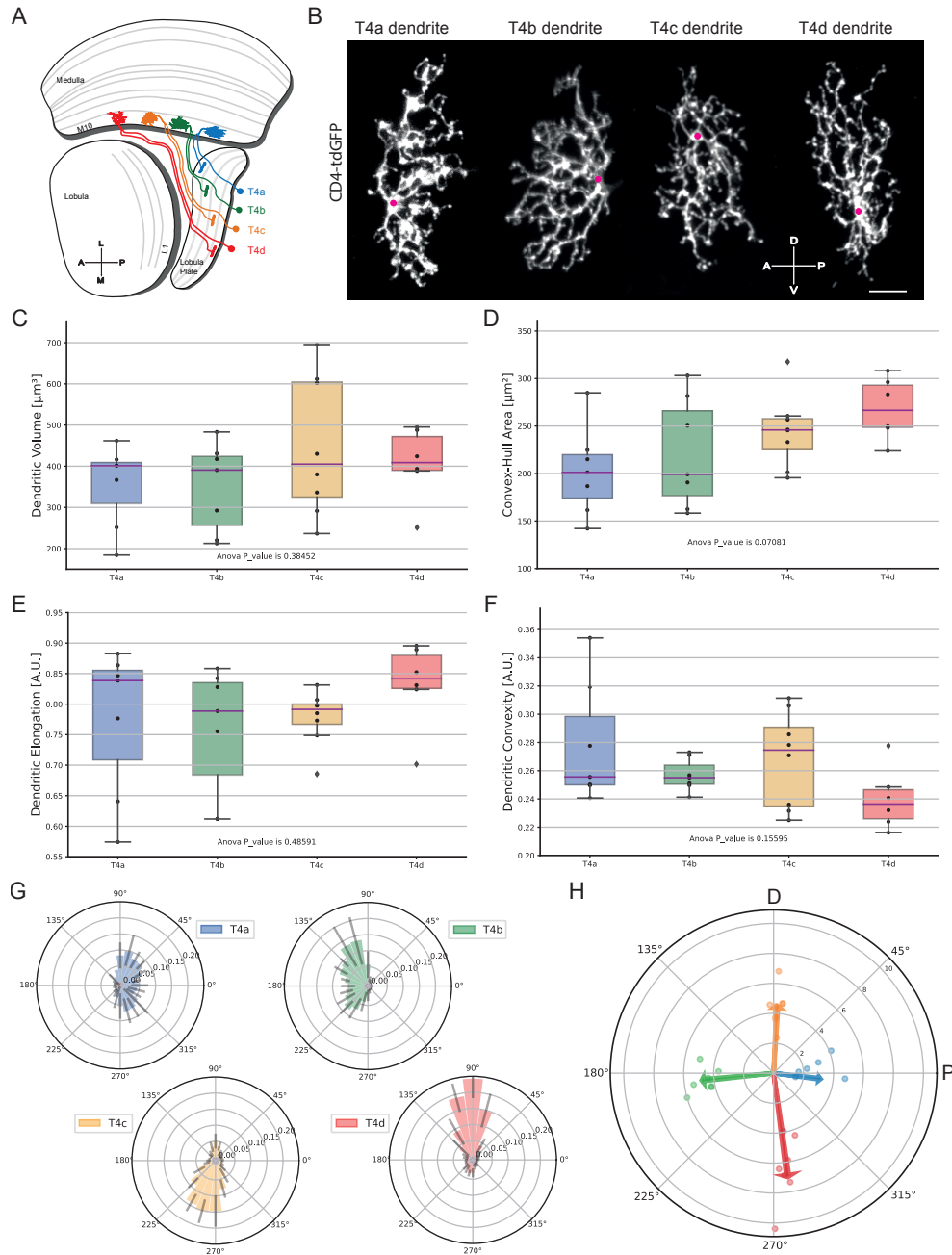


Fig. 1 Morphological analysis of adult T4 dendrites: (A) Illustration of a horizontal view for an adult optic lobe showing example neurons for the four T4 subtypes (*a*, *b*, *c* and *d*) in blue, green, orange and red, respectively. (B) Representative dendrite images of single-labelled adult T4 neurons from each subtype. The magenta dot indicates the dendritic entry point into M10 “Entry Point”. (C-F) 3D dendritic volume, 2D area of the convex-hull, convexity and elongation, respectively, for the adult T4 dendrites separated by subtype T4*a* (blue; $n=7$), T4*b* (green; $n=7$), T4*c* (orange; $n=8$) and T4*d* (red; $n=6$). The dark purple line indicates the median. (G) Polar histograms showing the average distribution of the normalized count of fluorescent pixels around the Entry Point (indicated by magenta dot at the center) for the different T4 subtypes (*a*, *b*, *c* and *d*) from left to right, respectively. Posterior side is considered to be 0° , and dorsal side is considered to be 90° . Error bars show \pm one standard deviation. (H) Dendritic orientation based on principle component analysis (PCA). Individual dots represents individual neurons, and arrows represents the mean of each subtype; M10, medulla layer 10; L1, lobula layer 1; L, lateral; M, medial; A, anterior; P, posterior; D, dorsal; V, ventral; A.U., arbitrary unit.

T4d have a slightly bigger convex hull area, overall they are not significantly different. Together these metrics for size show a higher variability and cannot be used to distinguish between T4 subtypes. In order to estimate how complex the dendrite is concerning the branch structure, we use convexity (see Materials and Methods 2) to compare the perimeters of the convex hull and the dendrite. If the dendrite has many branches (Fig.1B) the perimeter of the dendrite would be a lot larger compared to the perimeter of the convex hull. A small value close to zero, thus, indicates a more complex object in terms of its shape, which would translate to a dendrite that has a more elaborate branching pattern. The convexity value of the different subtypes is quite low showing that the dendrites are complex in terms of branching structure (Fig.1F). The next metric examines the dendrite based on the position of the voxels (Fig.1E). We used the principle components of the binary image coordinates to find the 2-dimensional axes which best describe the variance within the image. These help us to measure the elongation of the dendrite (see Materials and Methods 2). Since they have the same receptive field according to the EM studies [17, 18] the elongation in the dorso-ventral direction is present in all dendrites (Fig.1E). The results (Fig.1A-F) are not able to distinguish between T4 subtypes but can be used to describe them collectively. Consequently, we want to include a metric that should show a difference as described before [15, 17, 18]. The main difference between T4 dendrites is the orientation. However, it is not trivial to calculate the orientation of dendritic branches for our LM data. We used the entry point of the T4 neuron into the medulla as a point of reference (Fig.1B). We first plotted the distribution of voxels based on their angle (Fig.1G). While we find variability between the dendrites as depicted by the error bars, a clear bias for the directionality of the dendrite emerged (Fig1G). This is in agreement with previous EM findings [17, 18]. Additionally, subtypes T4a and b are more broadly distributed along the main direction of growth, whereas subtypes T4c and d have more voxels aligned in their respective preferred direction. T4c and d also have more voxels in the opposite side of their main growth direction. We calculated the main direction of growth for each dendrite using principle component analysis (PCA) (Fig1H). Thereby, the preferred direction of growth is obvious for each subtype, respectively. Altogether, we defined a set of metrics to analyse the morphology of T4 dendrites based solely on LM images. Furthermore, the dendrites of all T4 subtypes are highly similar in most metrics. We have confirmed the main differences found in the EM reconstructions in our LM data and can utilise them to separate the subtypes. These experiments provide the foundation to further investigate the development of T4 dendrites.

Dendritic growth of T4 neurons

In order to observe the growth of T4 dendrites, we implemented an *ex vivo* time lapse imaging (TLI) approach [23]. We built a custom-made two-photon microscope with two detection pathways in order to increase the signal-to-noise ratio in our imaging sessions (Fig.2A). We recorded an image stack every

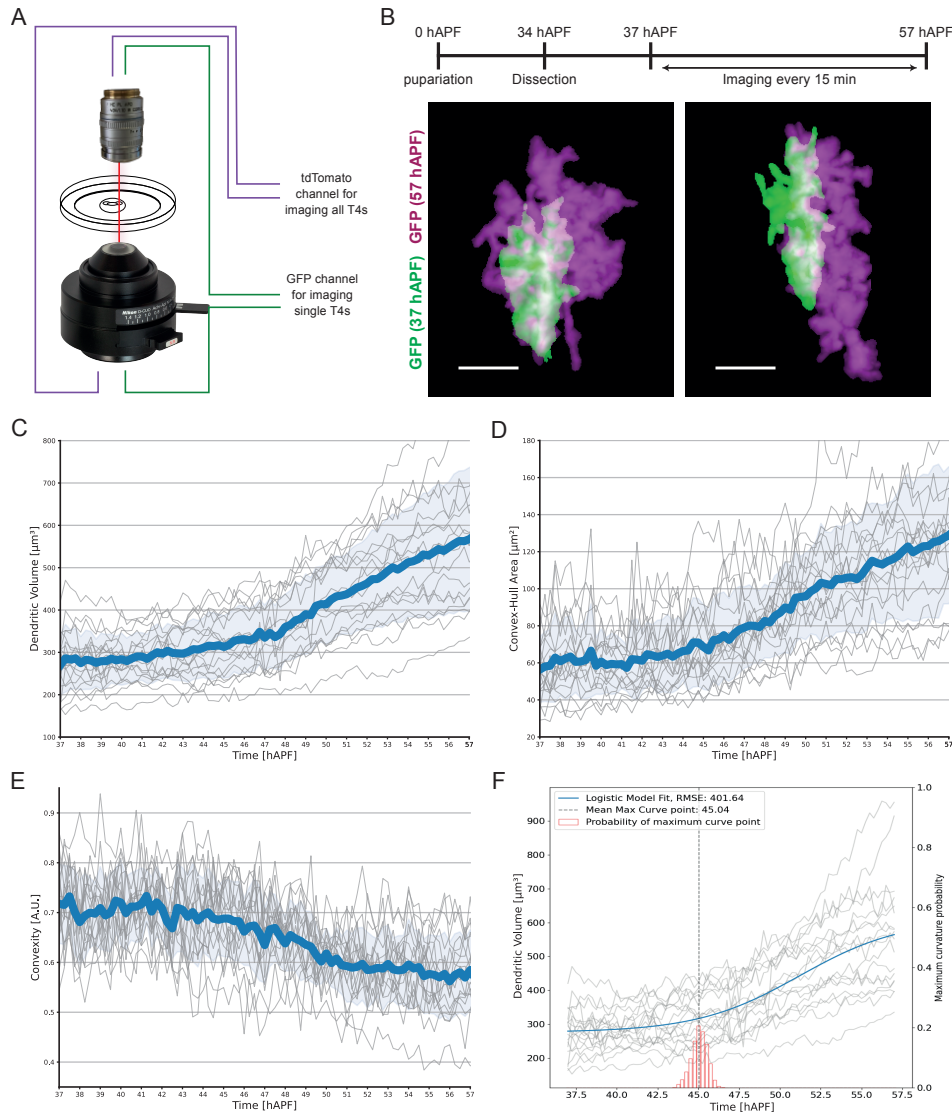


Fig. 2 *Ex-vivo* imaging of T4 dendrites shows non-linear growth during development. (A) Schematic of sample preparation and imaging settings. (B) Top: timeline for the sample preparation and imaging window. Bottom: two examples of overlay for neurons at the start (green) and after 20 hours at the end (violet) of time-lapse imaging. (C) 3D Volume in μm^3 of T4 dendrites in *ex-vivo* brains imaged over time from 37 hAPF until 57 hAPF ($n=18$). (D) 2D area in μm^2 of the bounding convex-hull for the same T4 dendrites, whose volume are shown in C. (E) Convexity value of the same T4 dendrites. Data shows individual traces with the mean (blue bold line) \pm standard deviation (shaded area). (F) 3D Volume in μm^3 of T4 dendrites as in C with the logistic model fit in blue. The histogram in red shows the probability distribution found using a permutation procedure for finding the time-point with the maximum curvature in the model fit (see Materials and Methods).

15 minutes to observe the dynamic process of dendritic development. Previous results assume the start of the dendritic growth to be at around 36 hours after pupa formation (hAPF) [15]. The timeline for the TLI experiment was arranged accordingly (Fig.2B). We were able to continuously record a single brain for at least 20 hours. Subsequently, the data was pre-processed to obtain single neurons for analysis (see Materials and Methods 2/2).

First, we wanted to prove that neurons grow similarly to previously published data validating our method and analysis. The z-projections of two example neurons at their starting point at 37 hAPF in green and at the end of the imaging session at 57 hAPF in magenta (Fig.2B) show a clear increase in size between the two time points. To quantify their growth we used the same metrics for size as in the adult. Starting with the volume, the increase in the beginning is moderate (Fig.2C). Fixed tissue samples revealed previously that the dendritic growth of T4 neurons is linear between 36 hAPF and 60 hAPF [15]. However, the temporal resolution for the fixed tissue samples were twelve hours. In comparison, our TLI data with a temporal resolution of 15 minutes allows us to fit a logistic function to the growth curves (Fig.3F). This reveals a non-linear fit is the best with the lowest root mean square error (Supp.Fig.1). Through permutation testing (see Materials and Methods 2), the first inflection point reveals that there is an increase in growth rate at around 45 hAPF (Fig.2F).

The convex hull area of the z-projection also increases throughout duration of the experiment, doubling in size from the beginning to the end (Fig.2D). The convexity starts with a higher value at the beginning of our TLI (Fig.2E). This means that the dendrite is not as intricate in structure, yet (Fig.2B). The shape changes during development with the extension of filopodia and branches. This is highlighted especially around 45-49 hAPF suggesting an increase in complexity that is maintained till the end of our experiment (Fig.2E). Comparing the values for convexity to the adult, it does not reach the elaborate dendritic branching in the course of our experiments. Nonetheless, our experiments show a non-linear growth for T4 dendrites in multiple metrics opposite to previous findings using only fixed tissues [15]. This increase in growth rate at around 45 hAPF could be evidence for specific growth phases during development.

We compared the values of these three metrics for the T4 dendrites at 57 hAPF of the TLI data to T4 dendrites in fixed samples at 54 hAPF and to adult data. The volume of TLI dendrites at 57hAPF is significantly larger than that of the fixed pupal control samples. However, this is likely due to the different axial resolutions used between the confocal and two-photon microscopes. Especially since the convex-hull area values are similar between the TLI samples at 57 hAPF and fixed tissue controls at 54 hAPF, where the z-axis is not considered (Supp. Fig.2).

Subtype-specific characteristics of T4 dendrites during development

All dendrites grew at a similar rate in our experiments. However, the previous metrics (Fig.2) do not divide the dataset into clusters of individual T4 subtypes. However, we noticed that some neurons grew more circularly, while others became more elongated by the end of the imaging session at 57 hAPF (Fig.2B). We wanted to see if these two types of growth corresponded to specific T4 subtypes. In order to identify the individual subtypes, we first used the approach of measuring the axon position of each neuron in the lobula plate

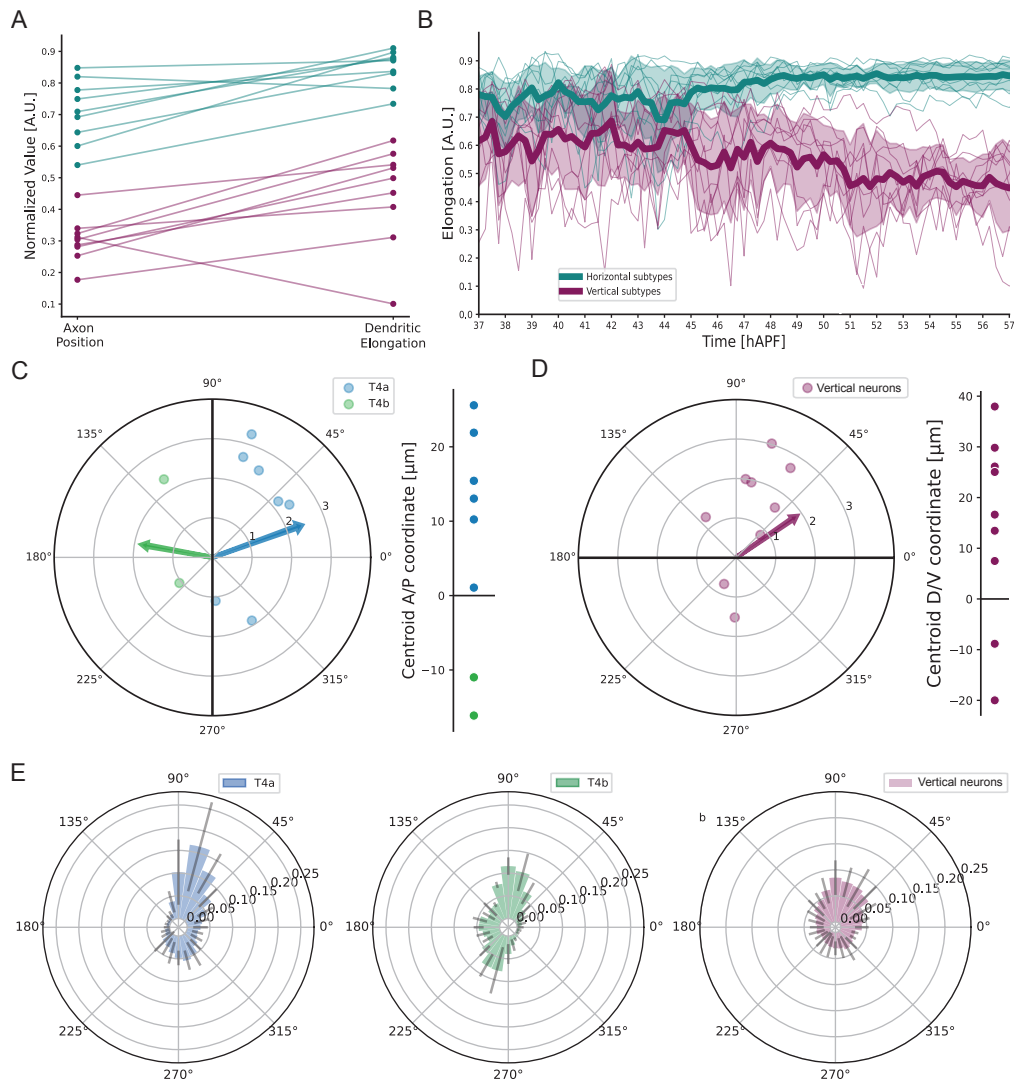


Fig. 3 T4 subtypes can be identified based on their dendritic morphology at 57 hAPF. (A) clustering of T4 neurons ($n=18$) at 57 hAPF after being imaged *ex-vivo* for 21 hours based on their relative axon position and dendritic elongation. (B) Dendritic elongation of T4 dendrites in *ex-vivo* brains imaged over time from 37 hAPF until 57 hAPF for horizontal subtypes ($n=9$) and vertical subtypes ($n=9$). Data shows individual traces with the mean (bold line) \pm standard deviation (shaded area). (C) Left: Polar plot of dendritic centroid to EP angle for T4a (blue; $n=7$) and T4b (green; $n=2$). The thick line represents the line of separation along the preferred growth axis. Right: the dendritic centroid distance from the EP along the preferred growth axis (A/P for the horizontal T4s) (D) Left: Polar plots of dendritic centroid to EP angle for vertical neurons (T4c and T4d) ($n=9$). Right: the dendritic centroid distance from the EP along the preferred growth axis (D/V for the vertical T4s). (E) Polar histograms showing the average distribution of fluorescent pixels around the Entry Point (indicated by magenta dot at the center) for the different T4 subtypes (a, b, c and d) from left to right, respectively. Posterior side is considered to be 0° , and dorsal side is considered to be 90° . Data is mean \pm standard deviation [A.U.]; P, posterior; D, dorsal; A/P, Anterior/Posterior axis; D/V, Dorsal/Ventral axis; A.U., arbitrary unit; EP, Entry Point. Individual thin lines represents individual neurons, thick lines represents the mean, and the shaded areas represents \pm one standard deviation from the mean.

to determine its subtype [15]. The thickness of the lobula plate layers during development and the larger z-step did not allow for the unequivocal identification of all T4 subtypes. Nevertheless, we were still able to distinguish between horizontal (a, b) and vertical (c, d) system neurons. We found that at the end of the imaged time window (57 hAPF), the dendrite elongation also separates the dataset into horizontal and vertical neurons (Fig.3A). We confirmed this result using fixed tissue samples at 54 hAPF (Supp.Fig.3B). This separation allowed us to divide the subtypes into pairs of two using only the value of dendritic elongation. In the following, we investigated when the dendritic elongation separates horizontal subtypes from vertical ones in the developmental process (Fig.3B). From 48 hAPF onward the horizontal subtypes become significantly different from the vertical ones. From this, we concluded that horizontal subtypes can be differentiated from vertical subtypes solely based on their dendritic elongation as early as 48 hAPF.

As mentioned before, individual subtypes could not be identified in our TLI dataset based on their axon position. However, we tested if we could identify them at 57 hAPF based on their dendritic orientation. The previous metric that we used for orientation in adult dendrites did not work (Supp.Fig.3C). This could be due to the circular shape of the vertical neurons or because the neuron’s dendritic field at this pupa age is different from the adult dendritic field. Therefore, we postulated that the centroid to entry point angle should still lean towards the preferred direction of growth for each dendrite according to its subtype. Therefore, we tested if we can separate the neurons into their 4 individual subtypes using this angle. We compared the dendritic orientation of horizontal (Fig.3C) and vertical (Fig.3D) subtypes separately. T4a and b show a clear directional bias in both the directional metric and the distribution of voxel angles from the entry point (Fig.3C and Fig.3E) based on what we would expect from the adult data. T4a and b subtypes resemble their adult counterparts more closely, allowing us to assign them accordingly. Both show a larger number of voxels in the dorsal direction (Fig.3E). Next, we compared the coordinates of the centroid along the main direction of growth with respect to the adult. For T4a and b, it corresponds to the x-axis (Fig.3C). The position relative to its entry point for these neurons distinguished T4a from T4b (Fig.3C). T4a has its x-coordinate leaning posterior relative to its entry point, while T4b is the opposite (Fig.3C). We also confirmed these results with fixed tissue samples at 54 hAPF (Supp.Fig.3D).

For the vertical system neurons, the orientation can separate the dataset based on the midline (Fig.3D). We used fixed tissue samples at 54 hAPF as controls, to obtain a higher resolution images in the lobula plate and determine the identity according to the layer of axon arborization. The centroid position relative to the entry point along the y-axis in the fixed samples show a variable orientation and do not allow us to classify the neurons as either c or d subtypes (Supp.Fig.3E). The distribution of voxels based on their angle (Fig.3E) also does not identify clearly with the adult distribution of either c or d subtypes. In conclusion, we managed to separate our data into horizontal and vertical

subtypes of T4. While *a* and *b* subtypes can be identified using only dendritic growth metrics in our TLI experiments (Fig.3E) subtypes *c* and *d* are harder to distinguish. Nevertheless, we find differences in orientation within the vertical T4 population.

Growth patterns of T4 dendrites

Next we analysed the growth patterns of horizontal and vertical subtypes. One growth metric is the centroid of the dendrite over time. We use the centroid of the first time point as our point of reference. First, we analyzed how the centroid shifts during development (Fig.4A-D). Individual dendrites of the horizontal subtypes (Fig.4A-B), first divide into groups growing either more dorsally or more ventrally. In the course of the experiments they slowly grow towards their main direction of growth as seen in the adult. We separated the vertical subtypes based on the growth direction along the dorso-ventral axis. Together, the vertical subtypes do not have as much of an orthogonal spread to their main orientation in the dorso-ventral axis. They grow more uniformly in either the dorsal or ventral direction. Interestingly, the last time points show that the centroid is moving into the opposite direction in each trajectory.

Taking a closer look at the movement of the centroid in the main direction of growth, we separated the movement of the centroid in the x- and y-axis (Fig.4E-F). The growth of T4*a* and *b* along the dorso-ventral axis does not show a clear bias in any direction but maintains its position very close to the position of the first time point where the dendrite is still mono columnar (SuppFig.4A). Focusing on the main direction of growth based on the adult dendrites, the horizontal subtypes at first don't grow in this direction until around 46 hAPF, which coincides with the change in growth rate. The centroid just moves around in the same area for the first few hours. After 46 hAPF the separation between subtypes becomes clear when considering the centroid position. This trend continues till the last time point (Fig.4E). For the vertical subtypes, the trajectory of the dendrite in the antero-posterior axis is biased towards the posterior for most neurons (Supp.Fig.4B). In the dorso-ventral axis neurons grow either dorsally or ventrally from 40 hAPF onward. In the last few time points it appears as if the centroid is starting to move into the opposite direction again (Fig.4F). The movement of the centroid can not be attributed to a retraction of branches since the absolute size of the dendrite does not change (Fig.2C-E). This means that the dendrite is first stabilizing its branches in one direction and afterwards extending neurites in the opposite direction.

Altogether, the horizontal subtypes divide into two groups which grow either first dorsally or ventrally independent of subtype. Afterwards they follow the expected growth direction. Vertical subtypes in comparison can be grouped into two groups that have opposing growth directions along the dorso-ventral axis. Furthermore, there seems to be a change in growth direction for vertical subtypes in the final part of our experiment. In conclusion, horizontal and

vertical subtypes follow different growth patterns during development, even though they need to fill the same receptive field.

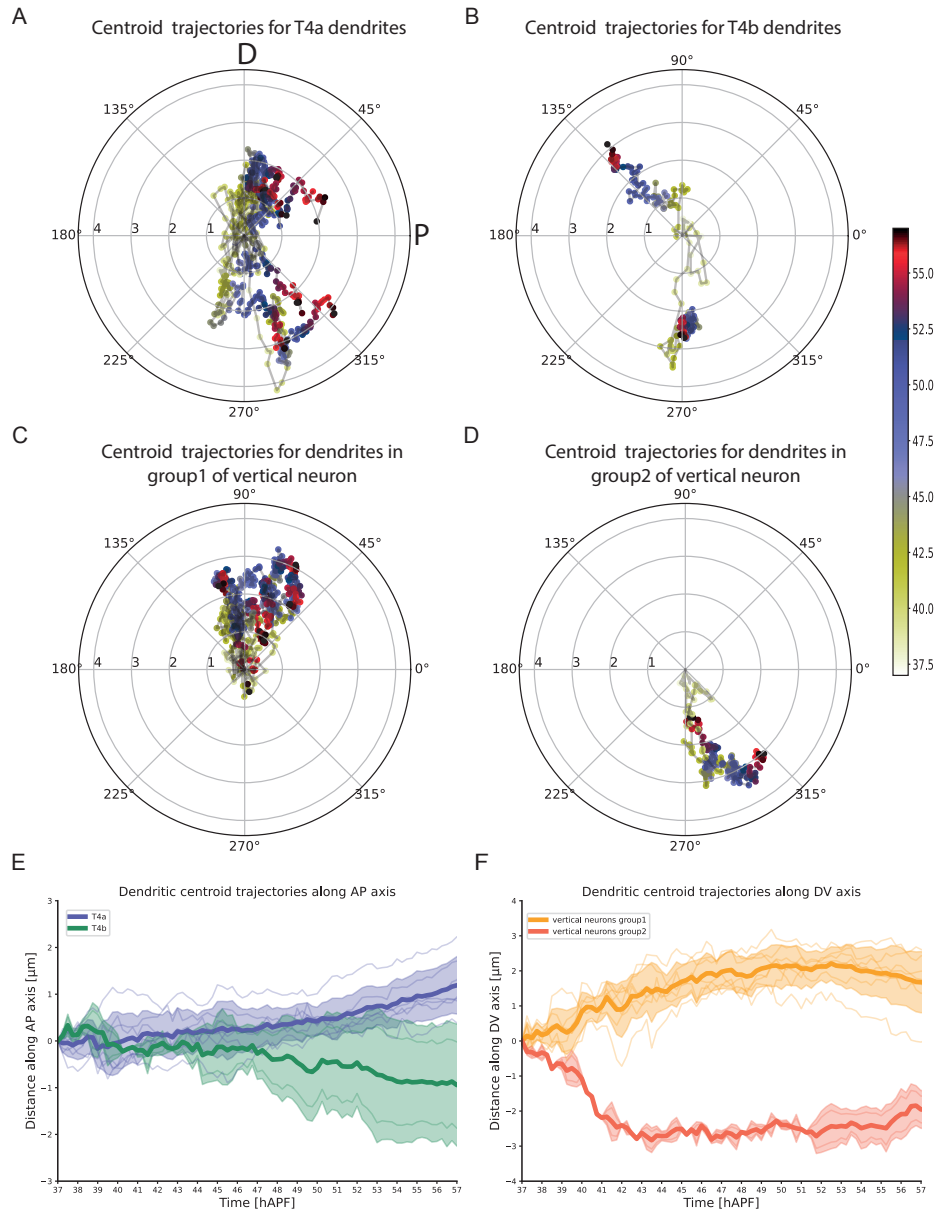


Fig. 4 Directional growth of T4 dendrites. (A-D) Trajectories of dendritic centroid over time for T4a ($n=7$), T4b ($n=2$), vertical neurons group 1 ($n=7$) and vertical neurons group 2 ($n=2$), respectively. Individual grey lines represent individual neurons. The dots' colors correspond to time (hAPF) as indicated by the color scale. (E) Shift in the centroid coordinate in μm along the posterior-anterior axis for T4a and T4b. Positive values correspond to shift toward the posterior side. (F) Shift in the centroid coordinate in μm along the dorsal-ventral axis for vertical neurons. Positive values correspond to shift toward the dorsal side. Two types of shift could be identified. Individual thin lines represents individual neurons, thick lines represents the mean, and the shaded areas represents \pm one standard deviation from the mean.

Discussion

Here, we investigated the dendritic development of T4 neurons in the *Drosophila* pupa using *ex-vivo* time lapse imaging. We established a set of metrics and used them to differentiate between T4 subtypes. Further, we investigated the growth patterns of horizontal and vertical subtypes in more detail by following the centroid of the dendrite over time and find different growth patterns between the T4 subtypes. Based on these results, T4 dendrites are not just filling their receptive field such as other neurons [12] but grow in a more elaborate way. They could potentially have two phases of growth during our experimental period, where in the first, they are searching in their vicinity and only stabilize branches in the second phase when they know the direction of growth based on external cue. Qualitative observations of the filopodia dynamics (data not shown) suggests the branches actively search for the next column to grow towards. This in turn could lead to the specific wiring sequence in the dendrite to compute the direction of motion [20, 22].

The classification of the vertical subtypes is not as easy, since their growth is more circular and does not show a clear bias in orientation. Their trajectory however, clearly separates them into two groups, growing either dorsally or ventrally first (Fig.3). This separation is also along the main direction of growth for the vertical subtypes. Additionally, they first grow into the one direction and towards the end of our experiment direct their growth in the opposite direction. This behaviour is interesting and could mean that changes in the temporal expression of certain genes lead to the dendrites redirecting their growth.

Another interesting characteristic is the transformation from a hexagonal to a square grid in the topographic map of M10 [17, 24, 25]. The ommatidia as well as the columns in the lamina and medulla are organised in a hexagonal fashion [26, 27]. This means that the lattice on which the T4 dendrites grow has three axis in contrast to the four subtypes which only calculate the direction of motion along two axis, horizontal and vertical [16]. Therefore, the information extracted along the horizontal axis does not come from points in space that follow a line, but the receptive fields of T4 need to be enlarged to calculate the direction of motion along the horizontal axis. This is reflected in the differences of growth we observed in the TLI data and in the adult shape of T4 neurons. The horizontal subtypes are elongated in the dorso-ventral axis, since columns in the horizontal axis are not arranged in a line but in a zigzag [18]. T4 dendrites need to extend more along the dorso-ventral axis, to get access to the same information. This is possibly one reason for the difference in width along the main direction of growth between the horizontal and vertical subtypes. Furthermore, the intrinsic elongation of the medulla columns [18] increases this bias even more.

For the dendritic development of T4 neurons, our results show that there are several steps. The dendrites of horizontal subtypes first stay within the orthogonal axis to their main growth. These branches correspond to the proximal region or the null side of the adult dendrite. This points towards the

dendrite first growing into the proximal receptive field [17, 20] and later extend towards the main direction of growth. Since the columnar structure of M10 does not show any apparent orientation, our results can be interpreted that the dendrites of T4 neurons first search for signals that could correspond to the input neurons on the null side. This includes Mi4, CT1 and C3 cells [17, 18]. This could be an indicator for the synaptotrophic hypothesis, where synaptic partners are necessary to stabilise dendritic branches [28–30].

Time lapse imaging of a later point of dendritic development could show if this is indeed the case. Moreover, it will be possible to use this information in the search of candidates for the molecular mechanism of directed growth. Taken together, our results show a time dependent growth pattern for T4 dendrites during development, which is likely guided by the topographical map of the medulla.

Materials and Methods

Drosophila stocks

Except when indicated, flies were raised on standard cornmeal agar medium at 25°C and 60% humidity with 12h light/dark cycle. All images of adult brain were obtained from female flies, while pupal images were from a mix of male and female flies. The following fly strains were used for obtaining all the pupal brain images: R42F04-Gal4 (BDSC: 41253), UAS-CD4-tdTomato (BDSC: 35837), UAS-*frt-stop-frt*-CD4-tdGAP ([31]), *hsflp-2-PEST* (BDSC: 62118). (*hsflp-2-PEST*/Y or w+; UAS-*frt-stop-frt*-CD4-tdGAP/+; UAS-CD4-tdTomato/R42F04-Gal4) was the final genotype of the pupae that were dissected for obtaining the pupal brains. For producing the adult brain images, male flies that had *hsflp-2-PEST* on the X-chromosome and recombined T4/T5-splitGal4 (VT043077AD;R39H12DBD) with UAS-*frt-stop-frt*-CD4-tdGFP were crossed with CantonS flies resulting in offspring with the genotype (*hsflp-2-PEST*/Y or w+; VT043077AD, UAS-*frtSTOPfrt*-CD4tdGFP/+; R39H12DBD/+). For the pupal control brain images, MultiColor FlpOut (MCFO; BDSC:64085) approach [32] together with the SS00324-splitGal4 line were used ([15]). To obtain sparse labelling of T4 cells, 1 day old pupae or younger were heat-shocked for 3:30 (m:ss) in a 37°C water bath in case of the samples for pupal brains. While, 4 min heat-shock was used on pupae younger than 3 days for the adult brain samples.

Immunostainings and confocal imaging

Fly brains were dissected in cold PBST (Phosphate Buffered Saline) with 0.3% Triton X-100 (Sigma-Aldrich) and fixed in 4% paraformaldehyde in PBST at room temperature for 25 min for adult brains, or 20 min for pupal brains. Afterwards, the samples were washed several times using PBST and blocked using 10% NGS (goat serum; Sigma-Aldrich) or 10% FBS (Fetal Bovine Serum; Thermo Fisher Scientific) in PBST for 1 hour at room temperature. The block

solution was discarded, and the primary antibody mix in PBST with 5% NGS or FBS was added. The samples were incubated on a shaker at 4°C for 2 days. After washing the samples several times with PBST, the secondary antibody mix in PBST with 5% NGS or FBS was added, and the samples were incubated on a shaker at 4°C for 2 days. The samples were then washed several times using PBST over several hours before mounting them in SlowFade Gold Antifade Mountant (Thermo Fisher Scientific). Fixed tissue samples were imaged using Leica SP8 laser scanning confocal microscope equipped with 488-, 561- and 633-nm lasers, and using a 63× glycerol-objective. All samples, except the MCFO pupal controls, were imaged at 0.076µm pixel resolution in X and Y, and 0.4 in Z, which is the same resolution pixel resolution used for the Time-Lapse Imaging.

Explant Dissection and sample preparation

We used a modified version of the protocol described earlier [23]. The imaging chamber for TLI was a 60x15 mm metal petri dish with 4 cm hole in the center (made in house), and a glued 4 cm coverslip that had a 50 mm thin layer of Sylgard 184 (Dow Corning) in the center. The growth medium used was Schneider’s insect media (Thermo Fisher Scientific) . White pupae, right after pupariation (0 hAPF), were collected and transferred to a new tube. The sample was heat-shocked as explained before, and incubated at 25°C until (34 hAPF). For brain dissection, we used a growth medium that has been oxygenated for at least 45 minutes with a tube slowly pumping a mixture of 95% oxygen and 5% carbon dioxide. Dissection was conducted at room temperature using fine forceps (Fine Science Tools). Once the brain was dissected with the intact ventral nerve-cord, it was transferred into a 20ul droplet of 0.4% low-melting agarose in the growth medium in the center of the imaging chamber. Three 460 mm thick 1x0.2 cm silicon mold spacers were placed diagonally to prevent the coverslip from crushing the brain. Another 4 cm coverslip was gently added on top of the bottom one, and the sample was left for 25 minutes at room for the agarose to solidify. Afterwards, around 900 µl growth medium was added into the space in between the two coverslips using a 1 ml pipette, and the sample was sealed using glue (Marabu Fixogum). The sample was then left for 1 hour for the glue to dry before the sample was imaged with the two-photon microscope.

Two-photon time lapse imaging

We used a custom-built two-photon microscope equipped with a 5W-pumped Ti:sapphire laser (MaiTai, Spectra Physics) and resonant scanner (CRS 8 KHz; Cambridge Technology). We used 920 nm as the excitation wavelength for both imaging channels. A beam attenuator (Newport VA-BB-2- CONEX) was used to control the laser intensity. We used a 40x water immersion objective (Leica: 506357). Photons were focused onto the detectors using both, the objective and an oil-immersion condenser (Nikon D-CUO DIC Oil Condenser, 1.4 NA,

Male D3N Dovetail). We used two pairs of photomultiplier tubes "PMTs" (Hamamatsu). 560 DXCR dichroic mirrors and 525/50 and 607/70 emission filters were used to separate green and red fluorescence. The microscope was controlled with ScanImage SI 5.6 R1 (Vidrio Technologies).

Image registration

The 3D images from each TLI session were first registered to correct for any drift. Three steps of image registration were performed on the images of the red channel using Python (ver: 3.9.6) employing first Phase Correlation using Scipy package (ver: 1.6.1), Rigid registration and then the SyNRA method [33] registration using Antspy package (ver: 0.3.1). The resulting transformation matrix after each registration step was used to shift images from both the red and green channels. The accuracy of registration was inspected after each step manually by checking the images in Fiji software package [34]. In case some time frames in the 4D image time-series were misaligned after the registration, they were replaced with the original unshifted frames. After the last registration step, if there was still any jitter in the time-series images, the misaligned frames were shifted manually to ensure the drift was as minimal as possible. This final manual shift was needed in only three out of the 18 time-series used in this study.

Image denoising

Images of the red channel from TLI were denoised by performing a median filter in Python. While, images of the green channel were denoised in two steps. First, denoising was achieved by running a Noise2Void model [35], which was previously trained on representative images of the same type. Then, image contrast was enhanced by running 'Contrast Limited Adaptive Histogram Equalization' (CLAHE).

Data alignment across imaging sessions

Images of each neuron were cropped using Fiji and rotated to make the dorsal side on top, and anterior side on the left. The entry point of each neuron into the M10 layer was determined manually. Then, background in the images was subtracted using the Otsu-threshold [36]. Scipy.ndimage.label was used to create the binary images of the isolated neurons. These steps were performed on both the confocal images of the fixed tissues and the images generated by TLI.

Image analysis

The subtype identification based on the relative axon position in the lobula plate was performed as described in [15]. Custom-written python scripts were used for the rest of image analysis. Dendritic volume was calculated as the

number of value voxels in the binary 3D image stack multiplied by the pixel-to- μm resolution in each dimension (z, y and x) to get the volume in μm^3 . The dendritic centroid was also calculated from 3D binary images using the `regionprops` function from the `scikit-image` package. Maximum z-projection of the images were then calculated to convert the 3D stacks into 2D images, for which the convex-hull was calculated using `scikit-image regionprops`. The convex-hull area was calculated using the same function, and multiplied by the pixel-to- μm resolution in x and y to get the area in μm^2 . Convexity was calculated as the ratio of the perimeter for the convex-hull over the neuron's perimeter, which was calculated also using `scikit-image`. In order to calculate dendritic orientation and elongation, we used a modified version of the PCA method described in [37], where the covariance matrix was determined for the 2D z-projection of the binary images and its eigenvectors and eigenvalues were calculated. Dendritic elongation was calculated as the absolute difference between the two eigenvalues divided by the largest eigenvalue. In order to calculate orientation, we first calculated the angle (theta) of the eigenvector with largest eigenvalue. We then rotated the image by angle theta, and recentered it to the dendrite's entry point. The percentage of pixels residing on each side of each eigenvector was calculated. The dendritic orientation was the angle of the eigenvector side that had the largest fraction of pixels plus theta, and the distance was calculated as the distance of that fraction's centroid from the entry point. For determining the histogram distribution of the dendrite, the angles of vectors between each pixel and the entry point were calculated. The angles' distribution was binned then into 24 bins, and normalised to the total number of vectors.

Growth curve fitting

A range of models were fit to the time lapse imaging data, comparing the goodness of fit using the residual mean square error (RMSE). We find that growth is best fitted by a non-linear function, although the difference between Quadratic, Cubic, Exponential, and Logistic model fits is comparably small. Ultimately, an Logistic model was chosen due to its common use when investigating biological growth [38], and that it provided the best fit to our data. In order to define the point in time at which our growth metric maximally increase, we find the point of maximum curvature along our fitted exponential. This is defined as the point at which $y = f(x)$ is maximally distant from the linear vector between $[y_{x0}, y_{xn}]$. In the case of the Logistic function n is equal to the first inflection point along the fitted curve. In order to better understand the possible variability around this point, we perform a permutation procedure. This involves drawing ten neurons randomly from our sampled set of neurons, without replacement, and calculating the point of maximum curvature from the logistic model fit to the permuted sample. Once this process is repeated 10,000 times a distribution of the time point of maximum curvature is generated and normalised to give the probability density of maximum curvature over time (hAPF).

Acknowledgments

This project would not have been possible without the help of some people. First, Jürgen Haag, Joseph Donovan and Robert Kasper have helped us tremendously with the building of the two-photon microscope. Neset Özel showed us how to conduct the TLI experiments. Michael Drews, Sumit Vohra and Philipp Schubert have helped us with the preprocessing of the TLI data. Tabea Schilling supplied us with *Drosophila* lines. Georg Ammer has given us valuable feedback on the manuscript. Lastly, Robin Hiesinger has provided us with tools, given us helpful advice about the project throughout the years and reviewed the manuscript with constructive feedback. We would like to thank all people above and the Borst Lab for helpful feedback and discussions.

Author contributions

Conceptualization: N.H., A.H.A, J.P.M., A.B., Data curation: A.H.A., N.H., Formal Analysis: A.H.A, N.H., N.D., C.C., M.Ö., Funding acquisition: A.B., Investigation: A.H.A., N.H., J.P.M., C.C., M.Ö., Methodology: N.H., A.H.A, N.D., Project administration: N.H., A.H.A, Resources: A.B., Software: N.H., A.H.A, N.D., Supervision: A.B., J.P.M, Validation: N.H., A.H.A, N.D., Visualization: A.H.A, N.H., N.D., Writing original draft: N.H., A.H.A, Writing review and editing: N.H., A.H.A, N.D., C.C., M.Ö., J.P.M., A.B., (order according to contribution)

References

- [1] Ramón y Cajal, S., Sánchez, D. & Madrid, U. C. d. *Contribución al conocimiento de los centros nerviosos de los insectos* (Imprenta de Hijos de Nicolás Moya, Madrid, 1915). Pages: 1-180.
- [2] Hassan, B. A. & Hiesinger, P. R. Beyond Molecular Codes: Simple Rules to Wire Complex Brains. *Cell* **163** (2), 285–291 (2015).
- [3] Hiesinger, P. R. & Hassan, B. A. The Evolution of Variability and Robustness in Neural Development. *Trends in Neurosciences* **41** (9), 577–586 (2018).
- [4] Sugimura, K., Shimono, K., Uemura, T. & Mochizuki, A. Self-organizing Mechanism for Development of Space-filling Neuronal Dendrites. *PLOS Computational Biology* **3** (11), e212 (2007).
- [5] Lefebvre, J. L., Sanes, J. R. & Kay, J. N. Development of Dendritic Form and Function. *Annual Review of Cell and Developmental Biology* **31** (1), 741–777 (2015).
- [6] Dong, X., Shen, K. & Bülow, H. E. Intrinsic and Extrinsic Mechanisms of Dendritic Morphogenesis. *Annual Review of Physiology* **77** (1), 271–300 (2015).

- [7] Baltruschat, L., Tavosanis, G. & Cuntz, H. A developmental stretch-and-fill process that optimises dendritic wiring (2020). Pages: 2020.07.07.191064 Section: New Results.
- [8] Schmucker, D. *et al.* Drosophila Dscam Is an Axon Guidance Receptor Exhibiting Extraordinary Molecular Diversity. *Cell* **101** (6), 671–684 (2000).
- [9] Moore, A. W., Jan, L. Y. & Jan, Y. N. hamlet, a Binary Genetic Switch Between Single- and Multiple- Dendrite Neuron Morphology. *Science* **297** (5585), 1355–1358 (2002).
- [10] Corty, M. M., Matthews, B. J. & Grueber, W. B. Molecules and mechanisms of dendrite development in Drosophila. *Development* **136** (7), 1049–1061 (2009).
- [11] Williams, D. W. & Truman, J. W. Mechanisms of Dendritic Elaboration of Sensory Neurons in Drosophila: Insights from In Vivo Time Lapse. *Journal of Neuroscience* **24** (7), 1541–1550 (2004).
- [12] Ferreira Castro, A. *et al.* Achieving functional neuronal dendrite structure through sequential stochastic growth and retraction. *eLife* **9**, e60920 (2020).
- [13] Hogg, P. W., Coleman, P., Dellazizzo Toth, T. & Haas, K. Quantifying neuronal structural changes over time using dynamic morphometrics. *Trends in Neurosciences* **45** (2), 106–119 (2022).
- [14] Kurmangaliyev, Y. Z., Yoo, J., LoCascio, S. A. & Zipursky, S. L. Modular transcriptional programs separately define axon and dendrite connectivity. *eLife* **8**, e50822 (2019).
- [15] Hoermann, N. *et al.* A combinatorial code of transcription factors specifies subtypes of visual motion-sensing neurons in *Drosophila*. *Development* dev.186296 (2020).
- [16] Maisak, M. S. *et al.* A directional tuning map of Drosophila elementary motion detectors. *Nature* **500** (7461), 212–216 (2013).
- [17] Takemura, S.-y. *et al.* The comprehensive connectome of a neural substrate for ‘ON’ motion detection in Drosophila. *eLife* **6**, e24394 (2017).
- [18] Shinomiya, K. *et al.* Comparisons between the ON- and OFF-edge motion pathways in the Drosophila brain. *eLife* **8**, e40025 (2019).
- [19] Pinto-Teixeira, F. *et al.* Development of Concurrent Retinotopic Maps in the Fly Motion Detection Circuit. *Cell* **173** (2), 485–498.e11 (2018).

- [20] Fendl, S., Vieira, R. M. & Borst, A. Conditional protein tagging methods reveal highly specific subcellular distribution of ion channels in motion-sensing neurons. *eLife* **9**, e62953 (2020).
- [21] Haag, J., Arenz, A., Serbe, E., Gabbiani, F. & Borst, A. Complementary mechanisms create direction selectivity in the fly. *eLife* **5**, e17421 (2016).
- [22] Groschner, L. N., Malis, J. G., Zuidinga, B. & Borst, A. A biophysical account of multiplication by a single neuron. *Nature* **603** (7899), 119–123 (2022).
- [23] Özel, M. N., Langen, M., Hassan, B. A. & Hiesinger, P. R. Filopodial dynamics and growth cone stabilization in *Drosophila* visual circuit development. *eLife* **4**, e10721 (2015).
- [24] Ting, C.-Y. *et al.* Photoreceptor-Derived Activin Promotes Dendritic Termination and Restricts the Receptive Fields of First-Order Interneurons in *Drosophila*. *Neuron* **81** (4), 830–846 (2014).
- [25] Zhao, A. *et al.* Eye structure shapes neuron function in *Drosophila* motion vision (2022). Pages: 2022.12.14.520178 Section: New Results.
- [26] Sanes, J. R. & Zipursky, S. L. Design Principles of Insect and Vertebrate Visual Systems. *Neuron* **66** (1), 15–36 (2010).
- [27] Borst, A. Fly visual course control: behaviour, algorithms and circuits. *Nature Reviews Neuroscience* **15** (9), 590–599 (2014).
- [28] Vaughn, J. E., Henrikson, C. K. & Grieshaber, J. A. A quantitative study of synapses on motor neuron dendritic growth cones in developing mouse spinal cord. *Journal of Cell Biology* **60** (3), 664–672 (1974).
- [29] Vaughn, J. E., Barber, R. P. & Sims, T. J. Dendritic development and preferential growth into synaptogenic fields: A quantitative study of Golgi-impregnated spinal motor neurons. *Synapse* **2** (1), 69–78 (1988).
- [30] Cline, H. & Haas, K. The regulation of dendritic arbor development and plasticity by glutamatergic synaptic input: a review of the synaptotrophic hypothesis. *The Journal of Physiology* **586** (6), 1509–1517 (2008).
- [31] Han, C., Jan, L. Y. & Jan, Y.-N. Enhancer-driven membrane markers for analysis of nonautonomous mechanisms reveal neuron–glia interactions in *Drosophila*. *Proceedings of the National Academy of Sciences* **108** (23), 9673–9678 (2011).
- [32] Nern, A., Pfeiffer, B. D. & Rubin, G. M. Optimized tools for multicolor stochastic labeling reveal diverse stereotyped cell arrangements in the fly

visual system. *Proceedings of the National Academy of Sciences* **112** (22), E2967–E2976 (2015).

- [33] Rana, S. S., Ma, X., Pang, W. & Wolverson, E. *A Multi-Modal Deep Learning Approach to the Early Prediction of Mild Cognitive Impairment Conversion to Alzheimer’s Disease*, 9–18 (IEEE, Leicester, UK, 2020).
- [34] Schindelin, J. *et al.* Fiji: an open-source platform for biological-image analysis. *Nature Methods* **9** (7), 676–682 (2012).
- [35] Krull, A., Buchholz, T.-O. & Jug, F. *Noise2Void - Learning Denoising From Single Noisy Images*, 2124–2132 (IEEE, Long Beach, CA, USA, 2019).
- [36] Otsu, N. A Threshold Selection Method from Gray-Level Histograms. *IEEE Transactions on Systems, Man, and Cybernetics* **9** (1), 62–66 (1979).
- [37] Mudrová, M. & Procházka, A. *Principle component analysis in image processing* (Prague, 2005).
- [38] Tsoularis, A. & Wallace, J. Analysis of logistic growth models. *Mathematical Biosciences* **179** (1), 21–55 (2002).

Supplementary information

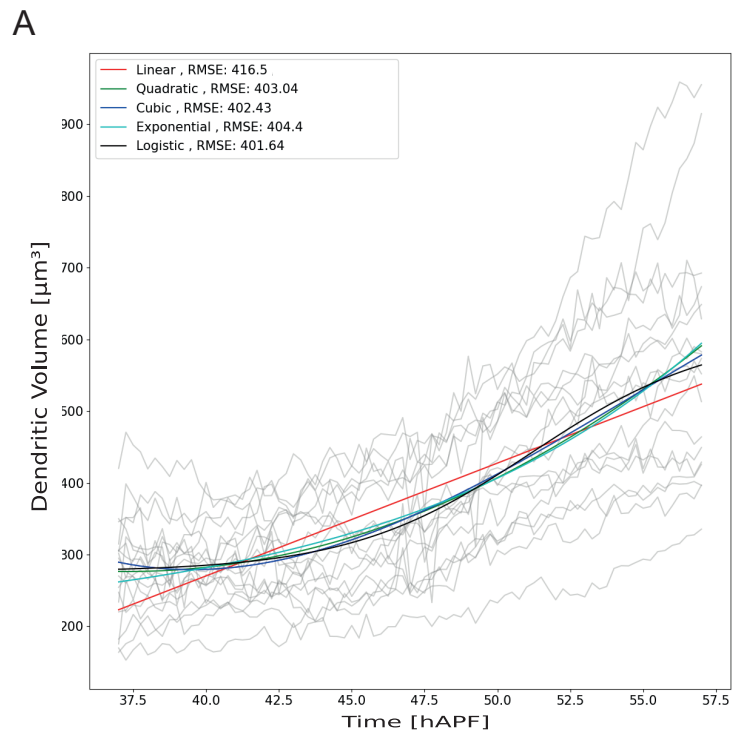


Fig. 1 Different model fits for T4 volumetric growth during Time-Lapse imaging. Grey lines are traces of individual neurons.

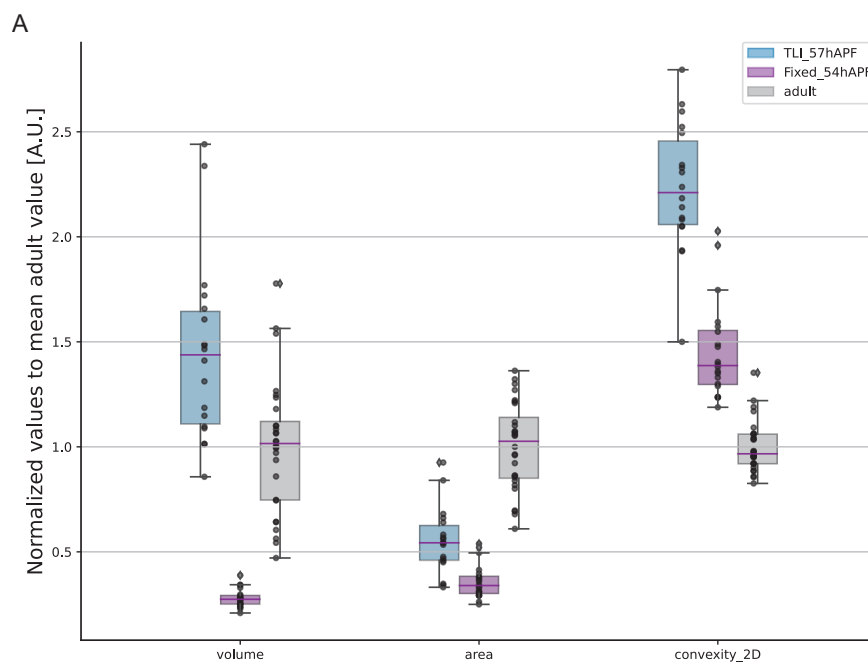


Fig. 2 Comparison of developing and mature T4 dendrites: Dendritic volume, convex-Hull area and convexity for T4 dendrites at the end of TLI sessions at 57hAPF (blue), in fixed tissues of 54 hAPF pupa brains, and in fixed adult brains. All values were normalized to the mean of the adult values. Dark violet lines indicates the medians.

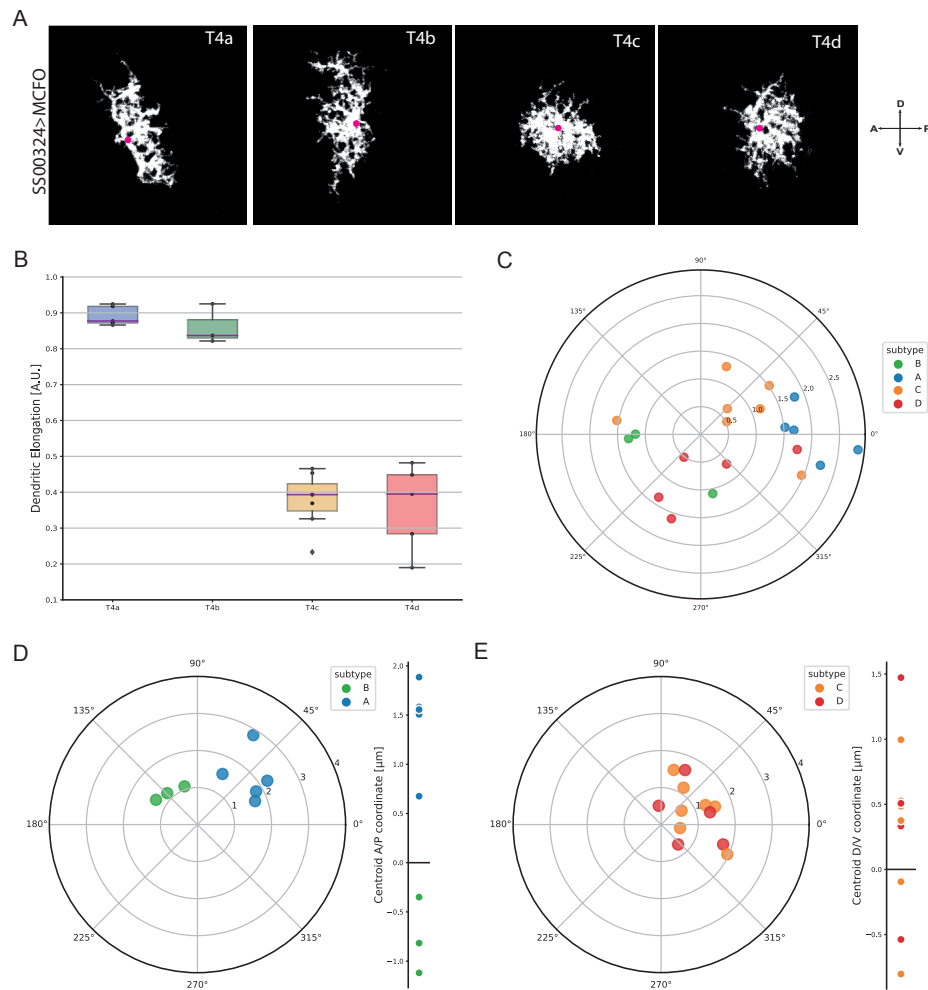


Fig. 3 Characterization of T4 dendrites at 54 hAPF (A) representative dendrite images of single-labelled T4 neurons from each subtype at 54 hAPF. The magenta dot indicates the dendrite entry point into M10 “Entry Point”. (B) Dendritic elongation for T4 dendrites at 54 hAPF separated by subtype T4a (blue; n=5), T4b (green; n=3), T4c (orange; n=7) and T4d (red; n=5). The dark purple line indicates the median. (C) Dendritic orientation based on PCA analysis. Individual dots represents individual neurons. Posterior side is considered to be 0°, and dorsal side is considered to be 90°. (D) Left: Polar plot of dendritic centroid to EP angle for T4a (blue; n=5) and T4b (green; n=3). The thick line represents the line of separation along the preferred growth axis. Right: the dendritic centroid distance from the EP along the preferred growth axis (A/P for the horizontal T4s) (E) Left: Polar plot of dendritic centroid to EP angle for T4c (orange; n=7) and T4d (red; n=5). The thick line represents the line of separation along the preferred growth axis. Right: the dendritic centroid distance from the EP along the preferred growth axis (D/V for the vertical T4s). Posterior side is considered to be 0°, and dorsal side is considered to be 90°. A, anterior; P, posterior; D, dorsal; V, ventral; A/P, Anterior/Posterior axis; D/V, Dorsal/Ventral axis; A.U., arbitrary unit; EP, Entry Point.

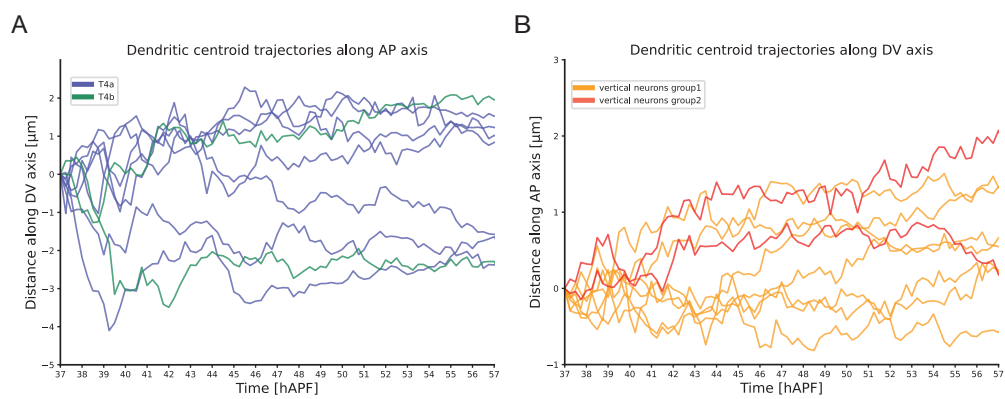


Fig. 4 Directional growth of T4 dendrites along the non preferred axis. (A) Shift in the centroid coordinate in μm along the antero-posterior axis for T4a and T4b. Positive values correspond to shift toward the dorsal side (B) Shift in the centroid coordinate in μm along the dorsal-ventral axis for vertical neurons. Positive values correspond to shift toward the posterior side. Individual lines represents individual neurons.

3

DISCUSSION

The genome is the blueprint from which the whole organism is built. However, how the genetic code is converted into distinct cellular morphologies is far from understood. Understanding brain development and the generation of complex dendritic shapes is especially challenging. The molecular mechanism guiding dendritic growth through differential expression of specific transcription factors (TFs) and cell surface molecules is of particular interest to me.

My system of choice to address this topic is the *Drosophila* motion vision circuit. T4 and T5 neurons have been studied well from a morphological, functional and transcriptional point of view in adult *Drosophila*, but their growth and development has not been investigated in detail. Their subtypes perform the exact same function of motion detection, albeit in different directions, while having distinct morphological characteristics such as their dendritic orientation and layer of axonal arborisation. Since the morphological differences have been precisely defined in the adult, differentially expressed genes between subtypes could be responsible for their individual morphologies.

The first aim of this thesis was to identify the specific genes responsible for the different subtypes, as reported in Manuscript 1. To identify the molecular mechanism that determine T4 and T5 morphologies, I have identified the transcriptomic profile of T4 and T5 subtypes at several stages during development. I found many cell surface molecules to be differentially expressed between subtypes. Most interestingly, I found that *grain*, a TF was necessary to distinguish between *a* and *b* as well as *c* and *d* subtypes. Overexpression and RNA interference (RNAi) experiments conducted as part of this work showed its importance in defining the separate morphologies of T4 and T5 subtypes.

After characterising T4 and T5 neurons transcriptionally, I next described their dendritic growth, as summarized in Manuscript 2. As a starting point, I focused on T4 neurons

in these experiments. Through time lapse imaging, I traced the growth process of individual dendrites, allowing me to differentiate between horizontal (*a/b*) and vertical (*c/d*) subtypes. Furthermore, *a* and *b* subtypes were separated through their distinct directional growth during dendritic development.

In the following, I will discuss gene regulatory networks, the underlying system through which genes are differentially expressed to generate the morphological characteristics of T4 and T5 subtypes. Then I focus on the chosen methodology including the challenges and pitfalls of single cell RNA sequencing (scRNA-seq) data, such as intrinsic biological variability, and the metrics to precisely define subtypes of T4 neurons morphologically. Subsequently, the findings are combined to formulate a hypothesis that could explain directional growth in T4 neurons.

3.1 Transcriptional regulation in T4 and T5 neurons

The number of genes in the genome is far higher compared to the number of factors regulating their transcription. Therefore, TFs are expressed in a combinatorial manner in gene regulatory networks to coordinate transcription through a network of positive and negative interactions [108, 109]. With the recent advances in single cell sequencing (see Introduction 1.4), it has become more feasible to study interactions of TFs during development.

3.1.1 Expression patterns of transcription factors in T4 and T5 neurons

Only a few TFs are expressed in fully differentiated T4 and T5 neurons, including *dachshund* (*dac*) [218], *optomotorblind* (*omb*) [218], and *Transcription factor AP-2* (*TfAP-2*) [149]. *dac* is expressed in *a/b* subtypes and *omb* in *c/d* subtypes. Both TFs could be involved in the migration and determination of T4 and T5 progenitors. Post-mitotically, they are necessary to specify morphologies of *a/b* subtypes by *dac* and *c/d* subtypes by *omb* [218]. Furthermore, *omb* represses the expression of *dac* in T4 and T5 neurons [218]. *TfAP-2* is only expressed in T4 neurons, but its specific function is still not understood [149]. These previous findings could now be used to assign cluster identities in the scRNA-seq results of this work (see Fig. 3/4 of Manuscript 1). However, the separation of *a* from *b* and *c* from *d* required an additional TF

grain expression in *b/c* subtypes can be used to separate *a* from *b* and *d* from *c* subtypes (see Fig. 3 of Manuscript 1 or [220]). Furthermore, the expression patterns of *grain* suggests a role in specifying morphological characteristics. *grain* overexpression and RNAi experiments conducted in this work showed that both dendritic orientation and the layer of axonal arborisation switch dependent on *grain* expression.

Based on the results from [scRNA-seq](#) experiments (see Fig. 4 of Manuscript 1), we know that *grain* is co-expressed with all TFs mentioned above. Therefore, it does not seem to regulate the transcription of either [dac](#), [omb](#) or [TfAP-2](#). However, it is able to fully transform the morphologies of *a/d* subtypes to *b/c* subtypes of T4 and T5 neurons.

It has been previously proposed that separate TFs are responsible for the specification of neuronal morphologies in T4 and T5 neurons [\[220\]](#). In Fig. 5/6 of Manuscript 1, I could show that this is not the case but rather *grain* specifies the layer of axonal arborisation and the dendritic orientation of T4 and T5 subtypes.

It is not easy to fit *grain* into a [TF](#) class as mentioned previously (see Intro [1.1.1](#)/[1.3.1](#)). The effect of *grain* on T4 and T5 is only observed after they are fully differentiated, therefore, excluding it as a temporal [TF](#). Furthermore, it does not specifically affect the morphology since the branching pattern between *a* and *b* or *c* and *d* subtypes does not differ more than the within subtype variability [\[221\]](#). It also does not classify as a terminal selector for T4 or T5 neurons, since all subtypes respond to the stimuli in the same manner and only half express *grain*. Altogether, the effect of *grain* appears to be transient and mainly during development, which could be a different class of [TF](#).

3.1.2 Temporal expression profiles

Developmental processes do not only depend on the TFs within the gene regulatory networks, but also require proteins, such as receptors, to build functioning neurons. Different stages of neuronal development are characterised by different expression patterns. Genes for axonal targeting are expressed early in morphogenesis, whereas genes for synapse formation are expressed at later stages. Thus, expression profiles change dynamically with time to satisfy the requirements of neuronal development.

In Fig. 1 of Manuscript 1, I could show the growth dynamics of T4 and T5 neurons, which increase the size of their dendrites especially from 36hours after pupa formation ([hAPF](#)) to 60[hAPF](#). The expression profiles at 36[hAPF](#) and 48[hAPF](#) corresponding to this growth process, include more cell surface molecules. These are presumably necessary for the contact-dependent search of growth cues and synaptic partners [\[128, 222\]](#) as well as self-avoidance [\[84, 223, 224\]](#). The expression profile at 60[hAPF](#) does not contain as many cell surface molecules, which could be due to protein expression lagging behind transcription. At later stages, the expression profile of T4 and T5 includes higher numbers of messenger RNA ([mRNA](#)) reads for ion channels and receptors (see Supp. Fig. 3 of Manuscript 1 or also [\[220, 225, 226\]](#)). This is in line with the increased neuronal activity observed in the optic lobe of *Drosophila* [\[227\]](#).

An open questions in temporal expression profiles is how neurons are able to switch between the expression of cell surface molecules and ion channels. Regulating the

expression of a set of genes for a specific function has been termed gene expression programs [228-231]. The aforementioned temporal changes in the transcription profile from cell surface molecules to ion channels and receptors in T4 and T5 could be due to a shift in gene expression program. A recent discovery of the global effect of the ecdysone hormone on changing the transcription in the *Drosophila* optic lobe, and also T4 and T5 neurons, is a strong indication for gene expression programs being linked across neuronal types [232].

3.1.3 Differentially expressed genes between T4 and T5 subtypes

Gene regulatory networks specify the subtypes of T4 and T5 neurons by activating transcription of subtype-specific genes. Detecting differentially expressed genes between clusters of subtypes is, however, not trivial. The thresholds for declaring a gene as differentially expressed can be quite arbitrary. To ensure the validity of the analysis in this work, the thresholds included three criteria:

- A difference in fold change to ensure a higher expression in one versus the other cluster.
- A minimum percentage of cells expressing the gene to ensure the use of more highly expressed genes.
- A difference in the percentage of cells expressing the gene to ensure that the gene is expressed in more cells in one cluster versus another.

These filters assure the identification of genes which are actually differentially expressed, at the risk of missing lowly expressed genes. Of the identified genes, most notable are the TFs *dac*, *omb*, *TfAP-2* and *grain* (see Fig. 4 of Manuscript 1). They have been used to assign cluster identities in this work. Most other differentially expressed genes in my dataset were cell surface molecules (see Supp. Fig. 3 of Manuscript 1).

To investigate the molecular mechanism underlying the transformation of T4 and T5 subtypes through *grain*, some of my collaborators performed preliminary experiments manipulating genes following the same expression pattern as *grain*. However, none of the tested cell surface molecules have shown a clear influence on the development of T4 and T5 neurons. This is in contrast to the results presented in Fig. 5/6 of Manuscript 1, where I show that *grain* can transform the subtypes of T4 and T5 neurons morphologically and functionally. The pilot experiments illustrate the difficulty of manipulating effector genes of TFs since there might be compensatory mechanisms in place to ensure proper dendritic development.

3.2 Variability of gene expression in T4 and T5 neurons

The basis for proper development and function of dendrites is the correct spatio-temporal expression of genes [69]. However, gene expression is subject to biological variability [233, 234] that needs to be compensated for proper circuit formation. Additionally, technical variability in **scRNA-seq** experiments further complicates the investigation of gene expression programs. Here, I want to discuss the issues with different types of variability in transcriptomic profiles and how it can be possible circumvent them.

3.2.1 Technical variability in scRNA-seq experiments

The technical progress leading to affordable **scRNA-seq** methods [12, 150] resulted in large datasets of transcriptomic profiles. One issue, however, is their low **mRNA** capture efficiency of below 50% [235]. To address the concern of technical variability, it is necessary to profile thousands of cells to get statistically accurate data. Dedicated algorithms determine cell types using the expression profile [236, 237]. However, the classification is not always as clear.

Since sample preparation is difficult, experiments do not always produce the same quality of **scRNA-seq** data. Consequently, it is necessary to use biological replicates to sequence high numbers of cells from different samples. Additionally, the same low and high thresholds of quality control measures should be applied to all samples. Even though technical variability between samples cannot be entirely removed, both replicates and common quality thresholds between them can reduce technical variability in **scRNA-seq** samples to a point of limited concern [238]. For T4 and T5 neurons, the expression profiles I reported in Manuscript 1 have been complemented by multiple different laboratories, showing their reproducibility (see Fig. 3 of Manuscript 1 and [148, 149, 220, 225, 226, 239]).

Measures, such as the number of expressed genes and unique mRNAs found, are used to exclude low-quality cells. The T4 and T5 datasets of this work (see Supp. Tab. 1 of Manuscript 1) were filtered more stringently to remove low-quality cells and to avoid additional noise in the datasets. This allows one to compare the datasets or integrate several samples. Large datasets of the whole optic lobe [226] suffer from high experimental variability, potentially distorting the results. For example, clusters with less than 100 cells might not correspond to a cell type but rather a technical artifact. These technical difficulties make the analysis more complicated and require control experiments to verify the cell types, which is why they were conducted for the work reported in Manuscript 1.

3.2.2 Biological variability in gene expression

Even when the technical variability is accounted for correctly, the natural variability in gene expression [233, 240] can be difficult to circumvent. On the one hand, genes can be expressed quite variably within one cell type. On the other hand, different genes can have expression levels ranging from tens to hundreds of mRNA copies per cell. For example, absolute numbers of mRNAs vary between less than ten for TFs, such as *grain*, and more than a hundred observed in some ion channels, such as *nicotinic Acetylcholine Receptor α 5* (see Fig. 4 of Manuscript 1). Genes with lower mRNA levels, which show differences in expression between subtypes, need to be carefully evaluated to make sure that the observed variability is not an artifact due to the natural variability in gene expression. Newly developed algorithms, such as consensus non-negative matrix factorization [231], for the identification of gene expression programs can help to counteract the natural variability because they take the covariance of genes into account.

Both types of variability require large datasets and a high number of sequencing reads per sample to be resolved, which is how they were addressed in the experiments presented in this work (see Supp. Tab. 2 of Manuscript 1). Nevertheless, it is best to identify expressed genes through a combination of methods, such as scRNA-seq and immunohistochemistry, to validate expression pattern, as I have shown in Fig. 3 of Manuscript 1. Additionally, proteins interact with each other as part of signaling cascades leading to co-expression of genes involved in the same pathway. Therefore, the analysis of gene expression programs can also help to identify lowly expressed genes if, for example, their interaction partners are expressed.

3.3 Morphological analysis of T4 dendrites during development

The complex tree structures and high variability in dendrites are a challenging subject for morphological analysis. Additionally, they have many small protrusions, such as filopodia [119] that are hard to resolve using conventional light microscopy (LM). Electron microscopy (EM) has the necessary resolution, but living samples cannot be used with this technique. Confocal [241] and two-photon scanning microscopy [242] are LM techniques with enhanced resolution but still require complex image processing techniques [11, 243] to identify the small, dynamic filopodia and follow the development of neurons [244].

Dendrites of *Drosophila* T4 cells are an especially challenging system to study dendritic development: first, they are located deep inside of the brain, which requires two-photon excitation to reduce scattering and increase the axial resolution. Second, the dendrites are comparatively small, around 5 μ m in the beginning of their growth at 36hAPF [52, 163]. Lastly, the dendrites of T4 neurons are structurally dense during development and in the adult (see Fig. 1 of Manuscript 2 or [163, 166]). Our investigation resulted in datasets

of growing T4 dendrites (see Fig. 2 of Manuscript 2), which we could follow over time. These data show subtype specific growth patterns for T4 subtypes *a* and *b*, whereas *c* and *d* could not be categorized from our data based on their dendrite.

3.3.1 Dendritic morphometrics

In order to analyse dendritic morphologies during development, neuronal subtypes of T4 need to be identified in every dataset for comparison. Therefore, it is important to define metrics, which can be inferred from measurements of microscopy images [245]. The morphological data for characterising dendrites can be divided into two categories: reconstructed or volumetric data. Reconstructed data refers to EM or LM reconstructions and can be skeletonised, creating a structure with well-defined branches [121, 207, 246]. When the dendrites are too small and only LM is an appropriate option for acquisition, the data cannot be fully reconstructed into a branching tree. This is called volumetric data and consists of two dimensional images stacked together in a non-isometric way creating an image volume (see Methods of Manuscript 2 or [247]).

One advantage of reconstructed data is that it enables the use of topological metrics which are independent of size metrics, such as dendritic branch length or field size [245]. There are several important terms for defining metrics relating to specific segments of the dendrite: root, branch point, and terminal tips. The root is the first branch of the dendrite. Branch points are segments of the dendrite which split into two separate branches. The terminal tips are the last segment of a branch and the points furthest away from the root. By using the branch points as reference, it is possible to calculate the branch order [248, 249]. Every branch segment is then numbered starting at 1 for the terminal tips and increasing the number at every branch point towards the root. The root will then have the highest number. This analysis makes dendritic trees more comparable [249] and differentiates between dendrites that are more or less branched. Another method for reconstructed data is Sholl analysis [250], which uses concentric rings around the soma or root of the dendrite with increasingly larger diameters. Sholl analysis then measures the number of intersection points between the dendrites and the concentric rings to identify the length of different branches from the centre of the circle. This can determine the total branch length, the dendritic span, and the straightness of branches [251]. These metrics are able to analyse the complexity of dendritic trees, but require reconstructed data.

The metrics mentioned above are all important for the characterisation of dendritic trees but cannot be transferred directly to volumetric data. Therefore, I developed a voxel-based analysis for volumetric data, together with my collaborators, to overcome the need for reconstructed data to investigate the development of T4 dendrites (see Fig.

2-4 of Manuscript 2). The analysis uses specific metrics to describe the characteristics of T4 dendrites in size, shape, complexity, and orientation.

Size metrics include volume and area spanned by the dendrite. Shape metrics, such as elongation of dendrites, show if the dendrite grows evenly or directed. These two metrics are easy to calculate from binarised image stacks, consisting of only ones or zeros.

Complexity metrics are challenging to determine. Nonetheless, the fields of computer vision and pattern recognition have presented many ways of characterising shapes, of which convexity has proven itself an appropriate metric for dendritic complexity [252]. The term 'convex' is used in a geometric sense, describing an object which consists of a convex set of points. This is the case if the line connecting every combination of two points in the convex set is also contained within the set [253]. Thus, a 'U' is not a convex shape, whereas a 'O' is convex. Another term necessary to calculate the convexity metric is the 'convex hull'. It is the smallest convex area encircling a set of points [254], in our case the z-projection of the dendrite. Convexity compares the perimeter of the convex hull to the perimeter of the dendrite. The perimeter of the dendrite can maximally be as small as the perimeter of the convex hull. By dividing the perimeter of the convex hull by the perimeter of the dendrite, the resulting value is between 1 and 0. This means that dendrites with a more elaborate branching pattern have small convexity values, whereas circular dendrites have values closer to 1 [252]. Convexity can also be calculated in three dimensions using the surface area of dendrites. Calculating the convex hull requires a careful evaluation of the dataset, since it considers every voxel that has been assigned to the dendrite. Therefore, it is necessary to remove any voxels that do not belong to the dendrite but to the axon because otherwise an artificially high convexity value would be calculated. I used convexity to discover an increase in dendritic elaboration observed in T4 dendrites during development (see Fig. 2 of Manuscript 2).

Lastly, dendritic orientation is especially important in the case of T4 dendrites, since it is one of their main distinctive features compared to other neurons. One of the difficulties in determining orientation metrics is the definition of a global reference frame to compare neurons across different brains. The anatomical axis of the neuropil can be used to align the image stacks along the same direction. However, in our case the curvature of the medulla needs to be taken into account as the dorso-ventral and antero-posterior axes are not always clearly determined. Through careful manual rotation, the dendrites could be transformed to the same global reference frame for this work (see Methods of Manuscript 1/2). The directionality of T4 dendrites falls into the four cardinal directions matching dorso-ventral and antero-posterior directions of the optic lobe [163]. To calculate dendritic directionality, a reference point available in each dendrite is needed. For this purpose, the entry point into the respective neuropil is a reasonable

choice, since it is the origin of all branches [163, 166]. The distribution of voxel angles from the entry point shows a clear bias between the subtypes and it is possible to identify T4 subtypes in the adult based on its histogram as reported in Fig. 2 of Manuscript 1. In Fig. 1 of Manuscript 2, we used principle component analysis (PCA) to align dendrites to each other without using a global reference frame. In addition, we calculated their directionality after the PCA. Applied to T4 data, PCA remaps voxels into a new coordinate space that captures the maximum variance of voxel positions for each dendrite. These align T4 dendrites to each other according to their variance in two axes. Using the entry point as point of reference, an unequal distribution of voxels along both axes can be seen. Since the entry point is located towards the proximal compartment of the dendrites [163], the voxels behind or in front of the entry point along the main direction of growth are not equal (see Fig. 1 of Manuscript 2). Both metrics for directionality, angles of voxels or PCA direction, work well for adult T4 dendrites. However, developing dendrites do not always have a clear distribution of voxel angles and their axes of variance do not fall into the same anatomical axes as in the adult. To calculate dendritic orientation during development, the dendritic centroid to entry point angle gives a robust result where the centroid is the dendrite's center of mass. In conclusion, the metrics of size, shape, complexity and directionality define subtypes of adult T4 dendrites. However, it was not possible to differentiate between T4 dendrites during development using the exact same metrics (see Fig. 3 of Manuscript 2). Therefore, it was important to find a characteristic to identify subtypes of developing T4 dendrites.

3.3.2 Morphological identification of T4 subtypes during development

In order to compare dendritic growth patterns between T4 dendrites, it is necessary to unambiguously determine their subtype identity. There are two main morphological differences between T4 subtypes: first, their dendrites are oriented and point into different directions. Second, axons arborise in different layers of the lobula plate for different subtypes. However, time lapse imaging of developing T4 dendrites shows that their dendritic arbors are not yet oriented at 36hAPF (see Fig. 2 of Manuscript 1). Furthermore, only high resolution images allow for precise determination of axon position in the lobula plate, which is thinner during early development [218]. Therefore, determination of T4 subtype identity is not as clear during development as it is in the adult.

Time lapse imaging experiments of T4 dendrites are limited to M10 and do not have information of the lobula plate. However, an image stack of the whole optic lobe allows the measurement of the relative axon position in the lobula plate. Due to a lower axial resolution, the exact positions are hard to determine and only distinguish between horizontal and vertical subtypes. At the same time, T4 dendrites could be divided into

the same groups with their elongation in the dorso-ventral direction because horizontal subtypes are more elongated compared to vertical subtypes. Calculating the directionality using the centroid to entry point angle allows separating *a* and *b* subtypes. However, *c* and *d* subtypes cannot be distinguished, with their angles showing a random distribution in the fixed tissue control. Morphologies of T4*a* and T4*b* diverge faster and are easier to distinguish during development compared to T4*c* and T4*d* subtypes. It is possible that EM reconstructions could show differences between dendrites of vertical subtypes, but based on the results of Manuscript 2, there are no clear indicators.

3.3.3 T4 morphologies during development

The morphologies of T4 subtypes change significantly during their development. After reaching M10, they do not extend their dendrites further than the column they grow towards (see Fig. 2 of Manuscript 2 or [52]). They start growing slowly from 37hAPF until around 44hAPF which could be induced by a global start signal of the ecdysone hormone pulse [232]. Afterwards, their growth accelerates as shown by the increase in volume reported in Fig. 2 of Manuscript 2. Other size metrics, such as dendritic area show a similar trajectory. Interestingly, they already reach a similar volume as the adult dendrites at 56hAPF while their span is still smaller compared to the adult. This indicates that pruning removes unnecessary branches at later stages of development (see Fig. 1 of both Manuscript 1/2). As dendrites are compact at the start of the time lapse imaging experiments, it is not possible to identify individual branches. Convexity increases from around 40hAPF until 50hAPF but stagnates afterwards. Both metrics are highly similar for all T4 subtypes, showing that their general growth is synchronised (see Fig. 2 of Manuscript 2).

The first metric found in this work to differentiate between subtypes is dendritic elongation along the dorso-ventral axis (see Fig. 3 of Manuscript 2). While T4 subtypes have similar dendritic field sizes in the adult, the dorso-ventral direction is elongated [163]. The dorso-ventral axis is the main direction of growth for the *c/d* subtypes. For *a/b* subtypes the growth is mainly orthogonal to this axis. Considering dendritic shapes, this means T4*a/b* are wider and shorter, whereas T4*c/d* are narrower and longer. Interestingly, the dendritic elongation along the dorso-ventral axis distinguishes horizontal from vertical subtypes, showing that horizontal subtypes first grow along the axis orthogonal to their main direction of growth. For vertical subtypes, this is not straight-forward to conclude since their dendritic shape is more circular throughout the imaging experiment. At this point, it is hard to judge if there are morphological differences between T4*c* and T4*d*. Thus, vertical subtypes cannot further be distinguished with the chosen metrics, even at advanced time points of time lapse imaging experiments. Horizontal subtypes, in comparison, show an increased growth in the orthogonal direction to their main direction of growth, which allows further separation into T4*a* and T4*b* (see Fig. 3 of Manuscript 2).

3.4 Dendritic growth strategies

The development of complex patterns in dendrites uses different strategies for growing. Dendrites achieve the minimal required growth adjusted to the limited resources [86]. Additionally, they need to self-avoid, tile and fill their receptive field from a growth perspective (see Fig. 1.2) [58, 84, 99]. During this process, dendrites rely on contact-dependent mechanisms to orient themselves in neuropils and grow dynamically searching for extrinsic cues [119]. Through dendritic growth cones probing the local environment, dendrites stabilize when they find the matching cell surface molecules [244]. These extrinsic cues can be organised in different ways, such as topographic maps (see Introduction 1.1.2) to guide dendritic growth.

3.4.1 Dendritic growth patterns of T₄ neurons

Growth patterns of T₄ subtypes can be distinguished between horizontal and vertical subtypes as discussed in Section 3.3.3. While it is not possible to differentiate between vertical subtypes (see Fig.3 of Manuscript 2), horizontal subtypes show a mirrored growth. At first, T_{4a} and T_{4b} grow towards the dorsal or ventral direction from their starting column. Subsequently, they extend along their main direction of growth in the antero-posterior axis. Interestingly, there does not seem to be a bias towards the dorsal or ventral side for either *a* or *b* subtypes. Therefore, it cannot be determined if a cue guides them in either direction of the dorso-ventral axis.

Vertical subtypes also show two groups of growth patterns. In the early stages of time lapse imaging experiments, they separate into dendrites growing either dorsally or ventrally. Throughout the imaging period, their centroid stays in this direction. However, near the end of the experiment, they start to slowly grow into the opposite direction to their first direction of choice. While they could not be separated based on their centroid to entry point angle, this growth pattern shows a strong bias and could be an indicator for their subtype identity. However, control dendrites in fixed tissue samples did not show a clear separation of the subtypes and therefore subtype identity could not be assigned accordingly. In the antero-posterior axis, growth is strongly biased towards the posterior direction (see Supp.fig. of Manuscript 2). This could, however, be an artifact due to the curvature of the optic lobe leading to an uneven growth along the antero-posterior direction.

Based on the results presented in this thesis, it is apparent that T₄ neurons do not follow the same growth rules as other neurons, such as dendritic arborisation (da) neurons in *Drosophila* larva. Most notably, they do not tile the medulla but overlap substantially [163, 166, 221]. A reason for this organisation could be to maintain a

higher resolution of visual flow fields. Since the computation of motion requires input from neighbouring points in space (see Introduction [1.5.2]), dendrites need to overlap. Additionally, different dendritic compartments (see Introduction [1.5.4]) are synaptically connected to different input neurons. Therefore, even though neurons of the same T₄ subtype occupy an overlapping space, they do not receive the same synaptic input in these overlapping locations. Since there is one T₄ subtype per column in the medulla, T₄ neurons are arranged in a structured manner. Even though they do not tile M10 in the conventional meaning, they occupy the whole M10 in a regular grid-like organisation.

3.4.2 Medulla topology

Topographic maps (see Introduction [1.1.2]) are essential to guide growing axons and dendrites to the right position for circuit formation [50]. They have been found in olfactory and visual systems of multiple organisms, including *Drosophila* [116]. In the medulla, two long-range signaling molecules from the planar cell polarity pathway, *DWnt4* and *DWnt10*, have been identified to construct a topographic map along the dorso-ventral axis. Their interaction partners include *derailed* [255, 256] and *frizzled* family receptors [257], among various other receptors [56]. However, transcriptomic data of T₄ neurons show low or late expression for receptors interacting with *DWnts*, which makes them an unlikely guide for the directional growth of T₄ dendrites (see Fig.3 of Manuscript 1). *DWnts* are secreted and could create a neuropil-wide map. Nevertheless, this map seems unsuitable to guide T₄ dendrites since directional cues need to be detectable along the span of the T₄ dendrite. Thus, T₄ neurons might need a more local cue to guide their growth, because it has been shown that all T₄ neurons have the same orientation across M10 in the adult [221].

One explanation would be that there is a topographic map in the medulla made of a locally repeating pattern. Medulla columns have a patterned organisation with columnar neurons growing only into certain parts of the columns [48, 192]. This would indicate that columns are directional, which could guide dendritic development of T₄, potentially also explaining their dynamic growth (see Fig. 4 of Manuscript 2).

The medulla columns are arranged in a hexagonal grid, which is inherited from the retina [166, 192]. This means that there are direct neighbours to each column in three axis following the sides of the hexagon. One of these axis falls onto the dorso-ventral axis of the medulla. The other two, however, do not fully align with the antero-posterior axis [192]. In order to sample the right space for the computation of motion (see Introduction [1.5.2]), T₄ subtypes *a/b* need to grow wider to enable the computation of motion in the horizontal axis of visual space. This could be one of the reasons for the difference in elongation observed in the growth pattern in horizontal subtypes of T₄ dendrites reported in this work.

3.4.3 Synaptotrophic hypothesis

The synaptotrophic hypothesis postulates, that there exist activity-independent and -dependent mechanisms of dendritic growth [258-261]. In the first step, dendrites grow into a specific area as described in the chemoaffinity hypothesis [262]. In the next step, they build synapses with presynaptic partners and stabilise the ones that are regularly active during the process.

The dendrites of horizontal subtypes of T4 neurons grow directionally starting with the proximal compartment and then extending towards the distal compartment (see Fig.4 of Manuscript 2). This could mean that dendrites first search for synaptic partners on the proximal side, such as Mi4 or CT1, and potentially use those to stabilise their branches. For the vertical subtypes, we cannot assign individual subtypes. Therefore, it is not possible to determine if they follow the same growth pattern. Additionally, the vertical subtypes have more branches in the proximal compartment (see Fig. 2 of Manuscript 1) [163] compared to horizontal subtypes. Therefore, it cannot be clearly determined in which direction they grow first.

Concerning the activity-dependent stabilization, it is possible that T4 and T5 neurons use synaptic activity to prune unnecessary branches. The reduction in volume (see Fig.1 of Manuscript 1) from 60-72hAPF in comparison with adult neurons could indicate that dendrites prune their branches dependent on neuronal activity. A conspicuous correlation is the timing of pruning and the start of calcium waves observed in the optic lobe. Both start at around 60hAPF [227]. Altogether, there are already some indicators that the synaptotrophic hypothesis could apply to dendritic development of T4 neurons.

3.4.4 Developmental comparison between T4 and T5 neurons

T4 and T5 neurons are highly similar in many aspects, such as transcription profile, function and morphology (see Manuscript 1/2) [163, 166, 206, 220]. Developmentally, only the last division of progenitors separates T4 from T5 subtypes. They innervate M10 and L01 at a similar time and grow their axons back to the same retiontopic locations [52, 166]. Using *grain*, both T4 and T5 neurons can be reprogrammed. Based on their volume at different time points during development, T4 and T5 neurons share similar growth curves (see Fig.1 of Manuscript 1). The neuropil grids are organised in a hexagonal fashion for both T4 and T5, albeit columns are smaller and more elongated in the dorso-ventral direction for T5 (Fig. 1.4e) [166]. These indicators argue for a similar growth pattern in T5 neurons as reported for T4 neurons in this work. However, it is left to future experiments to confirm this hypothesis, as shown in Fig. 4 of Manuscript 2.

3.5 Conclusions and outlook

My thesis focuses on the questions of how TFs influence dendritic development and how subtypes of T4 dendrites grow into different directions in the same environment. The characterisation of the transcriptome allowed to identify the important TFs to determine the morphologies of T4 neurons. Furthermore, the dendritic morphometrics of T4 neurons during development were determined in this work. In addition, for the first time clear indicators to identify T4a and T4b were established using only the dendrite.

Even though it is now clear that *grain* is able to control neuronal morphology of T4 neurons on a transcriptional level, the effectors further downstream have not been identified yet. It is likely that the effectors are different for T4b and T4c subtypes since their main direction of growth is along different axis. The combined analysis of different [scrRNA-seq](#) and single cell ATAC sequencing ([scATAC-seq](#)) datasets have the potential to identify how the different TFs expressed in motion-sensing neurons specify each T4 and T5 subtype and which genes are directly involved in the dendritic growth. Furthermore, the influence of identified genes on dendritic growth needs to be tested. With cell surface molecules having redundant roles in development, it can be challenging to see differences in branching structure of T4 and T5 dendrites. Therefore, it is necessary to have precise descriptions of T4 and T5 dendrites through the use of morphometrics. Accurate characterisation of adult and developing dendrites are quintessential for identifying subtypes. The accurate morphological characterisation, achieved in this work, can now enable the detection of small developmental defects, which might not become apparent to the observer otherwise.

Additionally, growth patterns of T4 and T5 neurons need to be precisely understood and determined as they can help to identify molecular mechanisms underlying the process of directed dendritic growth. Due to the limitations of time lapse imaging experiments, it is necessary to image two overlapping periods of dendritic growth from 36 [hAPF](#) to 56 [hAPF](#) and again at a later stage from around 44 [hAPF](#) to 64 [hAPF](#). At 64 [hAPF](#) the dendrites should be unambiguously identifiable. With these two imaging periods it should be possible to fully describe the growth patterns of T4 and T5 neurons in the future. Additionally, time lapse imaging experiments allow to observe the exact defect of a gene on the growth pattern with a genetic manipulation. To test potential effects certain genes could have *in silico*, it will be necessary to build a developmental model of T4 and T5 neurons. These models are necessary to narrow down the potential growth patterns of T4 and T5 neurons. They would allow to predict which molecular mechanism have the potential to generate the directional growth observed in time lapse imaging experiments. In conclusion, investigating the dendritic development of T4 and T5 neurons can provide us with a good understanding of how the genetic code translates

into specific morphologies of directional dendrites. This work contributes to this effort by employing state-of-the-art methods to collect and analyse data from T4 and T5 neurons of *Drosophila* providing first indicators on how their dendrites develop. However, both further experimental efforts, such as bigger datasets and additional detailed experiments, as well as theoretical efforts providing models behind growth processes are necessary to fully understand the molecular mechanism leading to complex dendritic morphologies.

LIST OF FIGURES

1.1	Developmental mechanisms in neuronal specification	3
1.2	Neuronal growth mechanisms	6
1.3	<i>Drosophila</i> optic lobe and neurons of the motion vision circuit	14
1.4	Synaptic connectivity and grid of T4 and T5 neurons	18

LIST OF ABBREVIATIONS

CSM	cell surface molecule
<i>dac</i>	<i>dachshund</i>
EM	electron microscopy
GPCR	G-protein coupled receptor
hAPF	hours after pupa formation
LM	light microscopy
mRNA	messenger RNA
<i>omb</i>	<i>optomotorblind</i>
PCA	principle component analysis
RNAi	RNA interference
scRNA-seq	single cell RNA sequencing
scATAC-seq	single cell ATAC sequencing
TF	transcription factor
<i>TfAP-2</i>	<i>Transcription factor AP-2</i>

REFERENCES

1. Crick, F. H. C., Barnett, L., Brenner, S. & Watts-Tobin, R. J. General Nature of the Genetic Code for Proteins. *Nature* **192**, 1227–1232 (Dec. 1961).
2. Basson, M. A. Signaling in Cell Differentiation and Morphogenesis. *Cold Spring Harbor Perspectives in Biology* **4**, a008151 (June 1, 2012).
3. Ramón y Cajal, S., Sánchez, D. & Madrid, U. C. d. *Contribución al conocimiento de los centros nerviosos de los insectos* 180 pp. (Imprenta de Hijos de Nicolás Moya, Madrid, 1915).
4. Zeng, H. & Sanes, J. R. Neuronal cell-type classification: challenges, opportunities and the path forward. *Nature Reviews Neuroscience* **18**, 530–546 (Sept. 2017).
5. Sanes, J. R. & Yamagata, M. Many Paths to Synaptic Specificity. *Annual Review of Cell and Developmental Biology* **25**, 161–195 (2009).
6. Luo, L. Rho GTPases in neuronal morphogenesis. *Nature Reviews Neuroscience* **1**, 173–180 (Dec. 2000).
7. Turing, A. M. The chemical basis of morphogenesis. *Philosophical Transactions of the Royal Society of London. Series B, Biological Sciences* **237**, 37–72 (Aug. 14, 1952).
8. Lewis, E. B. A gene complex controlling segmentation in *Drosophila*. *Nature* **276**, 565–570 (Dec. 1978).
9. Nüsslein-Volhard, C. & Wieschaus, E. Mutations affecting segment number and polarity in *Drosophila*. *Nature* **287**, 795–801 (Oct. 1980).
10. Liu, T.-L. *et al.* Observing the cell in its native state: Imaging subcellular dynamics in multicellular organisms. *Science* **360**, eaaq1392 (Apr. 20, 2018).
11. Von Chamier, L. *et al.* Democratising deep learning for microscopy with ZeroCostDL4Mic. *Nature Communications* **12**, 2276 (Apr. 15, 2021).
12. Macosko, E. Z. *et al.* Highly Parallel Genome-wide Expression Profiling of Individual Cells Using Nanoliter Droplets. *Cell* **161**, 1202–1214 (May 21, 2015).
13. Johnston, D. S. The Renaissance of Developmental Biology. *PLOS Biology* **13**, e1002149 (May 6, 2015).
14. Brody, T. & Odenwald, W. F. Regulation of temporal identities during *Drosophila* neuroblast lineage development. *Current Opinion in Cell Biology. Cell division, growth and death / Cell differentiation* **17**, 672–675 (Dec. 1, 2005).
15. Holguera, I. & Desplan, C. Neuronal specification in space and time. *Science* **362**, 176–180 (Oct. 12, 2018).
16. Puram, S. V. & Bonni, A. Cell-intrinsic drivers of dendrite morphogenesis. *Development* **140**, 4657–4671 (Dec. 1, 2013).
17. Santiago, C. & Bashaw, G. J. Transcription factors and effectors that regulate neuronal morphology. *Development* **141**, 4667–4680 (Dec. 15, 2014).
18. Waddington, C. *The Strategy of the Genes* 2nd ed. (Routledge, Apr. 29, 2014).
19. Rogers, K. W. & Schier, A. F. Morphogen Gradients: From Generation to Interpretation. *Annual Review of Cell and Developmental Biology* **27**, 377–407 (2011).

20. Sjöqvist, M. & Andersson, E. R. Do as I say, Not(ch) as I do: Lateral control of cell fate. *Developmental Biology. Signaling pathways in development* **447**, 58–70 (Mar. 1, 2019).
21. Urbach, R. & Technau, G. M. Neuroblast formation and patterning during early brain development in *Drosophila*. *BioEssays* **26**, 739–751 (2004).
22. Stiles, J. & Jernigan, T. L. The Basics of Brain Development. *Neuropsychology Review* **20**, 327–348 (Dec. 1, 2010).
23. Martin, A. C. The Physical Mechanisms of *Drosophila* Gastrulation: Mesoderm and Endoderm Invagination. *Genetics* **214**, 543–560 (Mar. 1, 2020).
24. Maroudas-Sacks, Y. & Keren, K. Mechanical Patterning in Animal Morphogenesis. *Annual Review of Cell and Developmental Biology* **37**, 469–493 (2021).
25. Nieto, M. A. Reorganizing the Organizer 75 Years On. *Cell* **98**, 417–425 (Aug. 20, 1999).
26. Akam, M. The molecular basis for metameric pattern in the *Drosophila* embryo. *Development* **101**, 1–22 (Sept. 1, 1987).
27. Ingham, P. W. The molecular genetics of embryonic pattern formation in *Drosophila*. *Nature* **335**, 25–34 (Sept. 1988).
28. Bhat, K. M. Segment polarity genes in neuroblast formation and identity specification during *Drosophila* neurogenesis. *BioEssays* **21**, 472–485 (1999).
29. Jaeger, J. The gap gene network. *Cellular and Molecular Life Sciences* **68**, 243–274 (Jan. 1, 2011).
30. Udolph, G., Prokop, A., Bossing, T. & Technau, G. A common precursor for glia and neurons in the embryonic CNS of *Drosophila* gives rise to segment-specific lineage variants. *Development* **118**, 765–775 (July 1, 1993).
31. Isshiki, T., Takeichi, M. & Nose, A. The role of the *msh* homeobox gene during *Drosophila* neurogenesis: implication for the dorsoventral specification of the neuroectoderm. *Development* **124**, 3099–3109 (Aug. 15, 1997).
32. McDonald, J. A. *et al.* Dorsoventral patterning in the *Drosophila* central nervous system: the *vnd* homeobox gene specifies ventral column identity. *Genes & Development* **12**, 3603–3612 (Nov. 15, 1998).
33. Von Ohlen, T. & Doe, C. Q. Convergence of Dorsal, Dpp, and Egfr Signaling Pathways Subdivides the *Drosophila* Neuroectoderm into Three Dorsal-Ventral Columns. *Developmental Biology* **224**, 362–372 (Aug. 15, 2000).
34. Wolpert, L. Positional information and the spatial pattern of cellular differentiation. *Journal of Theoretical Biology* **25**, 1–47 (Oct. 1, 1969).
35. *Patterning and Cell Type Specification in the Developing CNS and PNS (Second Edition)* (Academic Press, Jan. 1, 2020).
36. Fischbach, K.-F. & Hiesinger, P. R. in *Brain Development in Drosophila melanogaster* 115–136 (Springer, New York, NY, 2008).
37. Driever, W. & Nüsslein-Volhard, C. A gradient of bicoid protein in *Drosophila* embryos. *Cell* **54**, 83–93 (July 1, 1988).
38. Tomlinson, A. & Ready, D. F. Cell fate in the *Drosophila* ommatidium. *Developmental Biology* **123**, 264–275 (Sept. 1, 1987).
39. Frankfort, B. J. & Mardon, G. R8 development in the *Drosophila* eye: a paradigm for neural selection and differentiation. *Development* **129**, 1295–1306 (Mar. 15, 2002).
40. Treisman, J. E. Retinal differentiation in *Drosophila*. *WIREs Developmental Biology* **2**, 545–557 (2013).
41. Matsuno, K., Diederich, R., Go, M., Blaumueller, C. & Artavanis-Tsakonas, S. Deltex acts as a positive regulator of Notch signaling through interactions with the Notch ankyrin repeats. *Development* **121**, 2633–2644 (Aug. 1, 1995).

42. Maurange, C., Cheng, L. & Gould, A. P. Temporal Transcription Factors and Their Targets Schedule the End of Neural Proliferation in *Drosophila*. *Cell* **133**, 891–902 (May 30, 2008).
43. Mora, N. *et al.* A Temporal Transcriptional Switch Governs Stem Cell Division, Neuronal Numbers, and Maintenance of Differentiation. *Developmental Cell* **45**, 53–66.e5 (Apr. 9, 2018).
44. Doe, C. Q. Temporal Patterning in the *Drosophila* CNS. *Annual Review of Cell and Developmental Biology* **33**, 219–240 (2017).
45. Lowery, L. A. & Vactor, D. V. The trip of the tip: understanding the growth cone machinery. *Nature Reviews Molecular Cell Biology* **10**, 332–343 (May 2009).
46. Millard, S. S. & Pecot, M. Y. Strategies for assembling columns and layers in the *Drosophila* visual system. *Neural Development* **13**, 11 (June 7, 2018).
47. Nern, A., Zhu, Y. & Zipursky, S. L. Local N-Cadherin Interactions Mediate Distinct Steps in the Targeting of Lamina Neurons. *Neuron* **58**, 34–41 (Apr. 10, 2008).
48. Trush, O. *et al.* N-Cadherin Orchestrates Self-Organization of Neurons within a Columnar Unit in the *Drosophila* Medulla. *Journal of Neuroscience* **39**, 5861–5880 (July 24, 2019).
49. Winberg, M. L. *et al.* Plexin A Is a Neuronal Semaphorin Receptor that Controls Axon Guidance. *Cell* **95**, 903–916 (Dec. 23, 1998).
50. Kaas, J. H. Topographic Maps are Fundamental to Sensory Processing. *Brain Research Bulletin* **44**, 107–112 (Jan. 1, 1997).
51. Clandinin, T. R. & Zipursky, S. L. Making Connections in the Fly Visual System. *Neuron* **35**, 827–841 (Aug. 29, 2002).
52. Pinto-Teixeira, F. *et al.* Development of Concurrent Retinotopic Maps in the Fly Motion Detection Circuit. *Cell* **173**, 485–498.e11 (Apr. 5, 2018).
53. Hassenstein, B. & Reichardt, B. W. Systemtheoretische Analyse der Zeit-, Reihenfolgen- und Vorzeichenbewertung bei der Bewegungsperzeption des Rüsselkäfers *Chlorophanus*. *Zeitschrift für Naturforschung A* (Feb. 1, 1956).
54. Barlow, H. B. & Levick, W. R. The mechanism of directionally selective units in rabbit's retina. *The Journal of Physiology* **178**, 477–504 (1965).
55. Feldheim, D. A. & O'Leary, D. D. M. Visual Map Development: Bidirectional Signaling, Bifunctional Guidance Molecules, and Competition. *Cold Spring Harbor Perspectives in Biology* **2**, a001768 (Nov. 1, 2010).
56. Han, X. *et al.* DWnt4 and DWnt10 Regulate Morphogenesis and Arrangement of Columnar Units via Fz2/PCP Signaling in the *Drosophila* Brain. *Cell Reports* **33**, 108305 (Oct. 27, 2020).
57. Cheng, P.-l. & Poo, M.-m. Early Events in Axon/Dendrite Polarization. *Annual Review of Neuroscience* **35**, 181–201 (2012).
58. Dong, X., Shen, K. & Bülow, H. E. Intrinsic and Extrinsic Mechanisms of Dendritic Morphogenesis. *Annual Review of Physiology* **77**, 271–300 (2015).
59. Zolessi, F. R., Poggi, L., Wilkinson, C. J., Chien, C.-B. & Harris, W. A. Polarization and orientation of retinal ganglion cells in vivo. *Neural Development* **1**, 2 (Oct. 13, 2006).
60. Barnes, A. P. & Polleux, F. Establishment of Axon-Dendrite Polarity in Developing Neurons. *Annual Review of Neuroscience* **32**, 347–381 (2009).
61. Huber, A. B., Kolodkin, A. L., Ginty, D. D. & Cloutier, J.-F. Signaling at the growth cone: Ligand-Receptor Complexes and the Control of Axon Growth and Guidance. *Annual Review of Neuroscience* **26**, 509–563 (2003).
62. O'Donnell, M., Chance, R. K. & Bashaw, G. J. Axon Growth and Guidance: Receptor Regulation and Signal Transduction. *Annual Review of Neuroscience* **32**, 383–412 (2009).
63. Seiradake, E., Jones, E. Y. & Klein, R. Structural Perspectives on Axon Guidance. *Annual Review of Cell and Developmental Biology* **32**, 577–608 (2016).

64. Ledda, F. & Paratcha, G. Mechanisms regulating dendritic arbor patterning. *Cellular and Molecular Life Sciences* **74**, 4511–4537 (Dec. 1, 2017).
65. Inberg, S. *et al.* Lessons from Worm Dendritic Patterning. *Annual Review of Neuroscience* **42**, 365–383 (2019).
66. Zou, W. *et al.* A Dendritic Guidance Receptor Complex Brings Together Distinct Actin Regulators to Drive Efficient F-Actin Assembly and Branching. *Developmental Cell* **45**, 362–375.e3 (May 7, 2018).
67. Valnegri, P., Puram, S. V. & Bonni, A. Regulation of dendrite morphogenesis by extrinsic cues. *Trends in Neurosciences* **38**, 439–447 (July 1, 2015).
68. Lin, T.-Y., Chen, P.-J., Yu, H.-H., Hsu, C.-P. & Lee, C.-H. Extrinsic Factors Regulating Dendritic Patterning. *Frontiers in Cellular Neuroscience* **14** (2021).
69. Rossi, A. M., Jafari, S. & Desplan, C. Integrated Patterning Programs During Drosophila Development Generate the Diversity of Neurons and Control Their Mature Properties. *Annual Review of Neuroscience* **44**, 153–172 (2021).
70. Pasterkamp, R. J. Getting neural circuits into shape with semaphorins. *Nature Reviews Neuroscience* **13**, 605–618 (Sept. 2012).
71. Walter, J., Henke-Fahle, S. & Bonhoeffer, F. Avoidance of posterior tectal membranes by temporal retinal axons. *Development* **101**, 909–913 (Dec. 1, 1987).
72. Walter, J., Kern-Veits, B., Huf, J., Stolze, B. & Bonhoeffer, F. Recognition of position-specific properties of tectal cell membranes by retinal axons in vitro. *Development* **101**, 685–696 (Dec. 1, 1987).
73. Landis, S. C. Neuronal Growth Cones. *Annual Review of Physiology* **45**, 567–580 (1983).
74. Yamada, K. M., Spooner, B. S. & Wessells, N. K. Axon growth: roles of microfilaments and microtubules*. *Proceedings of the National Academy of Sciences* **66**, 1206–1212 (Aug. 1970).
75. Yamada, K. M., Spooner, B. S. & Wessells, N. K. Ultrastructure and function of growth cones and axons of cultured nerve cells. *Journal of Cell Biology* **49**, 614–635 (June 1, 1971).
76. Dent, E. W. & Gertler, F. B. Cytoskeletal Dynamics and Transport in Growth Cone Motility and Axon Guidance. *Neuron* **40**, 209–227 (Oct. 9, 2003).
77. Maskery, S. & Shinbrot, T. Deterministic and Stochastic Elements of Axonal Guidance. *Annual Review of Biomedical Engineering* **7**, 187–221 (2005).
78. Kidd, T. *et al.* Roundabout Controls Axon Crossing of the CNS Midline and Defines a Novel Subfamily of Evolutionarily Conserved Guidance Receptors. *Cell* **92**, 205–215 (Jan. 1998).
79. Yuan, W. *et al.* The Mouse SLIT Family: Secreted Ligands for ROBO Expressed in Patterns That Suggest a Role in Morphogenesis and Axon Guidance. *Developmental Biology* **212**, 290–306 (Aug. 1999).
80. Govek, E.-E., Newey, S. E. & Aelst, L. V. The role of the Rho GTPases in neuronal development. *Genes & Development* **19**, 1–49 (Jan. 1, 2005).
81. Koh, C.-G. Rho GTPases and Their Regulators in Neuronal Functions and Development. *Neurosignals* **15**, 228–237 (2006).
82. Shelly, M. *et al.* Semaphorin3A Regulates Neuronal Polarization by Suppressing Axon Formation and Promoting Dendrite Growth. *Neuron* **71**, 433–446 (Aug. 11, 2011).
83. Kantor, D. B. *et al.* Semaphorin 5A Is a Bifunctional Axon Guidance Cue Regulated by Heparan and Chondroitin Sulfate Proteoglycans. *Neuron* **44**, 961–975 (Dec. 16, 2004).
84. Grueber, W. B. & Sagasti, A. Self-avoidance and Tiling: Mechanisms of Dendrite and Axon Spacing. *Cold Spring Harbor Perspectives in Biology* **2**, a001750 (Sept. 1, 2010).
85. Grueber, W. B., Jan, L. Y. & Jan, Y. N. Tiling of the Drosophila epidermis by multidendritic sensory neurons. *Development* **129**, 2867–2878 (June 15, 2002).

86. Cuntz, H., Forstner, F., Borst, A. & Häusser, M. One Rule to Grow Them All: A General Theory of Neuronal Branching and Its Practical Application. *PLOS Computational Biology* **6**, e1000877 (Aug. 5, 2010).
87. Matthews, B. J. *et al.* Dendrite Self-Avoidance Is Controlled by Dscam. *Cell* **129**, 593–604 (May 4, 2007).
88. Lefebvre, J. L., Kostadinov, D., Chen, W. V., Maniatis, T. & Sanes, J. R. Protocadherins mediate dendritic self-avoidance in the mammalian nervous system. *Nature* **488**, 517–521 (Aug. 2012).
89. Schmucker, D. *et al.* Drosophila Dscam Is an Axon Guidance Receptor Exhibiting Extraordinary Molecular Diversity. *Cell* **101**, 671–684 (June 9, 2000).
90. Wässle, H., Peichl, L. & Boycott, B. B. Dendritic territories of cat retinal ganglion cells. *Nature* **292**, 344–345 (July 1981).
91. Lefebvre, J. L., Sanes, J. R. & Kay, J. N. Development of Dendritic Form and Function. *Annual Review of Cell and Developmental Biology* **31**, 741–777 (2015).
92. MacNeil, M. A. & Masland, R. H. Extreme Diversity among Amacrine Cells: Implications for Function. *Neuron* **20**, 971–982 (May 1, 1998).
93. Dacey, D. M. The mosaic of midget ganglion cells in the human retina. *Journal of Neuroscience* **13**, 5334–5355 (Dec. 1, 1993).
94. Sir Charles Scott, S. *The integrative action of the nervous system* xvi, 411 (C Scribner's sons, New York, 1906).
95. Hartline, H. K. The response of single optic nerve fibers of the vertebrate eye to illumination of the retina. *American Journal of Physiology-Legacy Content* **121**, 400–415 (Jan. 31, 1938).
96. Hubel, D. H. & Wiesel, T. N. Receptive fields of single neurones in the cat's striate cortex. *The Journal of Physiology* **148**, 574–591 (1959).
97. Hubel, D. H. & Wiesel, T. N. Receptive fields, binocular interaction and functional architecture in the cat's visual cortex. *The Journal of Physiology* **160**, 106–154 (1962).
98. Fiala, J. C., Spacek, J. & Harris, K. M. in *Dendrites* (Oxford University Press, Sept. 27, 2007).
99. Sugimura, K., Shimono, K., Uemura, T. & Mochizuki, A. Self-organizing Mechanism for Development of Space-filling Neuronal Dendrites. *PLOS Computational Biology* **3**, e212 (Nov. 16, 2007).
100. Dimitrova, S., Reissaus, A. & Tavosanlis, G. Slit and Robo regulate dendrite branching and elongation of space-filling neurons in Drosophila. *Developmental Biology* **324**, 18–30 (Dec. 1, 2008).
101. Parrish, J. Z., Xu, P., Kim, C. C., Jan, L. Y. & Jan, Y. N. The microRNA bantam Functions in Epithelial Cells to Regulate Scaling Growth of Dendrite Arbors in Drosophila Sensory Neurons. *Neuron* **63**, 788–802 (Sept. 24, 2009).
102. Masland, R. H. Neuronal cell types. *Current Biology* **14**, R497–R500 (July 13, 2004).
103. Mukamel, E. A. & Ngai, J. Perspectives on defining cell types in the brain. *Current Opinion in Neurobiology* **56**, 61–68 (June 2019).
104. Latchman, D. S. Transcription factors: An overview. *The International Journal of Biochemistry & Cell Biology* **29**, 1305–1312 (Dec. 1, 1997).
105. Hobert, O. & Kratsios, P. Neuronal identity control by terminal selectors in worms, flies, and chordates. *Current Opinion in Neurobiology* **56**, 97–105 (June 2019).
106. Bayraktar, O. A. & Doe, C. Q. Combinatorial temporal patterning in progenitors expands neural diversity. *Nature* **498**, 449–455 (June 2013).
107. Arendt, D. *et al.* The origin and evolution of cell types. *Nature Reviews Genetics* **17**, 744–757 (Dec. 2016).

108. de-Leon, S. B.-T. & Davidson, E. H. Gene Regulation: Gene Control Network in Development. *Annual Review of Biophysics and Biomolecular Structure* **36**, 191–212 (2007).
109. Davidson, E. H. Emerging properties of animal gene regulatory networks. *Nature* **468**, 911–920 (Dec. 2010).
110. Enriquez, J. *et al.* Specification of Individual Adult Motor Neuron Morphologies by Combinatorial Transcription Factor Codes. *Neuron* **86**, 955–970 (May 2015).
111. Claverie, J.-M. & Audic, S. The statistical significance of nucleotide position-weight matrix matches. *Bioinformatics* **12**, 431–439 (Oct. 1, 1996).
112. Spitz, F. & Furlong, E. E. M. Transcription factors: from enhancer binding to developmental control. *Nature Reviews Genetics* **13**, 613–626 (Sept. 2012).
113. Goillard, J.-M. & Marder, E. Ion Channel Degeneracy, Variability, and Covariation in Neuron and Circuit Resilience. *Annual Review of Neuroscience* **44**, 335–357 (2021).
114. Hille, B. *Ionic Channels of Excitable Membranes* 632 pp. (Oxford University Press, Incorporated, 1992).
115. Levitan, I. B. Modulation of ION Channels in Neurons and Other Cells. *Annual Review of Neuroscience* **11**, 119–136 (1988).
116. Imai, T., Sakano, H. & Vosshall, L. B. Topographic Mapping—The Olfactory System. *Cold Spring Harbor Perspectives in Biology* **2**, a001776 (Aug. 1, 2010).
117. Borst, A. & Helmstaedter, M. Common circuit design in fly and mammalian motion vision. *Nature Neuroscience* **18**, 1067–1076 (Aug. 2015).
118. Nava Gonzales, C. *et al.* Systematic morphological and morphometric analysis of identified olfactory receptor neurons in *Drosophila melanogaster*. *eLife* **10**, e69896 (Aug. 23, 2021).
119. Hogg, P. W., Coleman, P., Dellazizzo Toth, T. & Haas, K. Quantifying neuronal structural changes over time using dynamic morphometrics. *Trends in Neurosciences* **45**, 106–119 (Feb. 1, 2022).
120. Laturus, S., Daranyi, A. v., Huang, Z. & Berens, P. MorphoPy: A python package for feature extraction of neural morphologies. *Journal of Open Source Software* **5**, 2339 (Aug. 3, 2020).
121. Gouwens, N. W. *et al.* Classification of electrophysiological and morphological neuron types in the mouse visual cortex. *Nature Neuroscience* **22**, 1182–1195 (July 2019).
122. Kohashi, T. & Oda, Y. Initiation of Mauthner- or Non-Mauthner-Mediated Fast Escape Evoked by Different Modes of Sensory Input. *Journal of Neuroscience* **28**, 10641–10653 (Oct. 15, 2008).
123. Card, G. & Dickinson, M. H. Visually Mediated Motor Planning in the Escape Response of *Drosophila*. *Current Biology* **18**, 1300–1307 (Sept. 9, 2008).
124. Dayan, P. & Abbott, L. F. *Theoretical Neuroscience: Computational and Mathematical Modeling of Neural Systems* 477 pp. (MIT Press, Aug. 12, 2005).
125. Haag, J. & Borst, A. Amplification of high-frequency synaptic inputs by active dendritic membrane processes. *Nature* **379**, 639–641 (Feb. 1996).
126. London, M. & Häusser, M. Dendritic Computation. *Annual Review of Neuroscience* **28**, 503–532 (2005).
127. Ozbudak, E. M., Thattai, M., Kurtser, I., Grossman, A. D. & van Oudenaarden, A. Regulation of noise in the expression of a single gene. *Nature Genetics* **31**, 69–73 (May 2002).
128. Hassan, B. A. & Hiesinger, P. R. Beyond Molecular Codes: Simple Rules to Wire Complex Brains. *Cell* **163**, 285–291 (Oct. 8, 2015).
129. Hiesinger, P. R. & Hassan, B. A. The Evolution of Variability and Robustness in Neural Development. *Trends in Neurosciences* **41**, 577–586 (Sept. 1, 2018).
130. Morgan, T. H. Sex Limited Inheritance in *Drosophila*. *Science* **32**, 120–122 (July 22, 1910).

131. Rubin, G. M. & Spradling, A. C. Genetic Transformation of *Drosophila* with Transposable Element Vectors. *Science* **218**, 348–353 (Oct. 22, 1982).
132. Adams, M. D. *et al.* The Genome Sequence of *Drosophila melanogaster*. *Science* **287**, 2185–2195 (Mar. 24, 2000).
133. Brand, A. & Perrimon, N. Targeted gene expression as a means of altering cell fates and generating dominant phenotypes. *Development* **118**, 401–415 (June 1, 1993).
134. Luan, H., Peabody, N. C., Vinson, C. R. & White, B. H. Refined Spatial Manipulation of Neuronal Function by Combinatorial Restriction of Transgene Expression. *Neuron* **52**, 425–436 (Nov. 9, 2006).
135. Pfeiffer, B. D. *et al.* Tools for neuroanatomy and neurogenetics in *Drosophila*. *Proceedings of the National Academy of Sciences* **105**, 9715–9720 (July 15, 2008).
136. Pfeiffer, B. D. *et al.* Refinement of Tools for Targeted Gene Expression in *Drosophila*. *Genetics* **186**, 735–755 (Oct. 1, 2010).
137. Jenett, A. *et al.* A GAL4-Driver Line Resource for *Drosophila* Neurobiology. *Cell Reports* **2**, 991–1001 (Oct. 25, 2012).
138. Kvon, E. Z. *et al.* Genome-scale functional characterization of *Drosophila* developmental enhancers in vivo. *Nature* **512**, 91–95 (Aug. 2014).
139. Fire, A. *et al.* Potent and specific genetic interference by double-stranded RNA in *Caenorhabditis elegans*. *Nature* **391**, 806–811 (Feb. 1998).
140. Dietzl, G. *et al.* A genome-wide transgenic RNAi library for conditional gene inactivation in *Drosophila*. *Nature* **448**, 151–156 (July 2007).
141. Perkins, L. A. *et al.* The Transgenic RNAi Project at Harvard Medical School: Resources and Validation. *Genetics* **201**, 843–852 (Nov. 1, 2015).
142. Mank, M. *et al.* A genetically encoded calcium indicator for chronic in vivo two-photon imaging. *Nature Methods* **5**, 805–811 (Sept. 2008).
143. Tian, L. *et al.* Imaging neural activity in worms, flies and mice with improved GCaMP calcium indicators. *Nature Methods* **6**, 875–881 (Dec. 2009).
144. Grienberger, C. & Konnerth, A. Imaging Calcium in Neurons. *Neuron* **73**, 862–885 (Mar. 8, 2012).
145. Shimomura, O., Johnson, F. H. & Saiga, Y. Extraction, Purification and Properties of Aequorin, a Bioluminescent Protein from the Luminous Hydromedusan, *Aequorea*. *Journal of Cellular and Comparative Physiology* **59**, 223–239 (1962).
146. Verkhusha, V. V. & Lukyanov, K. A. The molecular properties and applications of Anthozoa fluorescent proteins and chromoproteins. *Nature Biotechnology* **22**, 289–296 (Mar. 2004).
147. Nern, A., Pfeiffer, B. D. & Rubin, G. M. Optimized tools for multicolor stochastic labeling reveal diverse stereotyped cell arrangements in the fly visual system. *Proceedings of the National Academy of Sciences* **112**, E2967–E2976 (June 2, 2015).
148. Konstantinides, N. *et al.* Phenotypic Convergence: Distinct Transcription Factors Regulate Common Terminal Features. *Cell* **174**, 622–635.e13 (July 26, 2018).
149. Davis, F. P. *et al.* A genetic, genomic, and computational resource for exploring neural circuit function. *eLife* **9**, e50901 (Jan. 15, 2020).
150. Zheng, G. X. Y. *et al.* Massively parallel digital transcriptional profiling of single cells. *Nature Communications* **8**, 14049 (Apr. 2017).
151. Buenrostro, J. D., Giresi, P. G., Zaba, L. C., Chang, H. Y. & Greenleaf, W. J. Transposition of native chromatin for fast and sensitive epigenomic profiling of open chromatin, DNA-binding proteins and nucleosome position. *Nature Methods* **10**, 1213–1218 (Dec. 2013).
152. Buenrostro, J. D. *et al.* Single-cell chromatin accessibility reveals principles of regulatory variation. *Nature* **523**, 486–490 (July 2015).

153. Cusanovich, D. A. *et al.* Multiplex single-cell profiling of chromatin accessibility by combinatorial cellular indexing. *Science* **348**, 910–914 (May 22, 2015).
154. O’Neill, L. P. & Turner, B. M. Histone H4 acetylation distinguishes coding regions of the human genome from heterochromatin in a differentiation-dependent but transcription-independent manner. *The EMBO Journal* **14**, 3946–3957 (Aug. 1995).
155. O’Neill, L. P. & Turner, B. M. in *Methods in Enzymology* 189–197 (Academic Press, Jan. 1, 1996).
156. Chen, X. *et al.* High-Throughput Mapping of Long-Range Neuronal Projection Using In Situ Sequencing. *Cell* **179**, 772–786.e19 (Oct. 2019).
157. Li, H. *et al.* Fly Cell Atlas: A single-nucleus transcriptomic atlas of the adult fruit fly. *Science* (Mar. 4, 2022).
158. Janssens, J. *et al.* Decoding gene regulation in the fly brain. *Nature* **601**, 630–636 (Jan. 2022).
159. Zheng, Z. *et al.* A Complete Electron Microscopy Volume of the Brain of Adult *Drosophila melanogaster*. *Cell* **174**, 730–743.e22 (July 26, 2018).
160. Scheffer, L. K. *et al.* A connectome and analysis of the adult *Drosophila* central brain. *eLife* **9**, e57443 (Sept. 3, 2020).
161. Dorkenwald, S. *et al.* FlyWire: online community for whole-brain connectomics. *Nature Methods* **19**, 119–128 (Jan. 2022).
162. Denk, W. & Horstmann, H. Serial Block-Face Scanning Electron Microscopy to Reconstruct Three-Dimensional Tissue Nanostructure. *PLOS Biology* **2**, e329 (Oct. 19, 2004).
163. Takemura, S.-y. *et al.* The comprehensive connectome of a neural substrate for ‘ON’ motion detection in *Drosophila*. *eLife* **6**, e24394 (Apr. 22, 2017).
164. Takemura, S.-y. *et al.* A connectome of a learning and memory center in the adult *Drosophila* brain. *eLife* **6**, e26975 (July 18, 2017).
165. Franconville, R., Beron, C. & Jayaraman, V. Building a functional connectome of the *Drosophila* central complex. *eLife* **7**, e37017 (Aug. 20, 2018).
166. Shinomiya, K. *et al.* Comparisons between the ON- and OFF-edge motion pathways in the *Drosophila* brain. *eLife* **8**, e40025 (Jan. 9, 2019).
167. Fermi, G. & Reichardt, W. Optomotorische Reaktionen der Fliege *Musca domestica*. *Kybernetik* **2**, 15–28 (Sept. 1963).
168. Götz, K. G. Optomotorische Untersuchung des visuellen systems einiger Augenmutanten der Fruchtfliege *Drosophila*. *Kybernetik* **2**, 77–92 (June 1, 1964).
169. Ribeiro, I. M. A. *et al.* Visual Projection Neurons Mediating Directed Courtship in *Drosophila*. *Cell* **174**, 607–621.e18 (July 26, 2018).
170. Kabra, M., Robie, A. A., Rivera-Alba, M., Branson, S. & Branson, K. JAABA: interactive machine learning for automatic annotation of animal behavior. *Nature Methods* **10**, 64–67 (Jan. 2013).
171. Pereira, T. D. *et al.* SLEAP: A deep learning system for multi-animal pose tracking. *Nature Methods* **19**, 486–495 (Apr. 2022).
172. Schilling, T., Ali, A. H., Leonhardt, A., Borst, A. & Pujol-Martí, J. Transcriptional control of morphological properties of direction-selective T4/T5 neurons in *Drosophila*. *Development* **146**, dev169763 (Jan. 29, 2019).
173. Borst, A. Fly visual course control: behaviour, algorithms and circuits. *Nature Reviews Neuroscience* **15**, 590–599 (Sept. 2014).
174. Meinertzhagen, I. A. & O’Neil, S. D. Synaptic organization of columnar elements in the lamina of the wild type in *Drosophila melanogaster*. *Journal of Comparative Neurology* **305**, 232–263 (1991).

175. Borst, A., Drews, M. & Meier, M. The neural network behind the eyes of a fly. *Current Opinion in Physiology. Vision Physiology* **16**, 33–42 (Aug. 1, 2020).
176. Carthew, R. W. Pattern formation in the Drosophila eye. *Current Opinion in Genetics & Development. Pattern formation and developmental mechanisms* **17**, 309–313 (Aug. 1, 2007).
177. Kumar, J. P. Building an ommatidium one cell at a time. *Developmental Dynamics* **241**, 136–149 (2012).
178. Miklos, G. L. G. & Rubin, G. M. The Role of the Genome Project in Determining Gene Function: Insights from Model Organisms. *Cell* **86**, 521–529 (Aug. 23, 1996).
179. Fortini, M. E. & Bonini, N. M. Modeling human neurodegenerative diseases in Drosophila: on a wing and a prayer. *Trends in Genetics* **16**, 161–167 (Apr. 1, 2000).
180. Zeleny, C. The effect of selection for eye facet number in the white bar-eye race of Drosophila melanogaster. *Genetics* **7**, 1–115 (Jan. 1, 1922).
181. Rister, J. *et al.* Dissection of the Peripheral Motion Channel in the Visual System of Drosophila melanogaster. *Neuron* **56**, 155–170 (Oct. 4, 2007).
182. Yamaguchi, S., Wolf, R., Desplan, C. & Heisenberg, M. Motion vision is independent of color in Drosophila. *Proceedings of the National Academy of Sciences* **105**, 4910–4915 (Mar. 25, 2008).
183. Yamaguchi, S., Desplan, C. & Heisenberg, M. Contribution of photoreceptor subtypes to spectral wavelength preference in Drosophila. *Proceedings of the National Academy of Sciences* **107**, 5634–5639 (Mar. 23, 2010).
184. Strausfeld, N. J. & Wells, G. P. Golgi studies on insects Part II. The optic lobes of Diptera. *Philosophical Transactions of the Royal Society of London. B, Biological Sciences* **258**, 135–223 (Apr. 21, 1970).
185. Nériec, N. & Desplan, C. in *Current Topics in Developmental Biology* 247–271 (Academic Press, Jan. 1, 2016).
186. Fischbach, K. -. & Dittrich, A. P. M. The optic lobe of Drosophila melanogaster. I. A Golgi analysis of wild-type structure. *Cell and Tissue Research* **258**, 441–475 (Dec. 1, 1989).
187. Langen, M. *et al.* The Developmental Rules of Neural Superposition in Drosophila. *Cell* **162**, 120–133 (July 2, 2015).
188. Joesch, M., Schnell, B., Raghu, S. V., Reiff, D. F. & Borst, A. ON and OFF pathways in Drosophila motion vision. *Nature* **468**, 300–304 (Nov. 2010).
189. Takemura, S.-y. *et al.* Cholinergic Circuits Integrate Neighboring Visual Signals in a Drosophila Motion Detection Pathway. *Current Biology* **21**, 2077–2084 (Dec. 20, 2011).
190. Silies, M. *et al.* Modular Use of Peripheral Input Channels Tunes Motion-Detecting Circuitry. *Neuron* **79**, 111–127 (July 10, 2013).
191. Meier, M. *et al.* Neural Circuit Components of the Drosophila OFF Motion Vision Pathway. *Current Biology* **24**, 385–392 (Feb. 17, 2014).
192. Ting, C.-Y. *et al.* Photoreceptor-Derived Activin Promotes Dendritic Termination and Restricts the Receptive Fields of First-Order Interneurons in Drosophila. *Neuron* **81**, 830–846 (Feb. 2014).
193. Wu, M. *et al.* Visual projection neurons in the Drosophila lobula link feature detection to distinct behavioral programs. *eLife* **5**, e21022 (Dec. 28, 2016).
194. Klapoetke, N. C. *et al.* Ultra-selective looming detection from radial motion opponency. *Nature* **551**, 237–241 (Nov. 2017).
195. Koenderink, J. J. Optic flow. *Vision Research* **26**, 161–179 (Jan. 1, 1986).
196. Keleş, M. F. & Frye, M. A. Object-Detecting Neurons in Drosophila. *Current Biology* **27**, 680–687 (Mar. 6, 2017).

197. Dvorak, D. R., Bishop, L. G. & Eckert, H. E. On the identification of movement detectors in the fly optic lobe. *Journal of comparative physiology* **100**, 5–23 (Jan. 1, 1975).
198. Joesch, M., Plett, J., Borst, A. & Reiff, D. F. Response Properties of Motion-Sensitive Visual Interneurons in the Lobula Plate of *Drosophila melanogaster*. *Current Biology* **18**, 368–374 (Mar. 11, 2008).
199. Borst, A., Haag, J. & Reiff, D. F. Fly Motion Vision. *Annual Review of Neuroscience* **33**, 49–70 (2010).
200. Muijres, F. T., Elzinga, M. J., Melis, J. M. & Dickinson, M. H. Flies Evade Looming Targets by Executing Rapid Visually Directed Banked Turns. *Science* **344**, 172–177 (Apr. 11, 2014).
201. Hall, J. C. The Mating of a Fly. *Science* **264**, 1702–1714 (June 17, 1994).
202. Reichardt, W. Evaluation of optical motion information by movement detectors. *Journal of Comparative Physiology A* **161**, 533–547 (July 1, 1987).
203. Egelhaaf, M., Borst, A. & Reichardt, W. The nonlinear mechanism of direction selectivity in the fly motion detection system. *Naturwissenschaften* **76**, 32–35 (Jan. 1, 1989).
204. Borst, A. & Egelhaaf, M. Principles of visual motion detection. *Trends in Neurosciences* **12**, 297–306 (Jan. 1989).
205. Haag, J., Arenz, A., Serbe, E., Gabbiani, F. & Borst, A. Complementary mechanisms create direction selectivity in the fly. *eLife* **5**, e17421 (Aug. 9, 2016).
206. Maisak, M. S. *et al.* A directional tuning map of *Drosophila* elementary motion detectors. *Nature* **500**, 212–216 (Aug. 2013).
207. Takemura, S.-y. *et al.* A visual motion detection circuit suggested by *Drosophila* connectomics. *Nature* **500**, 175–181 (Aug. 2013).
208. Behnia, R., Clark, D. A., Carter, A. G., Clandinin, T. R. & Desplan, C. Processing properties of ON and OFF pathways for *Drosophila* motion detection. *Nature* **512**, 427–430 (Aug. 2014).
209. Serbe, E., Meier, M., Leonhardt, A. & Borst, A. Comprehensive Characterization of the Major Presynaptic Elements to the *Drosophila* OFF Motion Detector. *Neuron* **89**, 829–841 (Feb. 17, 2016).
210. Arenz, A., Drews, M. S., Richter, F. G., Ammer, G. & Borst, A. The Temporal Tuning of the *Drosophila* Motion Detectors Is Determined by the Dynamics of Their Input Elements. *Current Biology* **27**, 929–944 (Apr. 3, 2017).
211. Fendl, S., Vieira, R. M. & Borst, A. Conditional protein tagging methods reveal highly specific subcellular distribution of ion channels in motion-sensing neurons. *eLife* **9**, e62953 (Oct. 20, 2020).
212. Groschner, L. N., Malis, J. G., Zuidinga, B. & Borst, A. A biophysical account of multiplication by a single neuron. *Nature* **603**, 119–123 (Mar. 2022).
213. Leong, J. C. S., Esch, J. J., Poole, B., Ganguli, S. & Clandinin, T. R. Direction Selectivity in *Drosophila* Emerges from Preferred-Direction Enhancement and Null-Direction Suppression. *Journal of Neuroscience* **36**, 8078–8092 (Aug. 3, 2016).
214. Borst, A. A biophysical mechanism for preferred direction enhancement in fly motion vision. *PLOS Computational Biology* **14**, e1006240 (June 13, 2018).
215. Mauss, A. S., Meier, M., Serbe, E. & Borst, A. Optogenetic and Pharmacologic Dissection of Feedforward Inhibition in *Drosophila* Motion Vision. *Journal of Neuroscience* **34**, 2254–2263 (Feb. 5, 2014).
216. Hofbauer, A. & Campos-Ortega, J. A. Proliferation pattern and early differentiation of the optic lobes in *Drosophila melanogaster*. *Roux's archives of developmental biology* **198**, 264–274 (Feb. 1, 1990).
217. Apitz, H. & Salecker, I. A region-specific neurogenesis mode requires migratory progenitors in the *Drosophila* visual system. *Nature Neuroscience* **18**, 46–55 (Jan. 2015).

218. Apitz, H. & Salecker, I. Spatio-temporal relays control layer identity of direction-selective neuron subtypes in *Drosophila*. *Nature Communications* **9**, 2295 (June 12, 2018).
219. Oliva, C. *et al.* Proper connectivity of *Drosophila* motion detector neurons requires Atonal function in progenitor cells. *Neural Development* **9**, 4 (Feb. 26, 2014).
220. Kurmangaliyev, Y. Z., Yoo, J., LoCascio, S. A. & Zipursky, S. L. Modular transcriptional programs separately define axon and dendrite connectivity. *eLife* **8**, e50822 (Nov. 5, 2019).
221. Zhao, A. *et al.* *Eye structure shapes neuron function in Drosophila motion vision* Dec. 15, 2022.
222. Sanes, J. R. & Zipursky, S. L. Synaptic Specificity, Recognition Molecules, and Assembly of Neural Circuits. *Cell* **181**, 536–556 (Apr. 30, 2020).
223. Zipursky, S. L. & Sanes, J. R. Chemoaffinity Revisited: Dscams, Protocadherins, and Neural Circuit Assembly. *Cell* **143**, 343–353 (Oct. 29, 2010).
224. Lawrence Zipursky, S. & Grueber, W. B. The Molecular Basis of Self-Avoidance. *Annual Review of Neuroscience* **36**, 547–568 (2013).
225. Kurmangaliyev, Y. Z., Yoo, J., Valdes-Aleman, J., Sanfilippo, P. & Zipursky, S. L. Transcriptional Programs of Circuit Assembly in the *Drosophila* Visual System. *Neuron* **108**, 1045–1057.e6 (Dec. 2020).
226. Özel, M. N. *et al.* Neuronal diversity and convergence in a visual system developmental atlas. *Nature* **589**, 88–95 (Jan. 7, 2021).
227. Akin, O., Bajar, B. T., Keles, M. F., Frye, M. A. & Zipursky, S. L. Cell-type-Specific Patterned Stimulus-Independent Neuronal Activity in the *Drosophila* Visual System during Synapse Formation. *Neuron* **101**, 894–904.e5 (Mar. 6, 2019).
228. Eisen, M. B., Spellman, P. T., Brown, P. O. & Botstein, D. Cluster analysis and display of genome-wide expression patterns. *Proceedings of the National Academy of Sciences* **95**, 14863–14868 (Dec. 8, 1998).
229. Segal, E. *et al.* Module networks: identifying regulatory modules and their condition-specific regulators from gene expression data. *Nature Genetics* **34**, 166–176 (June 2003).
230. Liberzon, A. *et al.* The Molecular Signatures Database Hallmark Gene Set Collection. *Cell Systems* **1**, 417–425 (Dec. 23, 2015).
231. Kotliar, D. *et al.* Identifying gene expression programs of cell-type identity and cellular activity with single-cell RNA-Seq. *eLife* **8**, e43803 (July 8, 2019).
232. Jain, S. *et al.* A global timing mechanism regulates cell-type-specific wiring programmes. *Nature* **603**, 112–118 (Mar. 2022).
233. Raj, A. & van Oudenaarden, A. Nature, Nurture, or Chance: Stochastic Gene Expression and Its Consequences. *Cell* **135**, 216–226 (Oct. 17, 2008).
234. Pelkmans, L. Using Cell-to-Cell Variability—A New Era in Molecular Biology. *Science* **336**, 425–426 (Apr. 27, 2012).
235. Mereu, E. *et al.* Benchmarking single-cell RNA-sequencing protocols for cell atlas projects. *Nature Biotechnology* **38**, 747–755 (June 2020).
236. Satija, R., Farrell, J. A., Gennert, D., Schier, A. F. & Regev, A. Spatial reconstruction of single-cell gene expression data. *Nature Biotechnology* **33**, 495–502 (May 2015).
237. Wolf, F. A., Angerer, P. & Theis, F. J. SCANPY: large-scale single-cell gene expression data analysis. *Genome Biology* **19**, 15 (Feb. 6, 2018).
238. Ilicic, T. *et al.* Classification of low quality cells from single-cell RNA-seq data. *Genome Biology* **17**, 29 (Feb. 17, 2016).
239. Pankova, K. & Borst, A. RNA-Seq Transcriptome Analysis of Direction-Selective T4/T5 Neurons in *Drosophila*. *PLOS ONE* **11**, e0163986 (Sept. 29, 2016).

240. Novick, A. & Weiner, M. Enzyme induction as an all-or-none phenomenon*. *Proceedings of the National Academy of Sciences* **43**, 553–566 (July 15, 1957).
241. Minsky, M. *US Patent* 3013467A (1961).
242. Denk, W., Strickler, J. H. & Webb, W. W. Two-Photon Laser Scanning Fluorescence Microscopy. *Science* **248**, 73–76 (Apr. 6, 1990).
243. Krull, A., Buchholz, T.-O. & Jug, F. *Noise2Void - Learning Denoising From Single Noisy Images in 2019 IEEE/CVF Conference on Computer Vision and Pattern Recognition (CVPR) 2019 IEEE/CVF Conference on Computer Vision and Pattern Recognition (CVPR) (IEEE, Long Beach, CA, USA, June 2019)*, 2124–2132.
244. Hossain, S., Sesath Hewapathirane, D. & Haas, K. Dynamic morphometrics reveals contributions of dendritic growth cones and filopodia to dendritogenesis in the intact and awake embryonic brain. *Developmental Neurobiology* **72**, 615–627 (2012).
245. Uylings, H. B. M. & van Pelt, J. Measures for quantifying dendritic arborizations. *Network: Computation in Neural Systems* **13**, 397–414 (Jan. 1, 2002).
246. Helmstaedter, M. *et al.* Connectomic reconstruction of the inner plexiform layer in the mouse retina. *Nature* **500**, 168–174 (Aug. 2013).
247. Özel, M. N., Langen, M., Hassan, B. A. & Hiesinger, P. R. Filopodial dynamics and growth cone stabilization in *Drosophila* visual circuit development. *eLife* **4**, e10721 (Oct. 29, 2015).
248. Horton, R. E. Erosional development of streams and their drainage basins; Hydrophysical approach to quantitative morphology. *GSA Bulletin* **56**, 275–370 (Mar. 1, 1945).
249. Vormberg, A., Effenberger, F., Muellerleile, J. & Cuntz, H. Universal features of dendrites through centripetal branch ordering. *PLOS Computational Biology* **13**, e1005615 (July 3, 2017).
250. Sholl, D. A. Dendritic organization in the neurons of the visual and motor cortices of the cat. *Journal of Anatomy* **87**, 387–406.1 (Pt 4 Oct. 1953).
251. Bird, A. D. & Cuntz, H. Dissecting Sholl Analysis into Its Functional Components. *Cell Reports* **27**, 3081–3096.e5 (June 4, 2019).
252. Rosin, P. L. Classification of pathological shapes using convexity measures. *Pattern Recognition Letters* **30**, 570–578 (Apr. 1, 2009).
253. Berger, M. Convexity. *The American Mathematical Monthly* **97**, 650–678 (1990).
254. Rockafellar, R. T. *Convex Analysis* 482 pp. (Princeton University Press, 1970).
255. Savant-Bhonsale, S., Friese, M., McCoon, P. & Montell, D. J. A *Drosophila* Derailed homolog, Doughnut, expressed in invaginating cells during embryogenesis. *Gene* **231**, 155–161 (Apr. 29, 1999).
256. Yoshikawa, S., McKinnon, R. D., Kokel, M. & Thomas, J. B. Wnt-mediated axon guidance via the *Drosophila* Derailed receptor. *Nature* **422**, 583–588 (Apr. 2003).
257. Lyuksyutova, A. I. *et al.* Anterior-Posterior Guidance of Commissural Axons by Wnt-Frizzled Signaling. *Science* **302**, 1984–1988 (Dec. 12, 2003).
258. Vaughn, J. E., Henrikson, C. K. & Grieshaber, J. A. A quantitative study of synapses on motor neuron dendritic growth cones in developing mouse spinal cord. *Journal of Cell Biology* **60**, 664–672 (Mar. 1, 1974).
259. Vaughn, J. E., Barber, R. P. & Sims, T. J. Dendritic development and preferential growth into synaptogenic fields: A quantitative study of Golgi-impregnated spinal motor neurons. *Synapse* **2**, 69–78 (1988).
260. Vaughn, J. E. Review: Fine structure of synaptogenesis in the vertebrate central nervous system. *Synapse* **3**, 255–285 (1989).

261. Cline, H. & Haas, K. The regulation of dendritic arbor development and plasticity by glutamatergic synaptic input: a review of the synaptotrophic hypothesis. *The Journal of Physiology* **586**, 1509–1517 (2008).
262. Sperry, R. W. Chemoaffinity in the orderly growth of nerve fiber patterns and connections*. *Proceedings of the National Academy of Sciences* **50**, 703–710 (Oct. 1963).

ACKNOWLEDGEMENTS

The effort of the last few years resulted in the work of this thesis. It could have not been accomplished without the help of colleagues, friends, and family supporting me in this endeavour. I would like to thank the following especially for their help and company during this journey.

Firstly, of course, Axel Borst! He gave me all the freedom and means to pursue different research directions, such as a two month stay in Konstanz or the Neural Systems and Behaviour summer school at the MBL. Additionally, he supported me in the organisation of the WireUp Max Planck PhD Symposium and other activities of the Max Planck Phdnet. He always reviewed any important application or thesis, even though there was little time left before the deadlines. Furthermore, he encouraged me to meet up with Florian Engert about a potential postdoc position, which turned out quite positive. Altogether, he shaped my way of scientific thinking and supported me in many different ways to advance my scientific career. I am grateful for all his support throughout the years.

Next, I would like to thank all my co-authors without whom this work could have not been completed. They created a supporting environment even when we got partially scoped and worked together to publish our work. Working collaboratively was rewarding and resulted in the two manuscripts above, which opened a new research direction for the lab. The rest of the Borst lab provided a supportive environment for scientific discussion and, not to forget, many fun lab outings and themed Happy Hours.

Additionally, I want to acknowledge the friends in Munich from the GSN, MPI and Phdnet that helped me to stay driven throughout the years and made the whole experience a lot more fun: Anna, Drago, Ksenia, Judy, Veronika and Vilim for our skiing trips and extravagant dinners; all of the PhDs for the experiences we had at our institute retreats, but especially my coorganisers of the WireUp conference; the motivated people of the Phdnet that helped me get a sense for the organisation and political side of academia, with a special thanks to Srinath, who was my partner in crime in the beginnings of the Offspring Podcast.

I am grateful to Armin, Katrin and Heike for the welcoming environment in Konstanz which allowed me to experience zebrafish research and gave me a lot of advice and motivation for staying in academia.

And I want to thank my fellow students from the "Neural Systems and Behaviour" summer school which lead to many new experiences from a scientific and social point of view. But also my reviewers, Drago Guggiana Nilo and Duncan Mearns for reading

the thesis on such short notice while still providing constructive feedback without fail. I would like to thank Lea Heckmann for reviewing the thesis as well as overall support during the writing process pushing me past the last few days of work for the submission.

Lastly, I would like to thank my family for supporting me throughout the years emotionally and with a lot of food.

List of publications and author contributions

Manuscript 1: A combinatorial code of transcription factors specifies subtypes of visual motion-sensing neurons in *Drosophila*

Authors: Nikolai Hörmann*, Tabea Schilling, Aicha Haji Ali, Etienne Serbe, Christian Mayer, Alexander Borst and Jesús Pujol-Martí*

*: Authors for correspondence: hoermann@neuro.mpg.de; pujolmarti@neuro.mpg.de

Author contributions: Conceptualization: **N.H.**, T.S., A.B., J.P.-M.; Methodology: **N.H.**, T.S., C.M., J.P.-M.; Software: **N.H.**, C.M.; Investigation: **N.H.**, T.S., A.H.A., E.S., J.P.-M.; Writing (original draft): J.P.-M.; Writing (review and editing): **N.H.**, T.S., C.M., A.B., J.P.-M.; Visualization: **N.H.**, T.S., J.P.-M.; Supervision: A.B., J.P.-M.; Funding acquisition: A.B. (order according to author list)

Manuscript 2: Topographic maps differently influence growth patterns in subtypes of *Drosophila* direction-selective neurons

Authors: Nikolai Hörmann^{†,*}, Aicha Haji Ali[†], Nikolas Drummond, Cemre Coskun, Melisa Özmen, Jesús Pujol-Martí and Alexander Borst

†: These authors contributed equally

*: Author for correspondence: nikolai.hoermann@bi.mpg.de

Author contributions: Conceptualization: **N.H.**, A.H.A, J.P.M., A.B., Data curation: A.H.A., **N.H.**, Formal Analysis: A.H.A, **N.H.**, N.D., C.C., M.Ö., Funding acquisition: A.B., Investigation: A.H.A, **N.H.**, J.P.M., C.C., M.Ö., Methodology: **N.H.**, A.H.A, N.D., Project administration: **N.H.**, A.H.A, Resources: A.B., Software: **N.H.**, A.H.A, N.D., Supervision: A.B., J.P.M, Validation: **N.H.**, A.H.A, N.D., Visualization: A.H.A, **N.H.**, N.D., Writing original draft: **N.H.**, A.H.A, Writing review and editing: **N.H.**, A.H.A, N.D., C.C., M.Ö., J.P.M., A.B., (order according to contribution)

Nikolai Hörmann
(Author)

Prof. Dr. Alexander Borst
(Supervisor)

Aicha Haji Ali
(Co-first author Manuscript 2)

EIDESSTÄTTLICHE VERSICHERUNG/AFFIDAVIT

Nikolai Hörmann

(Studierende/Student)

Hiermit versichere ich an Eides statt, dass ich die vorliegende Dissertation

"Transcriptional specification and dendritic growth patterns of motion-sensing neurons in Drosophila during development"

selbstständig angefertigt habe, mich außer der angegebenen keiner weiteren Hilfsmittel bedient und alle Erkenntnisse, die aus dem Schrifttum ganz oder annähernd übernommen sind, als solche kenntlich gemacht und nach ihrer Herkunft unter Bezeichnung der Fundstelle einzeln nachgewiesen habe.

I hereby confirm that the dissertation

"Transcriptional specification and dendritic growth patterns of motion-sensing neurons in Drosophila during development"

is the result of my own work and that I have only used sources or materials listed and specified in the dissertation.

München, 09. Januar 2023

(Datum/Date)

Nikolai Hörmann

(Unterschrift/Signature)